TRAJECTORY TRACKING CONTROL OF UNMANNED GROUND VEHICLES IN MIXED TERRAIN

A THESIS SUBMITTED TO
THE GRADUATE SCHOOL OF NATURAL AND APPLIED SCIENCES
OF
MIDDLE EAST TECHNICAL UNIVERSITY

BY

GÖKHAN BAYAR

IN PARTIAL FULFILLMENT OF THE REQUIREMENTS
FOR
THE DEGREE OF DOCTOR OF PHILOSOPHY
IN
MECHANICAL ENGINEERING

SEPTEMBER 2012

Approval of the thesis:

TRAJECTORY TRACKING CONTROL OF UNMANNED GROUND VEHICLES IN MIXED TERRAIN

submitted by **GÖKHAN BAYAR** in partial fulfillment of the requirements for the degree of **Doctor of Philosophy in Mechanical Engineering Department, Middle East Technical University** by,

Prof. Dr. Canan Özgen
Dean, Graduate School of **Natural and Applied Sciences** _____

Prof. Dr. Suha Oral
Head of Department, **Mechanical Engineering** _____

Assist. Prof. Dr. A. Buğra Koku
Supervisor, **Mechanical Engineering, METU** _____

Assist. Prof. Dr. E. İlhan Konukseven
Co-supervisor, **Mechanical Engineering, METU** _____

Examining Committee Members:

Prof. Dr. Samim Ünlüsoy
Mechanical Engineering, METU _____

Assist. Prof. Dr. A. Buğra Koku
Mechanical Engineering, METU _____

Prof. Dr. Tuna Balkan
Mechanical Engineering, METU _____

Assist. Prof. Dr. Yiğit Yazıcıuğlu
Mechanical Engineering, METU _____

Prof. Dr. Veysel Gazi
Electrical and Electronics Engineering, İstanbul Kemerburgaz University _____

Date: _____

I hereby declare that all information in this document has been obtained and presented in accordance with academic rules and ethical conduct. I also declare that, as required by these rules and conduct, I have fully cited and referenced all material and results that are not original to this work.

Name, Last Name: GÖKHAN BAYAR

Signature :

ABSTRACT

TRAJECTORY TRACKING CONTROL OF UNMANNED GROUND VEHICLES IN MIXED TERRAIN

Bayar, Gökhan

Ph.D., Department of Mechanical Engineering

Supervisor : Assist. Prof. Dr. A. Buğra Koku

Co-Supervisor : Assist. Prof. Dr. E. İlhan Konukseven

September 2012, 146 pages

Mobile robots are commonly used to achieve tasks involving tracking a desired trajectory and following a predefined path in different types of terrains that have different surface characteristics. A mobile robot can perform the same navigation task task over different surfaces if the tracking performance and accuracy are not essential. However, if the tracking performance is the main objective, due to changing the characteristics of wheel-ground interaction, a single set of controller parameters or an equation of motion might be easily failing to guarantee a desired performance and accuracy. The interaction occurring between the wheels and ground can be integrated into the system model so that the performance of the mobile robot can be enhanced on various surfaces. This modeling approach related to wheel-ground interaction can also be incorporated into the motion controller. In this thesis study, modeling studies for a two wheeled differential drive mobile robot and a steerable four-wheeled robot vehicle are carried out. A strategy to achieve better tracking performance for a differential drive mobile robot is developed by introducing a procedure including the effects of external wheel forces; i.e, traction, rolling and lateral. A new methodology to represent the effects of lateral wheel force is proposed. An estimation procedure to estimate the parameters of external wheel forces is

also introduced. Moreover, a modeling study that is related to show the effects of surface inclination on tracking performance is performed and the system model of the differential drive mobile robot is updated accordingly. In order to accomplish better trajectory tracking performance and accuracy for a steerable four-wheeled mobile robot, a modeling work that includes a desired trajectory generator and trajectory tracking controller is implemented. The slippage is defined via the slip velocities of steerable front and motorized rear wheels of the mobile robot. These slip velocities are obtained by using the proposed slippage estimation procedure. The estimated slippage information is then comprised into the system model so as to increase the performance and accuracy of the trajectory tracking tasks. All the modeling studies proposed in this study are tested by using simulations and verified on experimental platforms.

Keywords: autonomous, mobile robot, ground vehicle, trajectory tracking, control, terrain

ÖZ

İNSANSIZ KARA ARAÇLARININ DEĞİŞKEN YÜZEY ŞARTLARINDA YÖRÜNGE İZLEMESİ KONTROLÜ

Bayar, Gökhan
Doktora, Makina Mühendisliğ Bölümü
Tez Yöneticisi : Yrd. Doç Dr. A. Buğra Koku
Ortak Tez Yöneticisi : Yrd. Doç. Dr. E. İlhan Konukseven

Agustos 2012, 146 sayfa

Hareketli robot platformları referans bir yörüngenin otonom olarak takibi amacı ile yoğun olarak kullanılırlar. Referans yörünge değişik karakteristik özelliklere sahip yüzeylerden geçebilir. Eğer yörünge takip görevinde performans ve doğruluk çok önemli değilse, hareketli bir robot tek bir görevi değişik yüzey karakteristikleri olan yol şartlarında yapabilir. Fakat yörünge takip performansı ana amaçlardan bir tanesi ise bilinen yörünge takip modelleri ve sabit bir kontrolcü kullanılarak, hareketli robotun başarıyla görevini yapması beklenemez. Çünkü tekerlekler ve yüzey arasındaki ilişki sürekli değişmektedir ve robotun yörüngeden sapmasına sebeb olacaktır. Bu sorunları çözmek adına tekerlekler ve yüzey arasında etkileşim incelenebilir ve sistem modeline eklenebilir. Bu yörünge takip performansını iyileştirecektir. Bu etkileşimin kontrolcüyle de ilişkilendirilmesi performansa katkı sağlayacaktır. Bu tez çalışması kapsamında, iki tekerlekli diferansiyel sürüş özelliğine sahip bir hareketli robot ile dört tekerlekli, ön tekerlekleri döndürülebilen bir robot araç için modelleme çalışmaları yapılmıştır. Diferansiyel sürüşlü hareketli robot için, daha iyi bir yörünge takibi amacı ile tekerlek kuvvetlerinin (çekiş, yuvarlanma ve yanal) hesaba katıldığı bir prosedür geliştirilmiştir. Bu tekerlek kuvvetlerini tanımlamada kullanılan parametrelerin tahmin edilmesini sağlayan

bir mekanizma tanıtılmıştır. Tekerlek kuvvetlerinin yanı sıra, hareketli robotun hareket ettiği yüzeyin eğim bilgisininde hareket modeline dahil edilmesi sağlanmıştır. Dört tekerlekli robot araç ile daha iyi bir yörünge takibi yapabilmek için diğer bir modelleme çalışması yapılmıştır. Bu çalışma kapsamında referans yörünge üreteci ve yörünge takibini sağlayacak kontrolcü tasarımları gerçekleştirilmiştir. Robot aracın hareketini sağlayan arka tekerlekler ve dönüşünü sağlayan ön tekerleklerde oluşan kayma hızlarını baz alan bir kayma modeli geliştirilmiştir. Oluşan bu kayma hızlarını tahmin edibilen bir yapı oluşturulmuştur. Bu yapı referans yörünge takibi performansının ve doğruluğunun artırılması için sistem modeline dahil edilmiştir. Önerilen bütün modelleme çalışmaları deneysel platformlar kullanılarak test edilmiştir.

Anahtar Kelimeler: otonom, hareketli robot, kara aracı, yörünge takibi, kontrol, zemin

to my youth

ACKNOWLEDGMENTS

I would like to express my gratitude to my supervisor, Dr. A. Buğra Koku and my co-supervisor, Dr. E. İlhan Konukseven for their expertise, understanding, help and guidance. I appreciate their tremendous skills and knowledge in the field of mobile robotic research. They provided me an environment having vast of facilities required for my studies. I could be able to gain my research capabilities in mechatronics area via following their guidance. I must also acknowledge them for their interest and concern about my research that I have conducted in the Robotics Institute of Carnegie Mellon University. I would like to thank the other members of my Ph.D. thesis committee, Dr. Samim Ünlüsoy and Dr. Veysel Gazi for their assistance at the progresses of the thesis.

I would like to thank the members of the Mechatronics Laboratory of Mechanical Engineering Department of Middle East Technical University. A very special thanks goes out to Özgür Başer who is the senior member of this lab. I would also like to thank to the Mechatronics Laboratory, D-114, itself. It was my only friend at the long nights when I was doing my research. My thanks go to the members of Machine Shop of ME Department as well. I had to do lots of manufacturing in the Machine Shop and they helped me a lot.

I would like to thank the members of Comprehensive Automation for Specialty Crops Project conducted in the Field Robotics Center of Robotics Institute of Carnegie Mellon University. I did my researches related to mobility of an autonomous orchard vehicle by using the great facilities supplied. My special thanks go to Dr. Marcel Bergerman for his perfect guidance and perfect support. I would also like to thank Dr. Sanjiv Singh for his contributions in my research. My big thanks are to my office mates Gustavo Freitas and Ji Zhang. I also send my special thanks to Silvio Maeta for his vast effort and help in my studies. I should thank to Andrew Achamber and Joern Rehter for their significant friendship in the environment of the Field Robotics Center.

I must acknowledge my wife and best friend, Çağlar, whose boundless love, support and encouragement. She stood by me all the time.

TABLE OF CONTENTS

LIST OF TABLES

TABLES

LIST OF FIGURES

FIGURES

CHAPTER 1

INTRODUCTION

1.1 Motivation

An autonomous unmanned ground vehicle is a special vehicle which has capability for doing automatic navigation. Since the vehicle should be self behaving and self tuning, it is able to run and response to its work space in which it operates without any interaction from the outside. The vehicle that controls itself has the capabilities of sensing and modeling its work space, positioning itself, deciding the desired trajectory and executing the desired motion. There is lots of research in the area of unmanned ground vehicles within the past couple of decades. The reason of increasing in this new-age area is directly related to the advancement of the computing and recognizing technologies. Recently, with the incredible development in the digital world, sensors and computers can be able to achieve to give more accurate and more stable information about the work space of the robots. Moreover, these developments enable that more complicated and involved algorithms, which are prepared to be created an autonomous vehicle, are able to be run on the faster computers and larger memory. The improvements in these fields has fired up the intelligent ground vehicle research, and today unmanned autonomous space, air, land, underwater and sea vehicles are being rapidly modeled, constructed and used. In the autonomous vehicle research area, there are many research and application branches created in order to make simpler and safer the human life. The reasons of making the vehicles autonomous may be classified in four main groups: First is to reduce the risk of human life and injury accidents in hazardous areas, second is to access the location human cannot reach, the third is to relieve the human operators from the boring and repetitious tasks, and the last one is to obtain the exact location of the vehicle which gives the researchers to have the increased precision of navigation.

Therefore, unmanned ground robot vehicles are increasingly used for the applications in military, industry and service robotics area particularly when autonomous motion capabilities are required. The common main task for these vehicles is to track a reference trajectory. In order to achieve this, it should generate an appropriate desired trajectory according to the conditions, first and then run the controller that generates the required commands for completing the task.

1.2 Objectives of the Thesis

In this thesis study, the subject of autonomous ground vehicles are studied. In addition to ground wheel interaction, trajectory tracking control objective for these vehicles are targeted. The studies are focused for the applications conducted in indoor and outdoor environments. The indoor research studies are achieved by the opportunities of the Mechatronics Laboratory of Mechanical Engineering Department of Middle East Technical University, Ankara, Turkey. The studies are performed by using an autonomously driven small differential drive mobile robot on which plenty of sensors are mounted. The experiments are done on a specially constructed surface. The outdoor field studies are conducted in the Robotics Institute of Carnegie Mellon University, Pittsburgh, PA, USA. An autonomous orchard vehicle is used for these research activities. The vehicle is a typical four wheeled electrical vehicle. It is suited with number of sensors that are used for sensing, recognition, computation and communication. All the experiments are conducted in an experimental orchard located in the Robot City area of Carnegie Mellon University. The details of the indoor and outdoor studies conducted and the objectives of these studies can be briefly summarized as follows:

In order to increase the performance of localization, navigation and trajectory tracking control of a mobile robot, wheel forces resisting the motion needs to be studied. The first part of the study is related to investigation of wheel-ground interaction of a differentially driven mobile robot. In this part of the study, a differential mobile robot is modeled in a way that wheel forces (traction, rolling and lateral) are included in the overall robot dynamics. A lateral wheel force model is introduced in the mathematical model of the system along with traction and rolling forces. An estimation procedure for parameters of wheel forces is proposed. Together with the experiments simulation studies are conducted to investigate the performance of different models including traction force alone, traction and rolling forces and finally traction,

rolling and lateral forces altogether.

Mobile robots are effectively used for different applications in large number of areas. During these applications, the accuracy and performance of the mobile robot are very important. In order to satisfy the accuracy and performance of trajectory tracking control, localization and navigation, the external effects is needed to be included into the overall system like inclination information of the surface where mobile robot moves. In the second part of the study, wheeled mobile robot system is modeled in a way that in addition to wheel forces (traction, rolling and lateral); inclination effects of the terrain are included into the overall system dynamics. It is proposed and introduced to the system model that the normal forces, which the ground applies to the wheels, are affected by the change of mobile robot's orientation in an inclined surface. The overall modeling structure is validated by the results of experiment and simulation works.

In mobile robotics research area, trajectory tracking and path following are the valuable research subjects. The research results obtained in this field has shown that tracking a reference trajectory according to the constraints related to the mobile robot, environment and the task can be accomplished by having a good modeling and control procedures. The mobile robot may be well-designed and well-constructed and it may be decorated with efficient sensors. However, if the modeling issues that are developed according to the task defined does not meet the requirements and does not reflect the real conditions about the working environment, the task may not be achieved. The working environment including the terrain is one of the challenging point of trajectory tracking for a mobile robot. Different surface types create different working behavior for the mobile robot due to changing slippage characteristics that affect the wheel forces. In order to investigate the surface change and slippage detection, a methodology is constructed as the third part of the study. A two-wheeled differential mobile robot is used to illustrate the performance of the proposed structure.

Nowadays most of the areas like agriculture needs autonomous solutions. For instance in the agriculture world including cropping, seeding, cleaning, harvesting etc. are requiring some precision and automatic farming techniques. It is obvious that the motion of an autonomous vehicle in an working area is limited especially due to obstacles. Moreover its motion is restricted because of the surface whose characteristics are uncertain. This means that not only longitudinal but also lateral motion of the vehicle is important for the autonomous drive since it is an objective that there should always be success of trajectory tracking with minimum

trajectory errors in the applications where autonomous vehicles are used. The autonomous solutions for different missions performed in different terrains need more attention for the long distance autonomous drives as well. In order to bring new perspectives and new solutions, a desired trajectory generator is developed so as to perform autonomous drive by using an autonomous vehicle. Car-like robot approach is followed in order to develop a vehicle motion model. A model based controller strategy is focused for developing the control strategy to control the longitudinal velocity and steering angle of the vehicle. The methodologies and approaches proposed are adapted into an autonomous orchard vehicle as a field study. In this field study, the real-time position feedback is taken from a high accuracy positioning system (it may be called as differential or real time-kinematic (RTK) GPS. Another field study, which is related to the subject of trajectory tracking control of an autonomous ground vehicle is conducted by using the same autonomous orchard vehicle. In this field study, the objective is to develop an autonomous guidance of rows of trees and autonomous desired trajectory tracking in real-time orchard applications. In other words, the trajectory tracking control procedure which is proposed in this study is tested in the field for two different applications. In the first application, the procedure is implemented into a autonomous vehicle which has a RTK-GPS. The positioning feedback is taken from this high accuracy positioning system. In the second application, the methodology proposed is adapted in an autonomous orchard vehicle which does not have a RTK-GPS, has a laser scanner range finder. In this part of the study, the RTK-GPS is replaced with a laser scanning system. Within this study, new approaches for detecting the trees, rows (lines) of trees and creating desired trajectory that lies on the center line between two consecutive tree lines are proposed. In order to track the desired trajectory, the control strategy introduced is combined with the new guidance system which is composed of two detectors called as high and low level row detectors.

As stated above, the methodologies related to trajectory tracking control objectives are constructed without using slip information. This causes trajectory tracking errors especially in snowy, muddy and inclined surfaces. In order to make some improvements for trajectory tracking control of an autonomous vehicle, a procedure about estimating and including the effects of slippage into the overall system model is developed. In this study, the system model which is created by using the basis of car-like robot approach is included with the slippage information obtained by the slippage estimator proposed. Appropriate controllers for steering and driving systems are developed by using the methodology of backstepping controller as

well. The experimental works related to this studies are conducted by using an autonomous orchard vehicle and tested in an orchard environment as the third field study. Within this field study, the procedures proposed are implemented into the orchard vehicle. A high accuracy positioning system is used in order to estimate the slip velocities of the wheels in longitudinal and lateral directions. This estimation procedure is also performed by using the position information that is obtained by the usage of odometer and steering encoder of the vehicle. The experiments are performed not only on the flat surface but also on the inclined surface.

1.3 Contributions of the Thesis

Most of the mobile robots are used to achieve objectives including tracking a desired trajectory and following a predefined path in different types of terrains that have different surface characteristics. A mobile robot can perform a single task over different surfaces if the tracking performance and accuracy are not essential. However if the tracking performance is the main objective, owing to changing the characteristics of wheel-ground interaction, a single set of controller parameters or an unique equation of motion might be easily failing to guarantee a desired performance and accuracy. The interaction occurred between the wheels and ground can be investigated and combined with the system model so that the performance of the mobile robot would be enhanced. This modeling approach related to wheel-ground interaction can also be incorporated into the motion controller. To put it another way, if the modeling issues include the information about surface characteristics and wheel-ground interaction, and the controllers are updated according to this online information, it is possible to expect a better trajectory tracking performance of a mobile robot. The basic motion models constructed for the mobile robot applications use the simple assumptions which are ideal transmission, ideal rolling, no slippage, no lost of traction control, no external wheel forces, no surface change behavior, no disturbance, etc. In reality, all these assumptions are unusable since a mobile robot is faced with these facts. It is addressed that a new modeling study that includes the reality of the working environment of a mobile robot enables to accomplish a better tracking performance.

In this thesis study, modeling studies for a two wheeled differential drive mobile robot and a steerable four-wheeled robot vehicle are conducted. The following contributions are made in order to achieve better and accurate trajectory tracking:

- It is addressed that a better tracking performance for a differential drive mobile robot can be achieved by developing a procedure including the effects of external wheel forces, which are traction, rolling and lateral. A new modeling strategy for representing lateral wheel force is developed. An estimation procedure to estimate the parameters of external wheel forces is also introduced.

- A new modeling perspective that is related to show the effects of inclinations of the surface is developed and combined with the system model of the differential drive mobile robot. This procedure is also included with the effects of wheel forces.

- In addition to investigating the effects of external wheel forces and inclinations, a modeling approach to detect the surface changes via using slippage information is proposed. The surface change detection study is also conducted by using the information of current that is drawn by the actuated motors of the differential mobile robot.

- In order to get a better trajectory tracking performance and accuracy for a steerable four-wheeled mobile robot, a modeling study that includes a desired trajectory generator and trajectory tracking controller is introduced.

- It is focused that the admissible region of speed of steering angle change that are allowed by the steering system and steering actuator is taken into consideration while the desired trajectory is generated.

- Slippage is defined via the slip velocities of front and rear wheels of the mobile robot. A slippage estimation procedure is proposed and combined into the system model. Heading speed and steering angle of the four-wheeled mobile robot are commanded by the controller that takes into account the slippage information.

All the modeling studies mentioned above are tested by using the experimental platforms. A differential drive mobile robot, which has two wheels driven by DC motors and two spherical wheels used for stability, is used to perform the experiments related to detect the wheel-ground interactions of a differential drive mobile robot in indoor environment. This platform is suited with DC motors and their motion controllers, a six-axis IMU (inertial measurement unit), current sensors, tilt sensor and an embedded PC having a number of data acquisition interface boards. The experiments are conducted in a surface which is specially constructed and gives ability to be inclined for doing the tests aimed. The experimental surface also gives

ability to be covered with different materials. In order to detect the surface changes, the surface is covered with four different surface materials. A top-surface-camera is also used as a ground truth information. In order to conduct the experiments related to getting a better trajectory tracking performance for a steerable four-wheeled mobile robot, a mobile robot vehicle of which front wheels are steerable and rear wheels are actuated is used. The mobile robot is equipped with steering encoder, odometer, laser scanner, IMU, tilt sensor and RTK-GPS. Number of experiments related to achieve desired trajectory tracking are conducted in different types of terrains; smooth and dry, rough and dry, mixed and dry, smooth and snowy, rough and snowy, mixed and snowy, smooth and muddy, rough and muddy, and mixed and muddy. Moreover, the mobile robot is tested in a terrain which is rough, snowy and inclined.

1.4 Outline of the Thesis

In the introduction part, the brief information of the studies that are carried out within the scope of thesis are given. The detailed presentations of each studies can be found in the following chapters: Next chapter is related to the effects of wheel forces that resist mobile robot's motion. The detailed literature survey, mathematical modeling, simulation and experimental studies are presented in this chapter. In chapter 3, inclination effects to mobile robot's motion is given. The simulation studies are validated by the results of experimental studies. Chapter 4 is about the surface changes by using slip transitions. The literature survey, modeling and experimental studies are represented in detail. Chapter 5 is designed to show the modeling issue of trajectory tracking control of a mobile robot. A new perspective for developing a controller for achieving better trajectory tracking objective is introduced in this chapter. Chapter 6 is related to the improved trajectory tracking control of a mobile robot with including slip estimation procedure. The modeling issue given in chapter 5 is introduced with slippage term in this chapter. The experimental studies related to chapter 5 and 6 are illustrated in chapters 7, 8 and 9. The first field study is given in chapter 7. This is about trajectory tracking control of a mobile robot using high accuracy positioning feedback. The results of long distance desired trajectory tracking tasks, which are achieved by using a four wheeled autonomous ground vehicle, are shown in detail in this chapter. Chapter 8 is about the second field study. In this study, everything including models, controller procedure proposed, experimental mobile robot and experimental field, is same except that the high accuracy positioning feedback system is

replaced with a laser scanning range finder. In chapter 9, the system given in chapters 5, 6, 7, and 8 is introduced with a slippage estimation procedure. In order to achieve a better desired trajectory tracking, estimated slippage is included into the overall system. The whole system is tested in the same experimental area and the results are illustrated in chapter 9. A general conclusion about the research in this thesis study is made in chapter 10. Future works that can be ignited by the results of this thesis are listed in chapter 10 as well. The literature survey can be found after this chapter.

CHAPTER 2

EFFECTS OF WHEEL FORCES THAT RESIST MOBILE ROBOT'S MOTION

2.1 Introduction

Wheeled mobile robots are used to accomplish tasks involving trajectory tracking and path following on various types of terrain. Hence it is possible that a mobile robot will traverse over different surfaces during a single task. If the tracking performance is essential, due to changing wheel-ground interaction characteristics, a single set of controller parameters can fail to guarantee a desired performance. In order to improve the performance of a ground vehicle, the wheel-ground interaction can be incorporated into the motion controller. In other words, if a robot can use a surface model where model parameters are estimated online by the robot and motion controller is updated accordingly, a better tracking performance can be expected in comparison to the case where a fixed controller is used. Simple robot models generally start with a set of idealistic assumptions such as, there is ideal transmission and rolling, and yet there is no slip. However, in a realistic application these assumptions are doomed to fail. As a result, a broader model that is better represents the real physics of the process is necessary where the model includes traction, rolling and lateral forces.

2.2 Related Studies

In [Motte and Campion, 2000], external effects such as wheel slippage are included in the dynamic model. Traction force is modeled as a dependant force. While designing a feedback control system, this effect is taken into account. In [Ward and Iagnemma, 2008], traction and

rolling forces are modeled as a function of relative and forward velocity of the wheel. The study proposes a model-based approach in order to estimate the effects of wheel forces and detect immobilized conditions of a mobile robot. In [Tian et al., 2009], mathematical models for lateral and longitudinal forces are proposed. These forces are adapted into the overall system model. In [Sidek and Sarkar, 2008b], in order to improve the navigation performance of a mobile robot operating in an unstructured terrain, a procedure including wheel forces and slippage is constructed. In [Caracciolo et al., 1999], traction and lateral forces are modeled. These forces are coupled with the dynamic model of the mobile robot. A model based nonlinear controller is designed for tracking a desired trajectory. In [Li et al., 2006], longitudinal and lateral tire/road friction models are constructed and integrated with the whole vehicle system for monitoring the vehicle motion control. In [Yi et al., 2007], traction/braking and longitudinal forces including a friction model are developed for achieving adaptive trajectory tracking control of a skid steering mobile robot. In [Balakrishna and Ghosal, 1995], longitudinal force is considered as a tire force and included into the system model. In [Williams et al., 2002], wheel ground interaction is modeled and adapted into the system dynamics. In [Wong, 2001], it is proposed that if a mobile robot has non-negligible lateral force and this force doesn't give effect in yaw axis, it should be modeled, estimated and added to the dynamic model. In [Yun, 1995], control of mobile robot subjected to rolling contacts is studied. Rolling contacts are modeled and used in the control system. In [Ray, 2008], a methodology is constructed for autonomous terrain parameter estimation for wheeled vehicles. In this study, resistive forces are modeled by using sensor inputs, which are accelerometer, rate gyro, encoder, motor current drawn and ground speed. Then physical parameters of the surface are estimated. In [Iagnemma and Dubowsky, 2002], on-line surface parameter estimation method is proposed for high speed rough terrain autonomous vehicle navigation. Load on the robot vehicle and torque required for the desired motion are modeled. These models have dependent parameters to be estimated. The estimation procedure constructed is used to estimate the surface parameters like cohesion, internal friction angle, and drawbar pull force. Then a simulation study including parameters estimated is conducted. In [Ojeda et al., 2006a], a method related to terrain characterization, classification and implementation for motion control of a mobile robot is developed. Types of the terrain, which can be gravel, grass, sand, pavement, or dirt, are classified by using a complex terrain mechanics approach. The parameters of the models showing wheel terrain interaction are estimated. The methodology including the parameters estimated are simulated and compared with the experimental results. In [Song et al., 2004],

an identification method is proposed for the soil model parameters in an unmanned ground vehicle application. Interaction dynamics between surface and track is modeled by using terrain mechanics approach. Soil parameters, which are cohesion and internal friction angle, are estimated. In [de Wit, 1999], dynamic tire friction force model is proposed for vehicle traction control. The models are constructed by using magic formula approach. In [Han et al., 2008], wheel surface friction model is developed for monitoring tire pressure. Wheel forces are modeled by using LuGre modeling procedure and estimated by using a nonlinear observer.

2.3 Aim of the Study Related to Investigation of Effects of Wheel Forces Resisting Motion

As seen above, in the literature there are studies related to estimation procedures of external wheel forces and adaptation of these estimated forces into the system model. These estimation procedures are not enough to adapt the estimation systems to a differentially driven mobile robot. Especially, the approaches like terrain mechanics, Magic Formula approach, LuGre model, etc., are hard to implement into a differential small robot. Not only developing a motion model including wheel forces for a differential mobile robot but also implementation of the developed model into a real system has not been clearly improved yet. In this part of the study, a dynamic model including external wheel forces of a two wheeled mobile robot is introduced. Wheel and body forces are coupled with this model. Three wheel forces, which are traction, rolling and lateral forces, resisting the motion of mobile robot are considered. In order to model traction and rolling wheel forces, the related studies summarized in the literature section are followed. A new perspective for the lateral force model is introduced. An estimation procedure used to obtain the parameters of the wheel forces is proposed. The easy of use and adaptation of this approach are presented. Experimental studies are conducted by using a wheeled mobile robot on a surface specially constructed for this study. The test ground is made up of homogeneous rough surface. A camera is located at top of the constructed surface. Mobile robot is commanded to have a circular motion. During this motion, information coming from camera and sensors located on the robot is taken. Using these data, modal parameters of the wheel forces are estimated. The constructed model including the wheel forces and parameters estimated is tested to show the performance of the proposed method.

The outline of this chapter is as follows: the first part presents the robot model along with traction, rolling and lateral force models; part 2 introduces the experimental setup used in this work; following section presents the experimental process and parameter estimation procedure; finally before concluding the chapter part 4 illustrates the simulation results and compares experimental data with the simulation data.

2.4 Mathematical Modeling

Experiments as a part of this study is conducted on a two wheeled, differentially driven mobile robot. Hence, the simulation model is derived to model this robot including the effects of wheel and body forces where the following assumptions are made:

1. Mobile robot is considered as rigid.
2. It is moving on a horizontal flat plane without any slope.
3. Maximum longitudinal velocity of the mobile robot is limited to 1 m/sec.
4. In addition to body forces, longitudinal, rolling and lateral wheel forces acting on driving wheels are also taken into account.

2.4.1 Kinematic Modeling

The geometric model given in Figure 2.1 is used to derive the kinematic and dynamic models of the robot. G(X,Y) and g(x,y) indicate the fixed and body reference frames respectively. Body reference frame is located at the turning center of the robot. Longitudinal velocity of the robot in body reference frame is V_x and lateral velocity is V_y. Length and width of the robot are 2a and 2b. Longitudinal, lateral and angular velocities of the mobile robot are presented in frame g. The absolute velocities in frame G are given in equations given below:

$$\dot{X} = \dot{x}cos(\psi) - \dot{y}sin(\psi) \tag{2.1}$$

$$\dot{Y} = \dot{x}sin(\psi) + \dot{y}cos(\psi) \tag{2.2}$$

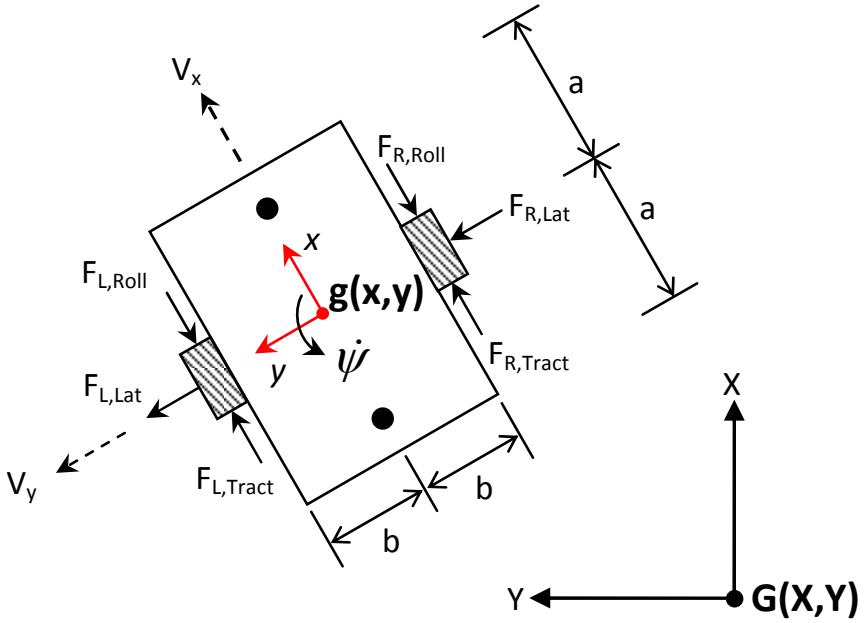

Figure 2.1: Free body diagram of the mobile robot

2.4.2 Dynamic Modeling and Equations of Motion

Forces acting on the mobile robot are gravitational, body and wheel forces. Combined wheel force is made up of traction, rolling and lateral forces as shown in Figure 2.1. Mobile robot used in this study has two driven and two spherical wheels. The spherical wheels, shown in Figure 2.2, are assumed that they have point contact with ground, they can spin freely and thus their effect on the overall robot dynamics is neglected.

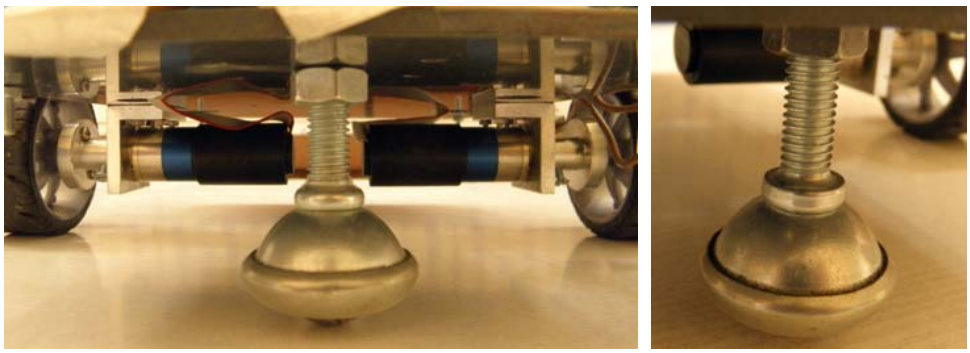

Figure 2.2: Spherical wheel used in the mobile robot

In Figure 2.3, normal and body forces are shown. During construction, the center of mass of the mobile robot is aligned with its turning center. W is the weight of the robot and h is the distance between the center of mass and the ground. N_R and N_L indicate the normal forces on right and left wheels, respectively.

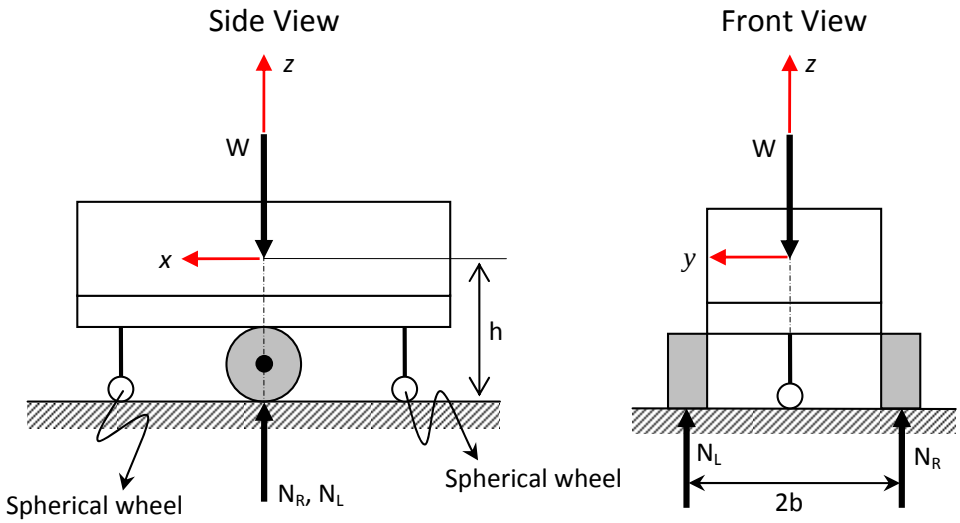

Figure 2.3: Free body diagram indicating normal and body forces of the mobile robot

For a mobile robot with a mass of m and inertia I, the equations of motion can be written in frame g(x,y) (i.e. along x- and y-axis) as follows:

$$\dot{V}_x m = F_{R,Trac} + F_{L,Trac} - F_{R,Roll} - F_{L,Roll} + F_{x,dist} \tag{2.3}$$

$$\dot{V}_y m = F_{R,Lat} + F_{L,Lat} + F_{y,dist} \tag{2.4}$$

where $F_{dist,x}$ and $F_{dist,y}$ are the disturbance forces in x- and y-directions, respectively. The angular acceleration of the robot can be defined as:

$$I\ddot{\psi} = (F_{R,Trac} - F_{R,Roll} - F_{L,Trac} + F_{L,Roll})b \tag{2.5}$$

The wheeled mobile robot system introduced above can be described by the following form. Considering that the system having n dimensional space is described as given in Equation 2.6. [Salerno and Angeles, 2007], [Caracciolo et al., 1999], [Yun and Yamamoto, 1997],

[Yun and Yamamoto, 1993], [Tian et al., 2009].

$$M(q)\ddot{q} + C(q, \dot{q}) = B(q)\tau + A^T(q)\lambda \tag{2.6}$$

where $q \epsilon R^{nx1}$ is the vector of generalized coordinates presented as $q = [x, y, \psi, \omega_1, \omega_2, \dot{\omega_1}, \dot{\omega_2}]$. $\dot{q}$ is the vector of linear and angular velocities along the generalized coordinates. M is the mass and inertia matrix of the system. Centrifugal and coriolis effects are taken into consideration in C. B is input transformation matrix where τ stands for input vector. Finally, A^T indicates matrix of constraint forces and λ represents the Lagrange multiplier.

2.4.3 Traction Force

In literature [Ward and Iagnemma, 2008], [Li et al., 2006] and [Salerno and Angeles, 2007], different traction force models are proposed. These models can be classified as empirical and analytical methods. The empirical approaches employ curve-fitting techniques. Such an approach may be good for obtaining the steady state characteristics but it falls short in predicting and reflecting external effects such as uneven surface condition, tire pressure fluctuations, surface inclination, etc. Analytical models however, if properly derived can include any effect that can be expressed by mathematical models including the relationship between wheel and terrain.

In [Li et al., 2006], Piecewise Linear, Burckhardt and Rill models are given. A Piecewise Linear model, being a rough estimation, is the simplest approach for developing an empirical traction force model. Burckhardt model is a friction model approach for modeling of traction force. The model contains some dependent parameters which can be determined based on experimental data. Rill model is another empirical model that is based on steady state characteristics of the system.

In [Ward and Iagnemma, 2008], a unified explicitly differentiable analytical model is proposed. Most of the traction force approaches in the literature are defined as a function of slip; however, traction force is defined as a function of relative speed of wheels. The simplified model of the traction force, proposed in [Ward and Iagnemma, 2008], is introduced as given in Equation 2.7. Note that traction force representation is continuously differentiable.

$$F_{i,Trac} = N_i(sign(V_{i,Rel})P_{i,1}(1 - exp(-P_{i,3}|V_{Rel}|)) + P_{i,2}V_{i,Rel}) \tag{2.7}$$

where $V_{i,Rel}$ are wheel velocities relative to the surface on which mobile robot moves. N_i is the normal forces between wheel and ground. $P_{i,1}$, $P_{i,2}$, and $P_{i,3}$ are wheel-surface parameters ($i = R, L$). Wheel relative velocity can be defined as:

$$V_{i,Rel} = r\omega_i - V_{i,wh} \tag{2.8}$$

where $V_{i,wh}$ ($i = R, L$) and ω are forward and angular velocities, and r is the radius of the wheels. Forward velocities of right and left wheels can be defined as a function of forward velocity of the mobile robot:

$$V_{R,wh} = V_x - b\dot{\psi} \tag{2.9}$$

$$V_{L,wh} = V_x + b\dot{\psi} \tag{2.10}$$

2.4.4 Rolling Force

[Ward and Iagnemma, 2008], [Wong, 2001], [Pacejka, 2006] and [Bekker, 1956] propose the rolling force as a function of velocity dependant forces. They offer a continuously differentiable model which has a similar form with the approach given in Equation 2.7. The proposed model [Ward and Iagnemma, 2008] is given as:

$$F_{i,Roll} = -sign(V_{i,wh})N_i(H_{i,1}(1 - exp(-H_{i,3}|V_{i,wh}|)) + H_{i,2}|V_{i,wh}|) \tag{2.11}$$

where $H_{i,j}$ are wheel-surface interaction parameters ($i = R, L$ and $j = 1, 2, 3$).

2.4.5 Lateral Force

In [Ray, 2008], [Iagnemma and Dubowsky, 2002] and [Ojeda et al., 2006a], ideal model approach is used for developing the dynamic models of the mobile robot. It is assumed that there is no lateral and slip force reacting. In [Tian et al., 2009], the wheeled mobile robot

is modeled with longitudinal and lateral force components. It is stated that in order to improve the maneuverability of a mobile robot in a real environment, lateral force should be included in the model. Considering lateral force representation given in [Tian et al., 2009], the essential information about the surface on which mobile robot moves cannot be obtained. In [Wong, 2001], lateral force is represented by using Magic formula. This approach is useful for simulating the relationship between wheel forces and slip angle. It is shown that Magic formula is very useful for generating wheel behavior characteristics which are closely match measured data ([Ward and Iagnemma, 2008], [Wong, 2001]) and is a rewarding approach for lateral force modeling. However, Magic formula contains lots of parameters and all of them should be estimated. Estimation process is not an easy work. Moreover usage of Magic formula in order to develop lateral force model may not be applicable to a small mobile robot, since it is developed for the large scale vehicles.

In this study a unified and simplified lateral force model is proposed and given in Equation 2.12. It is explicitly differentiable and it can meet the requirements of the modeling procedure for the mobile robot's motion. It contains only three variables which should be estimated.

$$F_{Lat} = N[sign(\alpha)L_1(1 - exp(-L_3|\alpha|)) + L_2|\alpha|] \tag{2.12}$$

where α represents side slip angle which is defined as a function of forward and lateral velocities of the robot. It can be represented in the following form [Wong, 2001]:

$$tan\alpha = \frac{V_y}{V_x} \tag{2.13}$$

Directions of V_x and V_y are shown in Figure 2.1.

2.5 Experimental Set-Up

Experimental setup contains two main parts. These are a wheeled mobile robot and a surface having a camera attached to top of it.

2.5.1 Wheeled Mobile Robot

In order to show the performance of the proposed method a mobile robot platform shown in Figure 2.4 is constructed. It has two driven wheels which can be separately controlled. These wheels are driven by using two Faulhaber - DC motors (Figure 2.5-a) that work in the range of $0 - 24V$. The DC motors have gearhead having ratio of $1 : 14$. They have also encoders having a resolution of 512 pulses/revolution. They are controlled by using motion controllers, Faulhaber MCDC-3003/06-S (Figure 2.5-a). A six axis inertial measurement unit (IMU), Microstrain (Figure 2.5-c) , is located at the turning center of the robot. Current sensors are also installed to the system to control the torque applied to the driving motors. In order to perform computation, control and communication purposes, an embedded $PC/104$, DiamondSystems (Figure 2.5-b) , is located on the robot. In order to get the encoder data, a quadrature encoder input PC/104 data module (Figure 2.6-a) is mounted into the embedded PC. Moreover a 16-Bit Analog I/O PC/104 module, DMM-32X-AT (Figure 2.6-b), is added to the embedded system to handle the input/outputs. The communication between the embedded PC and the main computer is achieved by using wireless Ethernet. All the computational and control objectives are done via xPC-Target toolbox of Matlab / Simulink.

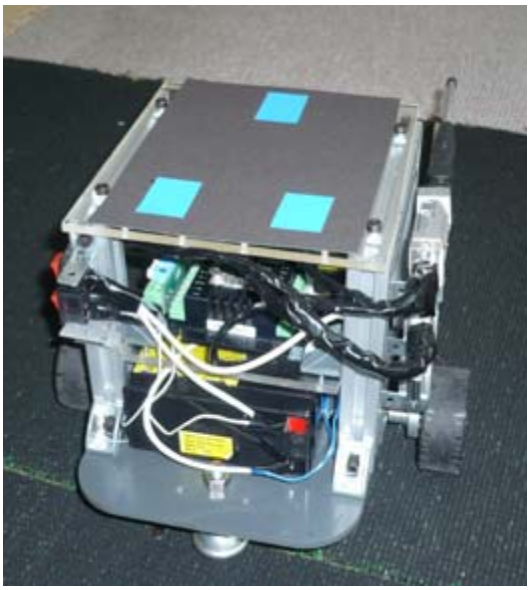

Figure 2.4: Two wheeled differentially driven mobile robot

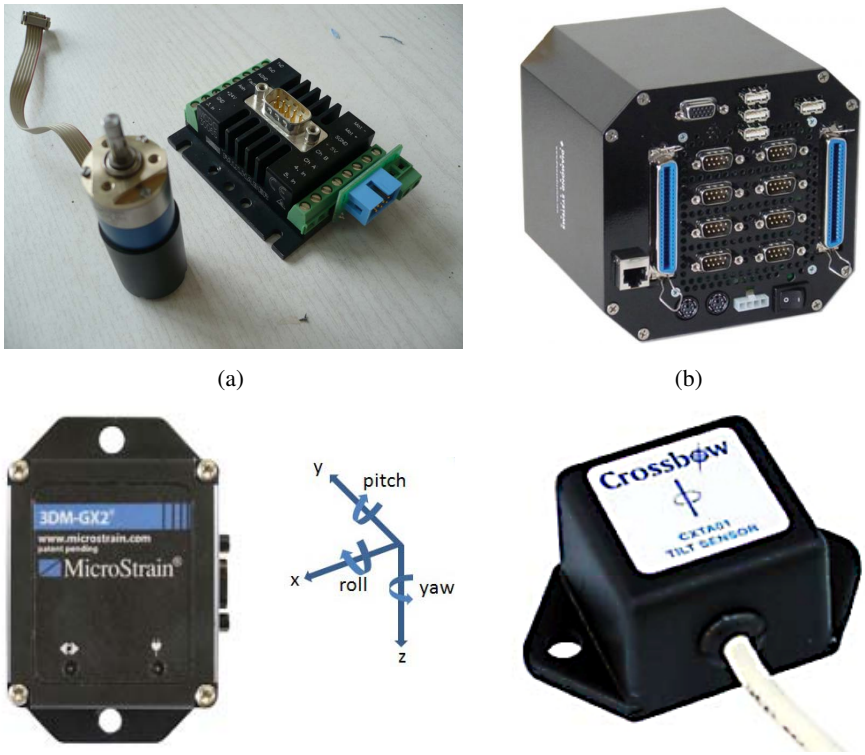

Figure 2.5: (a) DC motor and motion controller, (b) Embedded PC, (c) 6-Axis IMU, (d) Tilt sensor

2.5.2 Surface Set-Up

Test surface having a rectangular shape (1650 mm x 1650 mm) is constructed for performing the experiments (see Figure 2.7). It is covered with special material having a geometric profile as shown in Figure 2.7. Geometric profile has a rhomboidal shape (4 mm x 4 mm). Connections of these shapes create edges having 0.4 mm of thickness and 1 mm of depth. Such characteristics are preferred to create a homogenous-rough surface. A high resolution camera that works at 30 fps is attached to top of the surface. The camera processing that runs in real-time is performed by using an interface prepared in *C#* environment. There are three colored points on top of the mobile robot. They can be followed by the camera and used to get position and orientation information of the mobile robot. For observing the inclination of the surface, a two-axis inclination sensor, Crossbow (Figure 2.5-d) , is also used.

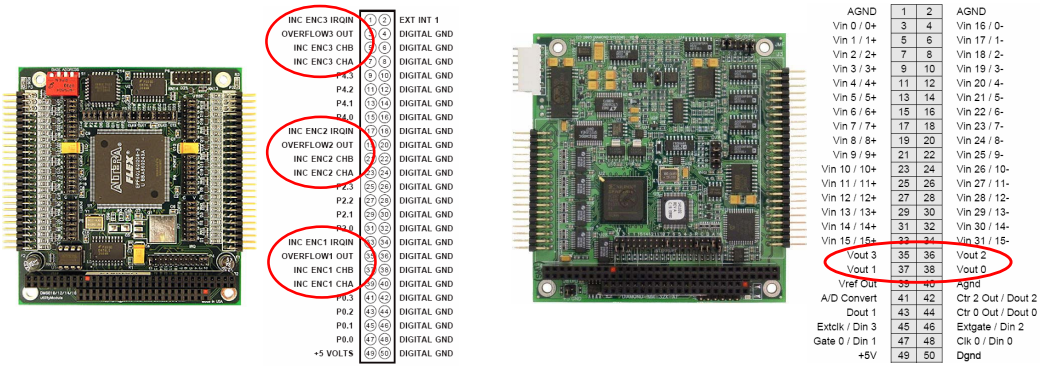

(a) (b)

Figure 2.6: (a) Quadrature encoder input PC/104 data module, (b) 16-Bit Analog I/O PC/104 data module

2.5.3 Velocity and Acceleration Estimation

The mobile robot is commanded to track a circular path. Position data coming from camera is stored while robot is moving. In order to find velocity and acceleration profiles, a function is fitted to the position data taken from camera in each X and Y directions separately as given in Figure 2.8. The function is selected to characterize a circular motion for both X and Y directions and given as follows:

$$f_P(z) = a_1 sin(b_1 z + c_1) + a_2 sin(b_2 z + c_2) \tag{2.14}$$

The curve fitting parameters of X and Y directions are given in Table 2.1. The curve fitting processes are performed by using curve fitting toolbox of Matlab.

Table 2.1: Curve fitting parameters obtained to develop the function in X and Y directions

	X-direction	Y-direction
a_1	385.3	645.504
b_1	0.02095	0.0004604
c_1	-3.351	0.7895
a_2	2389	480.2
b_2	0.0004103	0.01823
c_2	-0.02851	-1.402

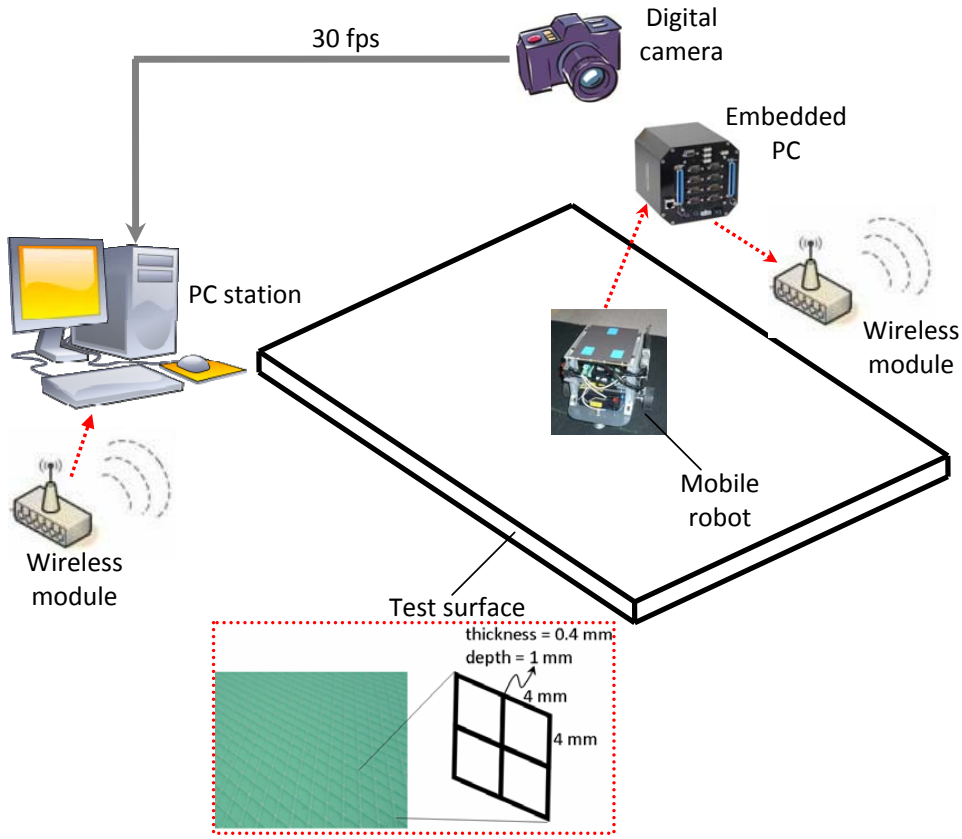

Figure 2.7: Experimental set-up involving surface constructed, mobile robot and camera attached at the top of the surface

The function given in Equation 2.14 specifies the motion of mobile robot. Since, it is continuously differentiable; the function of velocity can be obtained when it is differentiated as given in Equation 2.15. The velocity function can also be differentiated in order to obtain the function of acceleration (Equation 2.16).

$$f_V(z) = a_1 b_1 cos(b_1 z + c_1) + a_2 b_2 sin(b_2 z + c_2) \tag{2.15}$$

$$f_A(z) = -a_1 b_1^2 cos(b_1 z + c_1) - a_2 b_2^2 sin(b_2 z + c_2) \tag{2.16}$$

The velocities and acceleration of mobile robot in X and Y directions can be obtained by using the velocity and acceleration functions expressed in Equations 2.15 and 2.16. In Figures 2.9 and 2.10, velocities and accelerations in X and Y directions are shown, respectively.

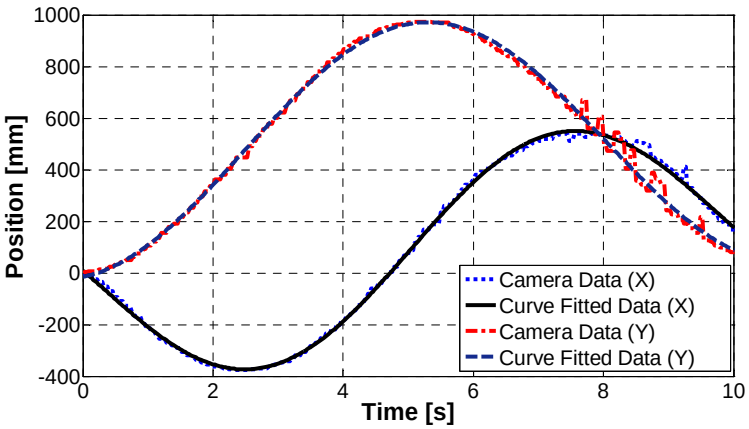

Figure 2.8: Position estimation in X and Y directions via curve fitting by using camera data as ground truth

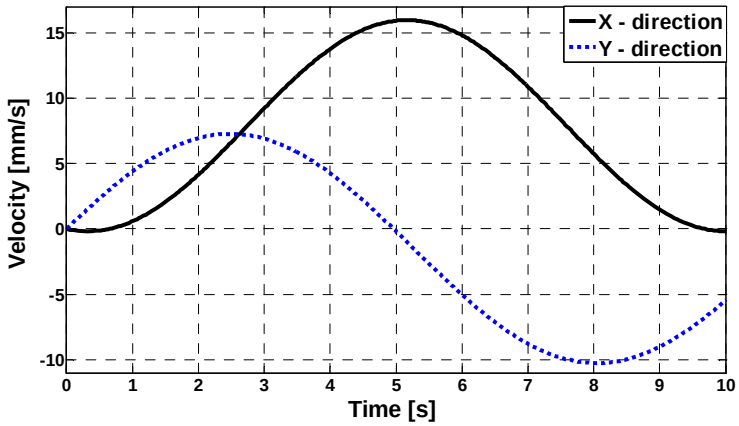

Figure 2.9: Velocities in X and Y directions

Angular velocities of right and left wheels during the circular motion are recorded and shown in Figure 2.11.

2.6 Parameter Estimation

Surface where mobile robot moves has a structured pattern as shown in Figure 2.7. Due to uneven structure of the surface, the robot is subjected to forces in both directions (i.e. longitudinal and lateral). As a result, the robot cannot be expected to complete a circular

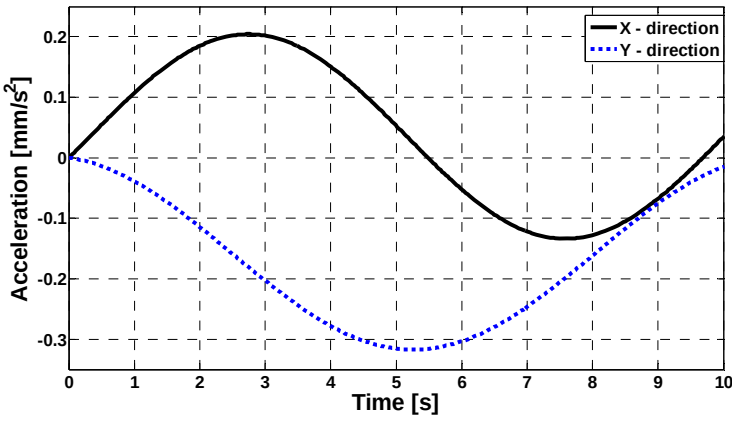

Figure 2.10: Accelerations in X and Y directions

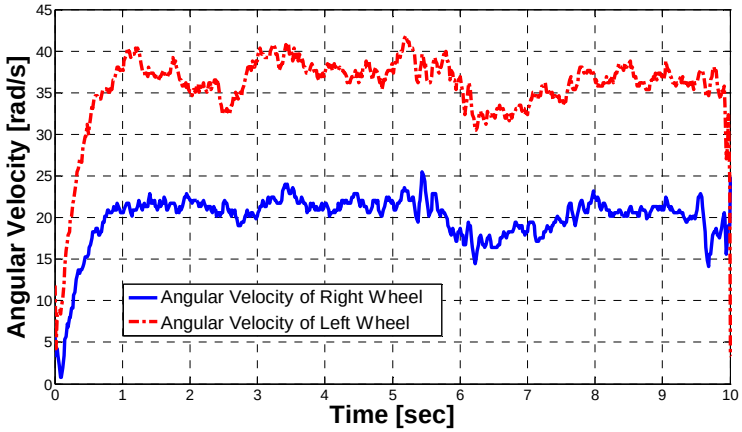

Figure 2.11: Angular velocities of the wheels

path using an open loop control scheme. In order to observe robot behavior on a circular path, following test repetitive experiments are conducted. In these experiments, the robot wheels are actuated with constant (but slightly different) velocities. The robot is run around the complete circles. Resulting paths recorded by the camera are given in Figure 2.12.

Observing the results given in Figure 2.12, it is evident that the mobile robot cannot follow a circular path due to the effects of wheel forces (traction, rolling and lateral) by using an open loop control scheme. This suggests that, in cases where external location fixes (such as GPS etc.) are not available, an improved dynamic model is essential for better motion tracking.

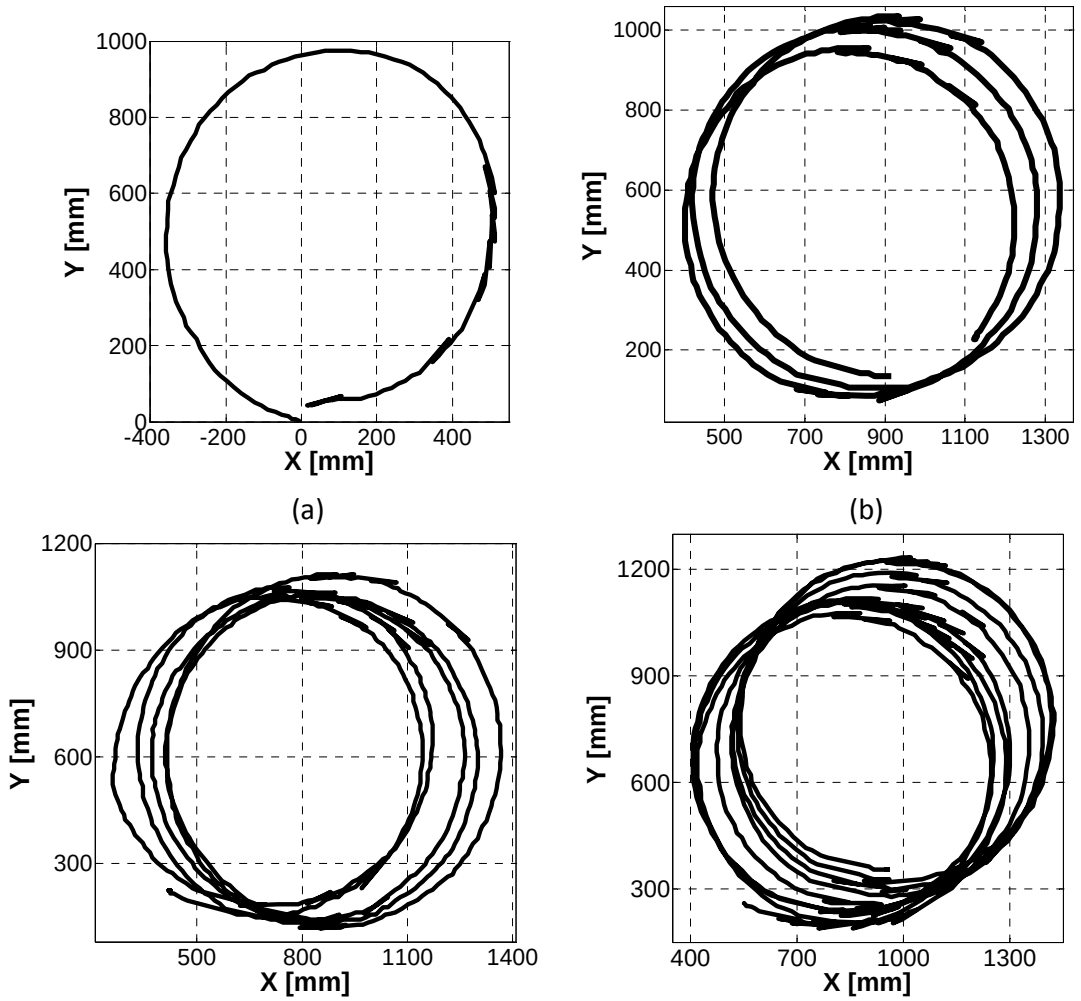

Figure 2.12: Paths formed by completing different number of circles: (a) 1, (b) 3, (c) 5, (d) 8 closed loops

2.6.1 Parameter Estimation Process of the External Forces and Simulation Studies

In the free body diagram of the system presented in Figure 2.1, there are three wheel forces including nine parameters for each wheel. The velocity and acceleration used in the parameter estimation process are estimated by using position information coming from camera (see Equations (2.14-2.16)). In addition to acceleration and velocity information, encoder and IMU data are also used. Angular velocities of each wheel are obtained by using encoders mounted to the shaft of the driving motors. Yaw rate of the mobile robot is taken from IMU.

Nonlinear least square method is used for parameter estimation, which is defined as:

$$minimize \sum_{i=1}^{m} J_i(u)^2 = \| J(u) \|^2 \tag{2.17}$$

where $J(u) = (J_1(u), J_2(u), ..., J_m(u))$. u is an input vector. There are methods for solving nonlinear least square problems. Some of them can be listed as: Newton's method, the steepest descent method, the Gauss-Newton method, the Levenberg-Marquardt method, Powell's Dog Leg method, trust region method and hybrid method, etc. Levenberg-Marquardt and trust regions are the mostly used methods. In this study, Matlab optimization toolbox "lsqnonlin" is used for estimating the parameters.

In order to estimate the parameters of the wheel forces proposed, number of experiments is conducted. The parameters of traction force obtained by using estimation process are given in Table 2.2. Minimum, maximum, mean and standard deviation values are listed in this table. Estimated values for rolling force are presented in Table 2.3. Table 2.4 shows the estimated parameters of lateral force's representation. The mean values of the estimated parameters are used in the simulation studies.

Table 2.2: Wheel parameters related to traction force

Parameters	Min	Mean	Max	Std. Dev.
$P_{1,1}$	0.0176	0.01871	0.0191	0.114
$P_{1,2}$	0.026	0.0288	0.0350	0.003
$P_{1,3}$	9.82 s/m	10 s/m	10.3 s/m	0.2646
$P_{2,1}$	0.010	0.01028	0.0112	8.32e-4
$P_{2,2}$	0.01288	0.01303	0.0141	0.001
$P_{2,3}$	48.1 s/m	48.69 s/m	50.67 s/m	0.2138

Table 2.3: Wheel parameters related to rolling force

Parameters	Min	Mean	Max	Std. Dev.
$H_{1,1}$	0.0281	0.0314	0.044	0.0117
$H_{1,2}$	0.0001 s/m	0.0015 s/m	0.0023 s/m	0.0011
$H_{1,3}$	20.01 s/m	23.32 s/m	25.53 s/m	0.1198
$H_{2,1}$	0.0012	0.018	0.0197	0.016
$H_{2,2}$	0.0001 s/m	0.0017 s/m	0.0019 s/m	0.0015
$H_{2,3}$	22.45 s/m	24.63 s/m	24.77 s/m	0.1124

Table 2.4: Wheel parameters related to lateral force

Parameters	Min	Mean	Max	Std. Dev.
$L_{1,1}$	0.065	0.086	0.097	0.0182
$L_{1,2}$	0.020	0.034	0.044	0.0125
$L_{1,3}$	39.35	40	40.60	0.1265
$L_{2,1}$	0.065	0.086	0.097	0.0182
$L_{2,2}$	0.020	0.034	0.044	0.0125
$L_{2,3}$	39.35	40	40.60	0.1265

2.7 Indoor Study-1: Experiment and Simulation Studies Related to Show the Effects of Wheel Forces to the Mobile Robot's Motion

In the estimation process, parameters of traction, rolling and lateral forces are obtained. These parameters are adopted into the system model. In the simulation studies, the mobile robot dynamic representation is simulated in Matlab/Simulink environment. The Simulink model of the system is shown in Figure 2.16. In the simulation process, three wheel forces, traction, rolling and lateral forces including estimated parameters are taken place in the dynamic model of the mobile robot using an open loop control scheme. In the same time the inputs are applied to the physical model in order to have a circular motion. The position of the mobile robot in X and Y directions is obtained. Then they are checked with the position information coming from the camera. The circular paths obtained from both simulation and experimental results are given in Figure 2.13. In the simulation and experiments, traction (T), traction and rolling (T+R), and traction, rolling and lateral (T+R+L) force combinations are tested on a circular motion to show the performance effects of the wheel forces. The performance of the system is evaluated according to the X and Y directional errors in the complete circular motion (Figures 2.14 and 2.15).

As seen in Figures 2.14 and 2.15, the error values in X and Y directions are decreased by using the model having T+R+L force combination.

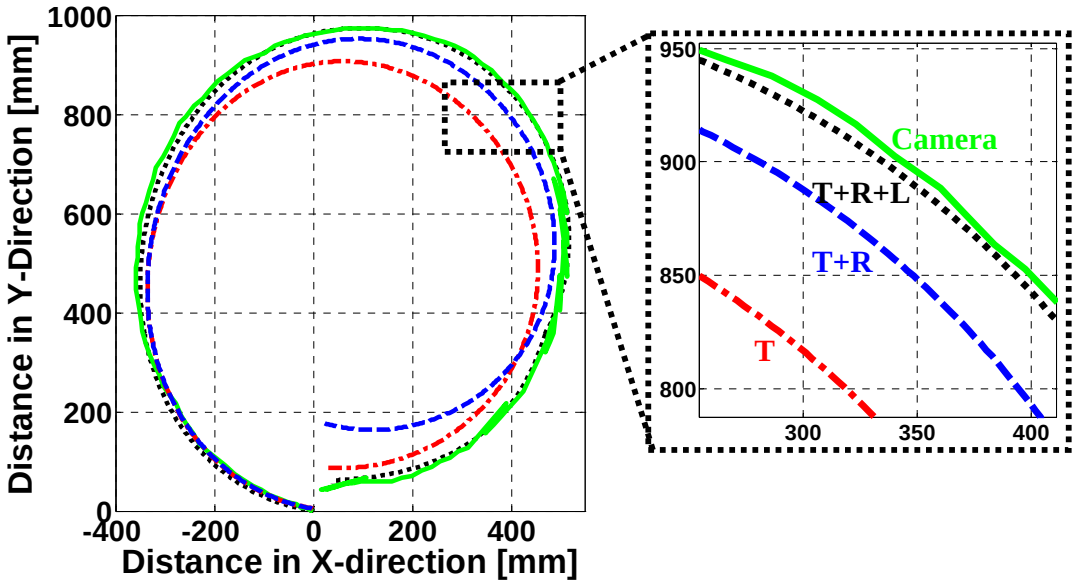

Figure 2.13: Position information obtained by simulations and camera

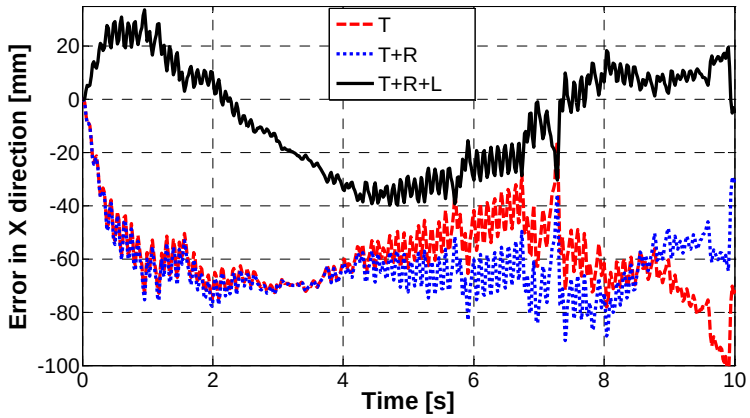

Figure 2.14: Position errors in X direction

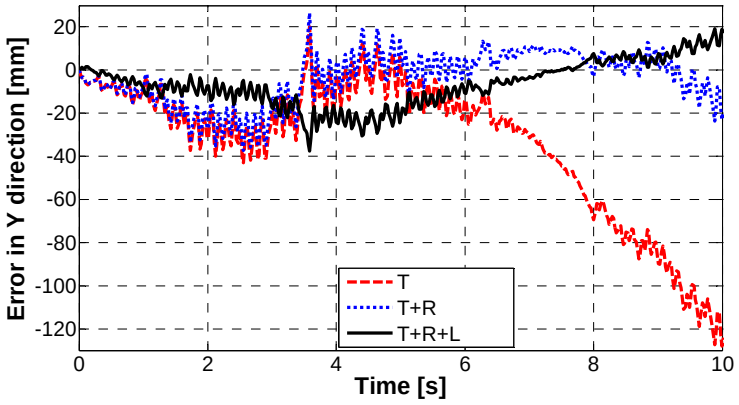

Figure 2.15: Position errors in Y direction

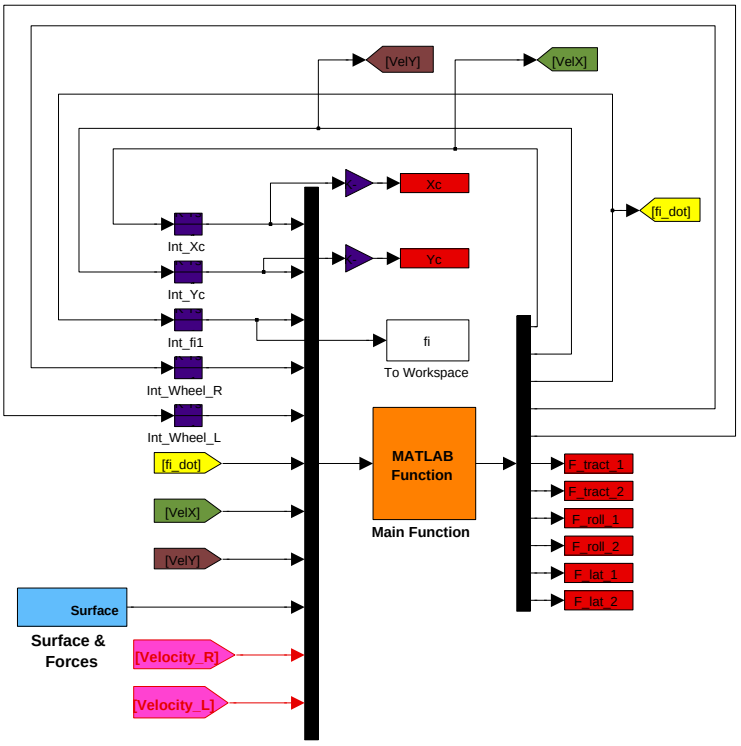

Figure 2.16: Simulation model constructed to simulate the effects of wheel forces

2.8 Conclusion and Discussions

In this part of the study, a simplified and differentiable lateral wheel force model is proposed and implemented on a differentially driven wheeled mobile robot. Dynamic effects of the wheel forces (traction, rolling and lateral) are investigated. A parameter estimation procedure is proposed and used to obtain the parameters of the wheel forces described. Both experimental and simulation results suggest that proposed method improves estimation performance of the vehicle model.

CHAPTER 3

INCLINATION EFFECTS TO MOBILE ROBOT'S MOTION

3.1 Introduction

Wheeled mobile robots have objectives for the operations conducted on different types of terrain having inclination. They are aimed to perform generally predefined trajectory tracking, desired path following and some autonomous motion planning tasks. Complete modeling for a wheeled mobile robot is necessary for obtaining adequate performance on a desired task. Particularly, outdoor mission requires detailed studies about modeling and control. Good control action can be done via having complete and proper models. Even if a mobile robot has an excellent design and construction, and uses perfect sensors, it is expected that desired objectives may not be achieving in case of having insufficient and/or incorrect mathematical modeling.

In general, ideal transmission, ideal rolling, zero inclination and no lateral slip assumptions are made in the modeling studies. However these assumptions may give improper approach when the robot works in an uneven surface having inclination. Furthermore, the modeled system which is stable on a flat surface can become an unstable system in an inclined surface.

3.2 Related Studies

In [Peters and Iagnemma, 2008], path tracking control in sloped terrain is studied. Mathematical model for the mobile robot and a path tracking controller based on the model predictive control framework are constructed. The proposed structure is simulated in Adams simulation package. In [Wei et al., 2009], navigation and slope detection system for a mo-

bile robot is designed. A slope detection procedure and local path planning algorithm are proposed. In [Zhu et al., 2010], a geometrical modeling is studied for sensing correctly an inclination. In order to estimate the slope characteristics, an estimation procedure is introduced. In [Ye and Borenstein, 2004], an obstacle detection method for mobile robot navigation in uneven terrain is presented. A slope estimation and adaptation procedure is introduced. In [Liegeois and Moignard, 1993], a terrain modeling study including slope and friction information is focused. An optimal motion planning of a mobile robot by using the terrain model is developed. In [Mester, 2010], intelligent mobile robot motion control in complex terrain is studied. A modeling and control procedure including obstacle detection and slope estimation is proposed. In [Silva et al., 2008], traction control for a mobile robot in rough terrain is focused and simulated. Speed and trajectory tracking control are targeted in case of that the terrain is slippery and has slope.

3.3 Aim of the Study Related to Investigation of Inclination Effects to Motion

In this part of the study it is contributed that in addition to wheel forces, inclination effects of the surface are studied. Three wheel forces are focused; traction, rolling and lateral. These forces are parametrically presented. An estimation process to obtain the parameters of these wheel forces is introduced. A complete mobile robot's motion model having wheel forces and slope information is constructed. It is indicated that while mobile robot moves in a surface having slopes in lateral and longitudinal directions; normal forces that are transferred from ground to the wheels are not constant (it is the general approach that normal forces are always considered constant while a wheeled mobile vehicle moves in a flat surface). They are changed according to orientation of the mobile robot. It is also pointed out that since wheel forces are described in terms of normal forces, the change of normal forces effects the wheel forces as well. In order to show such kind of effects to motion of a mobile robot, a differentially driven mobile robot is designed. It has two wheels located at the turning center and two spherical wheels for stability. It is commanded in a surface having slopes and the motion is observed by using a camera located at the top of the surface. The experimental system is adapted into a simulation environment so that the modeling studies proposed are confirmed by the results of experiment and simulation works.

The outline of this chapter is as follows: part 4 presents the robot model along with in addition

to slope information, traction, rolling and lateral force models; part 5 introduces the design of mobile robot used in this study; experimental surface setup specially constructed for this work is introduced in this part; following section presents the inclined surface experiments and simulations. Finally part 7 illustrated the concluding of the chapter.

3.4 Mathematical Modeling

3.4.1 Dynamic Model

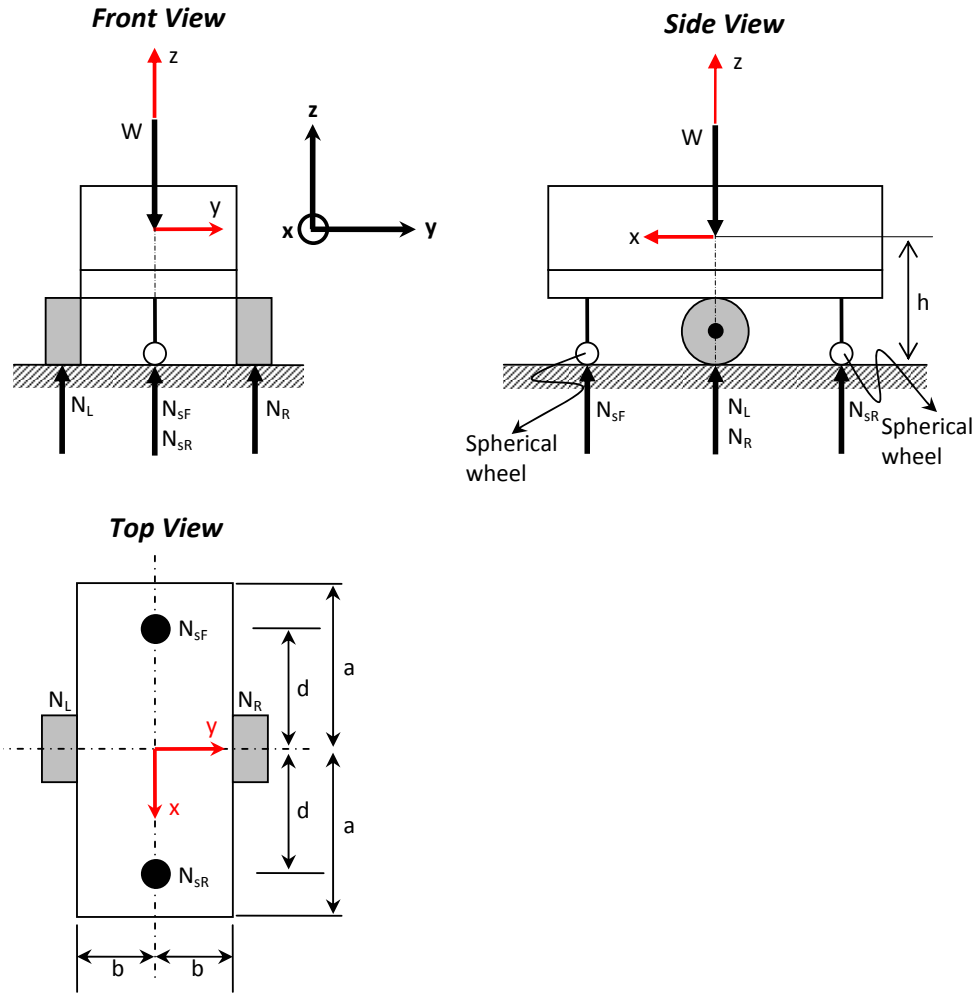

Figure 3.1: Free body diagram indicating normal and body forces acting on the mobile robot

Forces acting on the mobile robot are gravitational, body and wheel forces and their compo-

nents coming from the inclination effects. As shown in Figure 2.1, combined wheel forces are composed of three forces; traction, rolling and lateral forces. Traction forces for left and right wheels are shown by $F_{L,Tract}$ and $F_{R,Tract}$, respectively. $F_{L,Roll}$ and $F_{R,Roll}$ show rolling forces at left and right wheels, respectively. Left and right wheels' lateral forces are specified by using $F_{L,Lat}$, $F_{R,Lat}$, respectively. The lateral forces acting on front and rear spherical wheels are described by $F_{sF,Lat}$ and $F_{sR,Lat}$, respectively. Normal and body forces are shown in Figure 3.1 in the views of side, front and top. The center of mass of the mobile robot aligns with its turning center. The distance between the center of mass and the ground is specified by h. The total weight of the robot is W. N_L and N_R indicate the normal forces for left and right wheels, respectively. N_{sF} and N_{sR} show the normal forces at front and rear spherical wheels, respectively.

Normal forces that the ground applies to the wheels can be shown in vector form as follows:

$$\bar{N}_L = \begin{pmatrix} 0 \\ 0 \\ N_L \end{pmatrix} \quad \bar{N}_R = \begin{pmatrix} 0 \\ 0 \\ N_R \end{pmatrix} \quad \bar{N}_{sL} = \begin{pmatrix} 0 \\ 0 \\ N_{sL} \end{pmatrix} \quad \bar{N}_{sR} = \begin{pmatrix} 0 \\ 0 \\ N_{sR} \end{pmatrix} \tag{3.1}$$

In order to obtain the normal forces, the static case assumption is taken into account. In a static condition the following form of the moment equilibrium about point N_{sF} can be constructed:

$$\bar{r}_L \; x \; \bar{N}_L \; + \; \bar{r}_R \; x \; \bar{N}_R \; + \; \bar{r}_{sR} \; x \; \bar{N}_{sR} \; + \; \bar{r}_{sF} \; x \; \bar{N}_{sF} \; + \; \bar{r}_m \; x \left[R(\theta)\, R(\alpha)\, R(\phi) \right]^T \; \bar{W} \; = \; 0 \tag{3.2}$$

where r_L, r_R, r_{sR} and r_m are the distance vectors represented in Equation 3.3. W indicates the gravity vector. The mass of the robot is indicated by m. g shows the gravitational acceleration. $R(\theta)$, $R(\alpha)$ and $R(\phi)$ are the (3x3) rotation matrices represented in Equation 3.4.

$$\bar{W} = \begin{pmatrix} 0 \\ 0 \\ -mg \end{pmatrix} \quad \bar{r}_L = \begin{pmatrix} a \\ b \\ 0 \end{pmatrix} \quad \bar{r}_R = \begin{pmatrix} a \\ -b \\ 0 \end{pmatrix} \quad \bar{r}_{sR} = \begin{pmatrix} 2a \\ 0 \\ 0 \end{pmatrix} \quad \bar{r}_m = \begin{pmatrix} a \\ 0 \\ -h \end{pmatrix} \tag{3.3}$$

$$R(\theta) = \begin{pmatrix} 1 & 0 & 0 \\ 0 & cos(\theta) & -sin(\theta) \\ 0 & sin(\theta) & cos(\theta) \end{pmatrix} \quad R(\alpha) = \begin{pmatrix} cos(\alpha) & 0 & sin(\alpha) \\ 0 & 1 & 0 \\ -sin(\alpha) & 0 & cos(\alpha) \end{pmatrix}$$
$$R(\phi) = \begin{pmatrix} cos(\phi) & -sin(\phi) & 0 \\ sin(\phi) & cos(\phi) & 0 \\ 0 & 0 & 1 \end{pmatrix} \tag{3.4}$$

After performing the normal force calculations in a static case, the following equalities for the normal forces can be derived:

$$\begin{aligned} N_L &= \tfrac{h}{2b}\Big(cos\theta sin\alpha sin\phi + sin\theta cos\phi\Big)mg + \tfrac{1}{2\lambda}\Big(cos\theta sin\alpha cos\phi - sin\theta sin\phi - \mu_{sw}\Big)mg \\ N_R &= \tfrac{h}{2b}\Big(- cos\theta sin\alpha sin\phi - sin\theta cos\phi\Big)mg + \tfrac{1}{2\lambda}\Big(cos\theta sin\alpha cos\phi - sin\theta sin\phi - \mu_{sw}\Big)mg \end{aligned} \tag{3.5}$$

where $\lambda = \mu_w - \mu_{sw}$. μ_w and μ_{sw} indicate static friction coefficients of the driven and spherical wheels, respectively. Equation 3.5 states that normal forces depend on not only inclination angles of the surface but also orientation angle of the mobile robot. Furthermore normal forces are determined by the type of surface where mobile robot moves.

The accelerations of the mobile robot along x and y axes are introduced in Equations 2.3 and 2.4, respectively. Mobile robot's angular acceleration is represented in Equation 2.5 as well. In this part of the study, the procedure for developing the models for traction, rolling and lateral wheel forces which is proposed in Chapter 1 are also used in the modeling structure. Traction, rolling and lateral wheel forces are introduced in Equations 2.7, 2.11 and 2.12 respectively. Because of that as stated above spherical wheels are used for stability and are not driven, the effects of $F_{sF,Lat}$ and $F_{sR,Lat}$ are considered as small and can be neglected. Therefore the representation of angular acceleration of mobile robot is constructed without including the effects of these lateral forces.

The system showing the wheeled mobile robot system having n dimensional space illustrated in Equation 2.6 can be described in the following matrix form:

$$\begin{pmatrix} m & 0 & 0 \\ 0 & m & 0 \\ 0 & 0 & I \end{pmatrix} \begin{pmatrix} \ddot{X} \\ \ddot{Y} \\ \ddot{\phi} \end{pmatrix} + \begin{pmatrix} C_1 \\ C_2 \\ C_3 \end{pmatrix} = \begin{pmatrix} B_{11} & B_{12} \\ B_{21} & B_{22} \\ B_{31} & B_{32} \end{pmatrix} \begin{pmatrix} \tau_L \\ \tau_R \end{pmatrix} \tag{3.6}$$

where τ_L and τ_R are inputs for the motors located at left and right sides of the mobile robot, respectively. Assuming ideal transmission, torque equations can be developed as:

$$\begin{aligned} \tau_L &= r\, F_{L,Trac} \\ \tau_R &= r\, F_{R,Trac} \end{aligned} \tag{3.7}$$

where r is radius of each wheel. Note that $F_{L,Tract}$ and $F_{R,Tract}$ are traction forces at left and right wheels, respectively. Considering the equations given above, the elements of matrices B and C can be obtained as follows:

$$\begin{aligned} C_1 &= \Big(F_{L,Roll} + F_{R,Roll}\Big)\, cos(\phi) - W_x\, cos(\phi) \\ C_2 &= \Big(F_{L,Trac} + F_{R,Trac}\Big)\, sin(\phi) - \Big(F_{L,Lat} + F_{R,Lat}\Big)\, cos(\phi) - \\ & W_y\, cos(\phi) + \Big(F_{sF,Lat} + F_{sR,Lat}\Big)\, cos(\phi) \\ C_3 &= \Big(F_{L,Roll} - F_{R,Roll}\Big)\, b \end{aligned} \tag{3.8}$$

$$B = \begin{pmatrix} \left(\frac{cos(\phi)}{r}\right) & \left(\frac{cos(\phi)}{r}\right) \\ \left(\frac{sin(\phi)}{r}\right) & \left(\frac{sin(\phi)}{r}\right) \\ \left(\frac{b}{r}\right) & \left(\frac{b}{r}\right) \end{pmatrix} \tag{3.9}$$

The set of equations derived here show that the overall dynamics of the mobile robot is defined in terms of wheel forces and inclinations of the surface.

3.5 Experimental Surface Setup

The inclination angles are illustrated in Figure 3.2. θ and α represent the inclination angles about x and y axes, respectively. In this figure, angular rotation of the mobile robot is also indicated by ϕ.

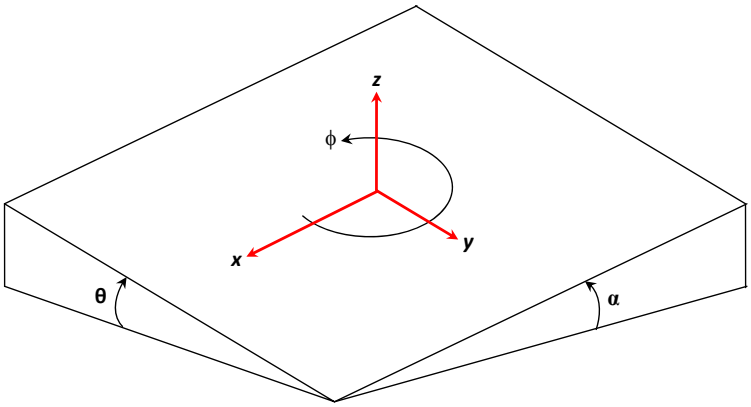

Figure 3.2: Description of inclination angles

3.6 Indoor Study-2: Experiments and Simulation Studies Related to Show the Effects of Inclinations to the Mobile Robot's Motion

In order to see the effects of inclination to the motion of the mobile robot, the platform is tilted as described in Figure 3.2. Then, mobile robot is commanded to have a circular motion. The platform is tilted in several conditions and the mobile robot is driven on this tilted platform. As seen in Figures 3.3, 3.4 and 3.5, mobile robot is driven for six different cases. These are ($\theta = 0^0$ and $\alpha = 0^0$), ($\theta = 4^0$ and $\alpha = 5^0$) (see Figure 3.3), ($\theta = 5^0$ and $\alpha = 2^0$), ($\theta = 6^0$ and $\alpha = 3^0$) (see Figure 3.4), ($\theta = 8^0$ and $\alpha = 5^0$), and ($\theta = 11^0$ and $\alpha = 5^0$) (see Figure 3.5). Note that inclination angle of 11^0 is the limit for the mobile robot (see right image of Figure 3.5). The bigger inclination angles than this value is not controllable for the mobile robot. Representation of the angles θ and α would be seen in Figure 3.2. The experimental results indicate that inclination angles given in x and y directions effect the mobile robot motion. They change wheel, normal and gravitational forces. These results show that the mobile robot cannot track a desired path in an inclined surface without having a model that includes the effects of the inclination information in the dynamics of the robot. (Note that starting position and initial heading angle of the mobile robot are same for all experiments).

Dynamic model of the mobile robot proposed in this study is simulated in Matlab environment. Simulations are performed for same inclination conditions used in the experiments

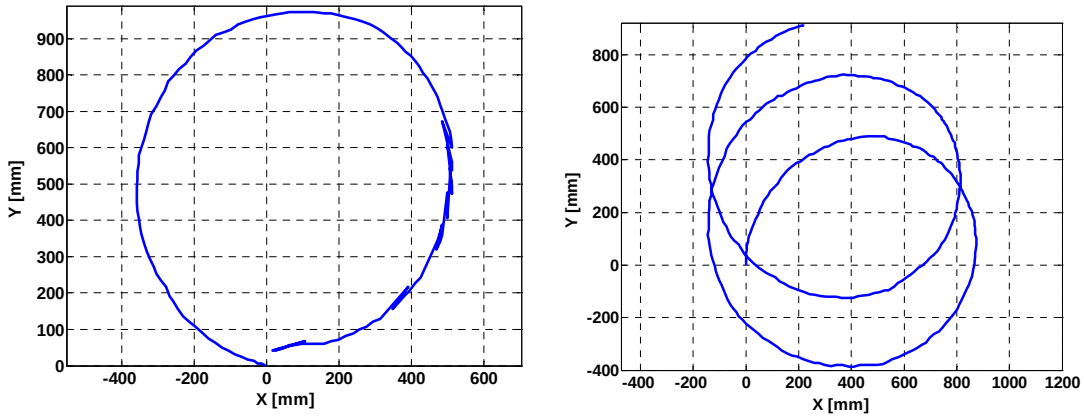

Figure 3.3: Effects of inclinations to circular motion of the mobile robot; ($\theta = 0^0$ and $\alpha = 0^0$), ($\theta = 4^0$ and $\alpha = 5^0$)

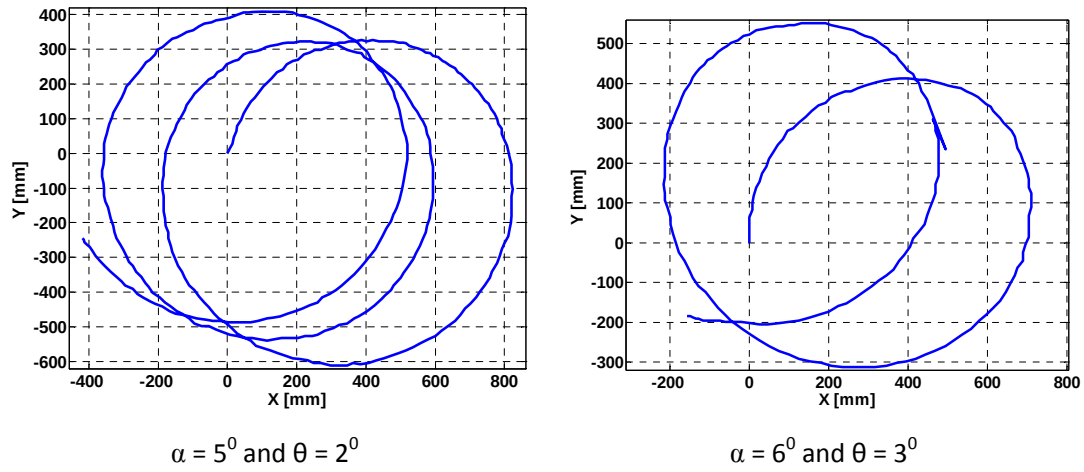

Figure 3.4: Effects of inclinations to circular motion of the mobile robot; ($\theta = 5^0$ and $\alpha = 2^0$), ($\theta = 6^0$ and $\alpha = 3^0$)

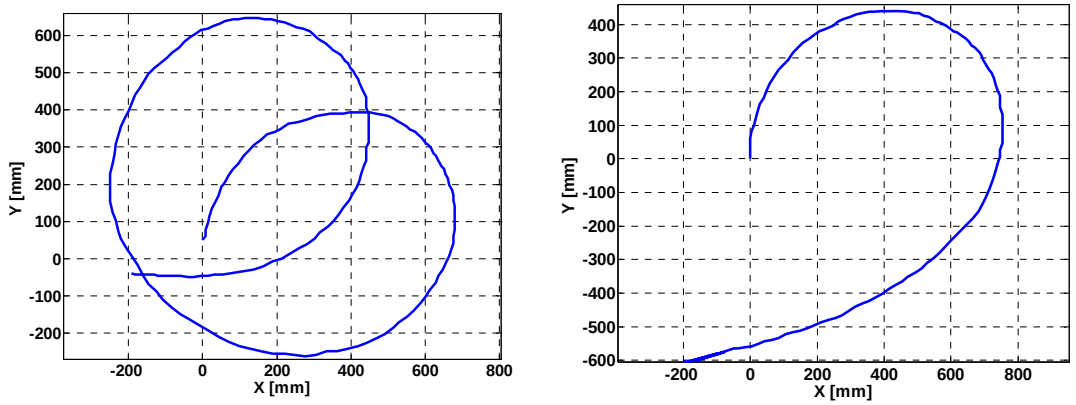

$\alpha = 8^0$ and $\theta = 5^0$ $\alpha = 11^0$ and $\theta = 5^0$

Figure 3.5: Effects of inclinations to circular motion of the mobile robot; ($\theta = 8^0$ and $\alpha = 5^0$), ($\theta = 11^0$ and $\alpha = 5^0$)

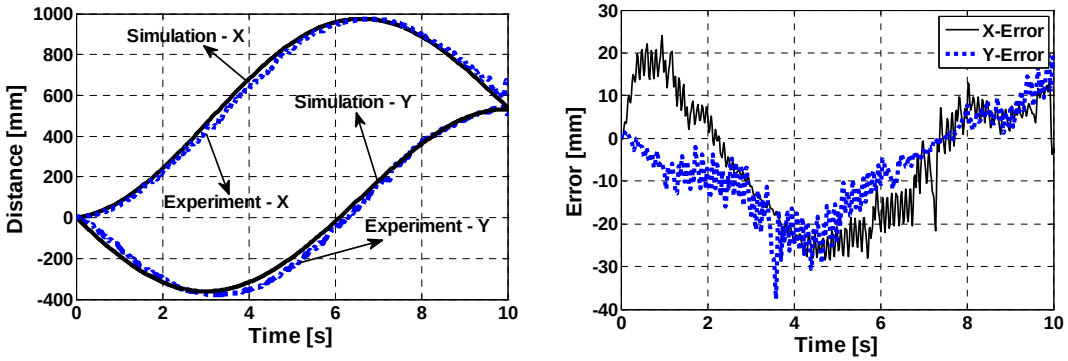

$\alpha = 0^0$ and $\theta = 0^0$

Figure 3.6: Simulation studies including effects of inclination angles; ($\theta = 0^0$ and $\alpha = 0^0$)

described above. The Simulink model is illustrated in Figure 3.10. Inclination values in x and y directions are taken about ($\theta = 0^0$ and $\alpha = 0^0$), ($\theta = 5^0$ and $\alpha = 4^0$), ($\theta = 3^0$ and $\alpha = 6^0$) and ($\theta = 5^0$ and $\alpha = 8^0$) in simulations and results are presented in Figures 3.6, 3.7, 3.8 and 3.9. Left columns of these figures show the position results of both simulation and experiments performed for different inclination conditions. Position results are illustrated in both X and Y directions. Right columns of the figures indicate the position errors showing the differences between the experimental and simulation results for both X and Y directions.

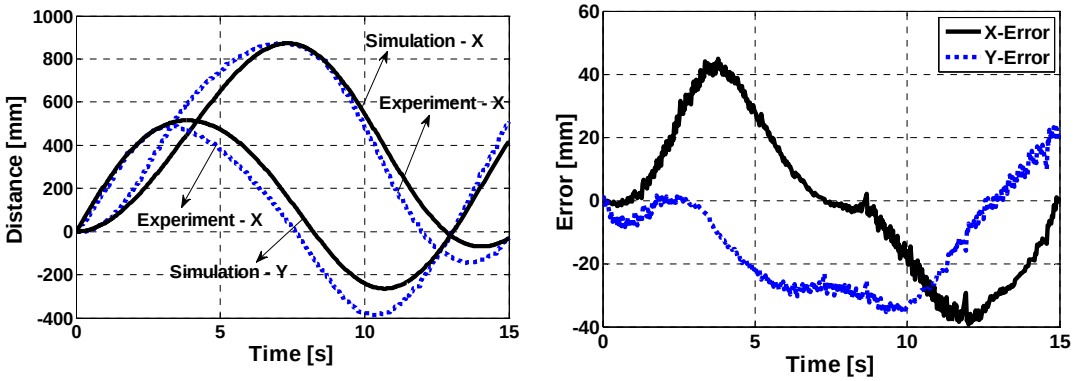

$\alpha = 4^0$ and $\theta = 5^0$

Figure 3.7: Simulation studies including effects of inclination angles; ($\theta = 4^0$ and $\alpha = 5^0$)

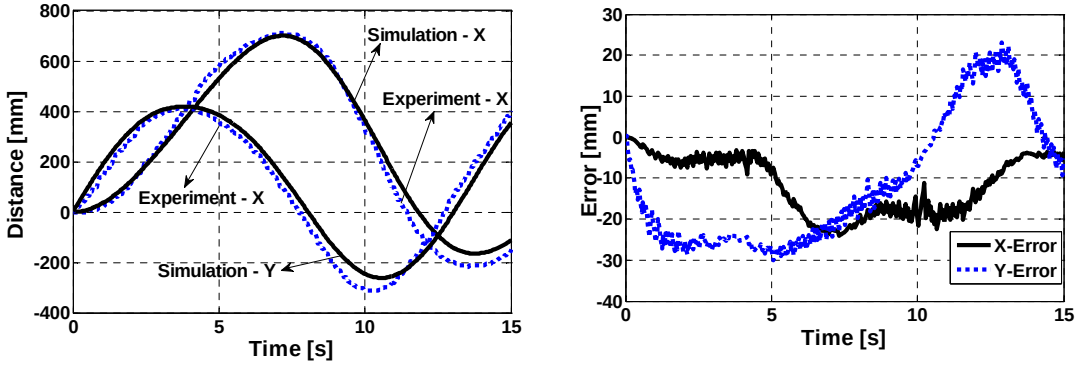

$\alpha = 6^0$ and $\theta = 3^0$

Figure 3.8: Simulation studies including effects of inclination angles; ($\theta = 3^0$ and $\alpha = 6^0$)

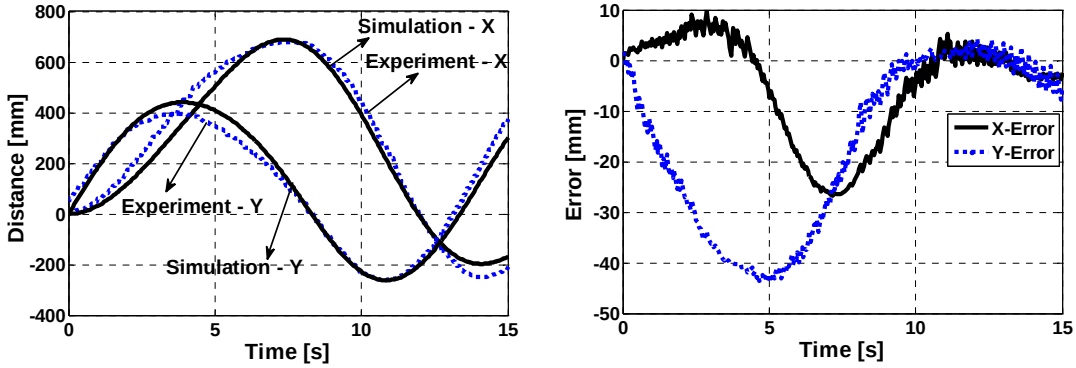

$\alpha = 8^0$ and $\theta = 5^0$

Figure 3.9: Simulation studies including effects of inclination angles; ($\theta = 5^0$ and $\alpha = 8^0$)

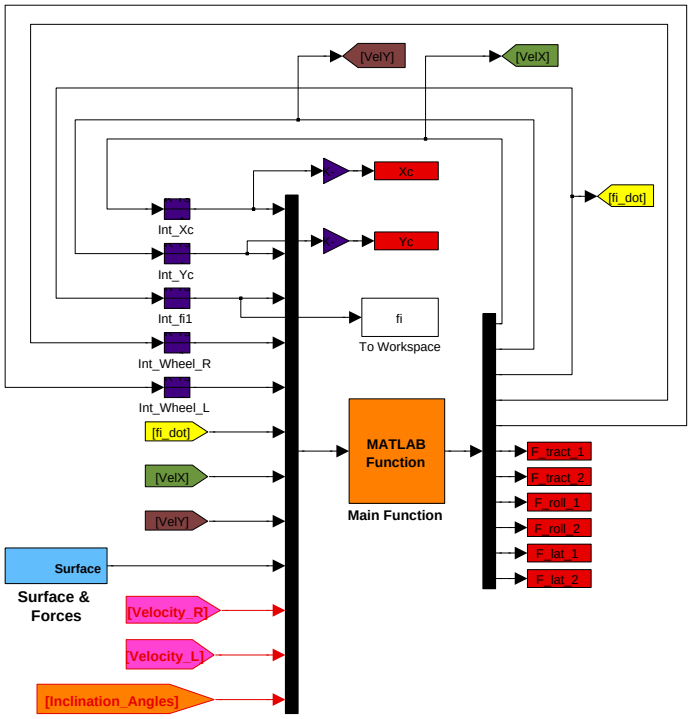

Figure 3.10: Simulation model constructed to simulate the surface inclination effects

3.7 Conclusion and Discussions

In this part of the study, a new perspective for incorporating inclination effects to motion model of a mobile robot is introduced. Wheel forces and inclination information are inserted into the overall system equations. It is shown that normal forces between wheels and ground change according to the inclination angles of the surface and orientation angle of the mobile robot. Both experimental and simulation results are provided to indicate the performance of the method proposed.

CHAPTER 4

DETECTING SURFACE CHANGES USING SLIP TRANSITIONS

4.1 Introduction

Desired trajectory tracking and path following tasks are the core objectives in mobile robotics research area. Furthermore in the real life usage of mobile robots, these tasks constitute the basis of the mobile robotic applications. Desired trajectory tracking can be achieved via a good modeling, estimation and control. Even if efficient sensors are used, the tasks may not be achieved in case of having deficient modeling.

One of the important point of trajectory tracking requires knowledge about surface on which mobile robot works. Surface characteristics create different slippage behaviors that affect the wheel forces. Then the model without having surface information develops deficient control commands that send the robot away from the desired trajectory.

4.2 Related Studies

In [Ward and Iagnemma, 2008], it is shown that surface change creates different slippage characteristics. This difference causes the positioning errors based on odometer. The slippage occurred when a mobile robot passes from one region to another prevents accomplishing good trajectory tracking and velocity control. Furthermore, it disallows the braking system to work better. In [Sidek and Sarkar, 2008a], it is mentioned that the ideal surface conditioned like no slippage is generally assumed in the mobile robotic applications. However, in reality the slippage is unavoidable since traction force causes slippage and provides required force that

drives the mobile robot. [Gustafsson, 1997] detects the slippage by comparing the speeds of the driven and undriven wheels. However, this methodology does not work while the robot crosses from one surface to another that have different characteristics. [Ojeda et al., 2006b] uses the current information coming from the actuated wheels so as to get the slippage information. [Stonier et al., 2007] develops a model including surface characteristic and slippage information. The model developed is used for navigation problems.

4.3 Aim of the Study Related to Surface Change Detection

In order to get information about the surface where mobile robot is aimed, a surface detection study is conducted via observing the change of slippage. Surface change detection is achieved by observing only the longitudinal slippage in this study. A differential drive test platform is used in order to perform the experiments for this purpose. The mobile robotic platform is equipped with and embedded PC/104 computer and communicates with the main computer through wireless ethernet. In order to measure the longitudinal velocity and angular velocity of the robot, encoders located on the wheels, current sensors, and an IMU (Inertial Measurement Unit) are interfaced into the system. The mobile robot is tested on a surface where the surface area is divided into four regions that have significantly different surface characteristics. The interaction between the wheels and the surfaces is used to determine the dynamic forces acting on the wheels. An extended Kalman Filter is used for accomplishing the purposes mentioned. During the experiments, the platform is driven at low speeds in order to ignore lateral slippage. The experiments show that longitudinal slip transitions give an opportunity to detect the surface changes. While the mobile robot travels from one surface to another, region of surface change is able to be detected by observing longitudinal slippage. These capability gives the ability for improving the trajectory tracking performance of mobile robots. Furthermore improved traction and braking performance of the mobile robot can also be achieved.

The outline of this chapter is as follows: next part is related to the modeling part. Then state space representation is given in the following section. The extended Kalman filter is presented in part 6 of this chapter. Experimental studies related to this chapter is shown in part 7.

4.4 Motion Modeling

The geometric model of the mobile platform is shown in Figure 2.1. 3D view of the geometric model is also illustrated in Figure 4.1. In this figure, weight of the mobile robot is shown by W. Longitudinal velocity is specified by V. The wheel forces are given as: $F_{Longitudinal}$, $F_{Rolling}$ and $F_{Lateral}$ indicate longitudinal, rolling and lateral forces, respectively. As seen from this figure, the platform has two wheels driven by DC-motors. The stability of the platform is provided by using two spherical wheels that are located at front and back. The kinematic model of the platform is given in Equation 2.1 and 2.2.

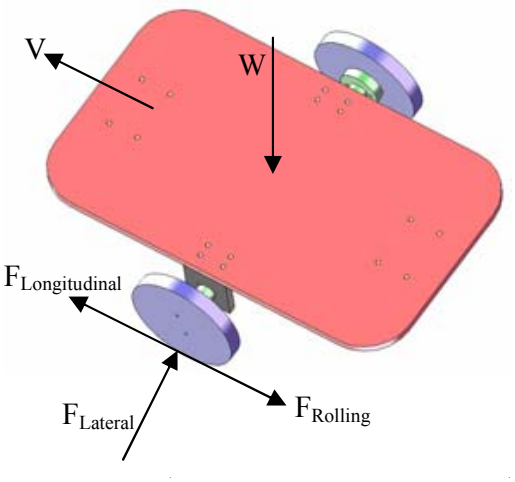

Figure 4.1: Wheel forces.

4.5 State Space Representation

The state space representation of the system can be defined by using the dynamics of the mobile platform and the sensors used as:

$$X = \left[x, y, \theta, V, \dot{\theta}, b_{ax}, b_{ay}, b_{\theta}, \omega_L, \omega_R\right]^T \tag{4.1}$$

where ω_R and ω_L are the rotational velocity of the right and the left wheels, respectively. b_{ax} and b_{ay} are the walking biases of the x and y accelerometers, respectively. b_{ω} is

the walking bias of the gyroscope. The walking bias is defined as in the following form [Ward and Iagnemma, 2008]:

$$\dot{b} = \frac{b}{\tau} + \left(\frac{2 f_s E[b^2]}{\tau}\right)^{0.5} \Psi_0 \tag{4.2}$$

where τ is the time constant of the inertial measurement system. f_s is the system frequency. Ψ_0 is the white noise of the sensor. The state space representation of the system can be written in the discrete domain as follows:

$$f_x = x_{k+1} = x + \Delta D_k \, cos\left(\theta_k + \frac{\Delta\theta_k}{2}\right) \tag{4.3}$$

$$f_y = y_{k+1} = y + \Delta D_k \, sin\left(\theta_k + \frac{\Delta\theta_k}{2}\right) \tag{4.4}$$

$$f_\theta = \theta_{k+1} = \theta_k + \Delta\theta_k \tag{4.5}$$

$$f_V = V_{k+1} = V_k + \Delta V_k = V_k + T A_w \tag{4.6}$$

$$f_{\dot{\theta}} = \dot{\theta}_{k+1} = \dot{\theta}_k + \Delta\dot{\theta}_k = \dot{\theta}_k + T\Gamma_w \tag{4.7}$$

$$f_{b_{ax}} = b_{ax_{k+1}} = b_{ax_k} + \Delta b_{ax_k} \tag{4.8}$$

$$f_{b_{ay}} = b_{ay_{k+1}} = b_{ay_k} + \Delta b_{ay_k} \tag{4.9}$$

$$f_{b_\theta} = b_{\theta_{k+1}} = b_{\theta_k} + \Delta b_{\theta_k} \tag{4.10}$$

$$\Delta D_k = \frac{\Delta D_{k,R} + \Delta D_{k,L}}{2} \tag{4.11}$$

$$\Delta\theta_k = \frac{\Delta D_{k,R} - \Delta D_{k,L}}{b} \tag{4.12}$$

where A_w and Γ_w are acceleration and angular acceleration of the mobile robot introduced in Equation 2.3 and 2.5, respectively. T indicates the sampling time of the system running. ΔD_k and $\Delta\theta_k$ are the displacement of the wheels and the orientation of the moving platform.

4.6 Extended Kalman Filter

In order to observe the surface changes using slip transitions, state space representation of the system is constructed and solved by using an extended Kalman filter. Extended Kalman filter is used for the integration of information coming from the sensor located in the robot

and the mobile robot's mathematical model. The filter is constructed based upon a discrete and nonlinear basis. This basis consists of two steps; prediction and correction.

$$\hat{X}_k^- = A_k \hat{X}_{k-1} + B_k U_k \tag{4.13}$$

$$P_k^- = A_k P_{k-1} A_k^T + B_k Q B_k^T \tag{4.14}$$

$$K_k = P_k^- H_k^T \left(H_k P_k^- H_k^T + R_n \right)^{-1} \tag{4.15}$$

$$\hat{X}_k = \hat{X}_k^- + K_k \left(Z_k - h_k \right) \tag{4.16}$$

$$P_k = \left(I - K_k H_k \right) P_k^- \left(I - K_k H_k \right)^T + K_k R K_k^T \tag{4.17}$$

The prediction steps for the extended Kalman filter are given in Equations 4.13 and 4.14. By the way, Equations 4.16 and 4.17 show the correction steps. Kalman gain is specified by matrix K. Q and R_n define the system noise and measurement noise, respectively. While solving this equation set, the initial values for $\hat{X}_{k-1}$ and P_{k-1} are specified (Equations 4.13 and 4.14). Then the resultant values are fed into Equations 4.15, 4.16 and 4.17. Hence a solution loop for the prediction and correction steps are able to be constructed. The Jacobian matrices (A, B, H) used in the representation of the extended Kalman filter can be defined as:

$$A_{i,j} = \frac{\partial f_i}{\partial X_j} \quad B_{i,j} = \frac{\partial f_i}{\partial U_j} \quad H_{i,j} = \frac{\partial h_i}{\partial X_j} \tag{4.18}$$

In this study, system noise (Q) and measurement noise R_n matrices are constructed as follows:

$$Q = \begin{pmatrix} 0.4 & 0 \\ 0 & 0.88 \end{pmatrix} \tag{4.19}$$

$$R_n = \begin{pmatrix} 0.1 & 0 & 0 & 0 & 0 \\ 0 & 0.6 & 0 & 0 & 0 \\ 0 & 0 & 0.9 & 0 & 0 \\ 0 & 0 & 0 & 0.4 & 0 \\ 0 & 0 & 0 & 0 & 0.5 \end{pmatrix} \tag{4.20}$$

The information about the rotation of the wheels in every time instant given in Equations 4.11 and 4.12 can be demonstrated as follows:

$$U_k = \begin{bmatrix} \Delta D_{k,L} & \Delta D_{k,R} \end{bmatrix}^T \tag{4.21}$$

The sensor measurement vector can be defined as:

$$Z_k = \left[\ddot{x}_k, \ddot{y}_k, \dot{\theta}_k, \omega_{encoder,R_k}, \omega_{encoder,L_k} \right]^T \tag{4.22}$$

It should be taken into account that the information coming from the sensors contain offset (C_0), walking bias (b_w), disturbance (a_d) and sensor noise (S_n) The actual sensor measurement can be defined as [Ward and Iagnemma, 2008]:

$$Z_{measurement} = Z_{actual} + C_0 + b_w + a_d + S_n \tag{4.23}$$

4.7 Indoor Study-3: Experiments Related to Show the Detection of Surface Changes By Using Slippage

Experiments are conducted by using the mobile robot system introduced in Figure 2.7. As stated in Chapter 2, two wheeled mobile robot is equipped with DC motors and encoders having resolution of 512 pulses/revolution, a six-axis IMU, and current sensor that are used for getting current information and achieving torque control tasks (Figure 4.2). As shown in Figure 4.3, an embedded PC is placed in the robot to perform all computational and communication issues. In order to get the encoder pulses, a 16-bit encoder card (Real Time Devices, DM6814) is also mounted in the embedded PC (Figure 4.3). Moreover, an analog-digital I/O card is plugged in this embedded PC in order for controlling the limit switches and relays. The I/O card is also used for getting current information coming from current sensor. All the experiments are performed by using xPC Target toolbox of Matlab. The motion of the mobile robot is followed by using a camera located at the top of the surface (Figure 4.6). The camera pursues the colored circles located at the top of the mobile robot (see Figure 4.4). Bigger circle indicates the turning center of the mobile robot whereas smaller circle is used for getting the heading information of the mobile robot.

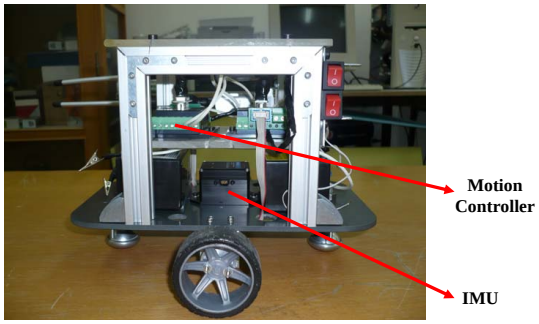

Figure 4.2: Differential drive mobile robot

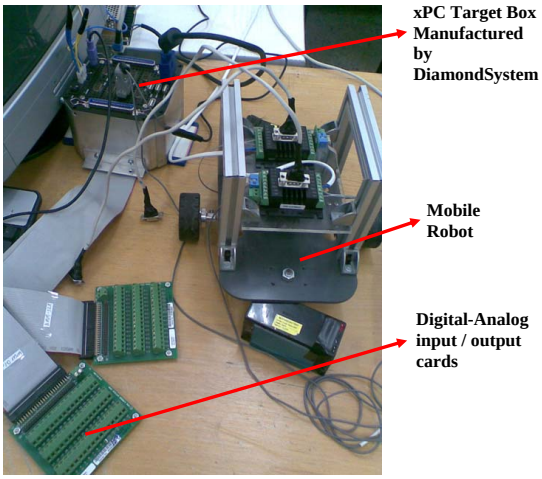

Figure 4.3: Mobile robot coupled with an embedded PC

4.7.1 Introduction to Experimental Surface

In order to detect the surface changes and slippage, a special surface is constructed (Figure 4.6). The surface is constructed by using four different regions as shown in Figure 4.5. Four different surfaces having different surface characteristics are specified by the letters A, B, C, and D. The biggest slippage is expected in region B since it is made up of hard and steep hairs.

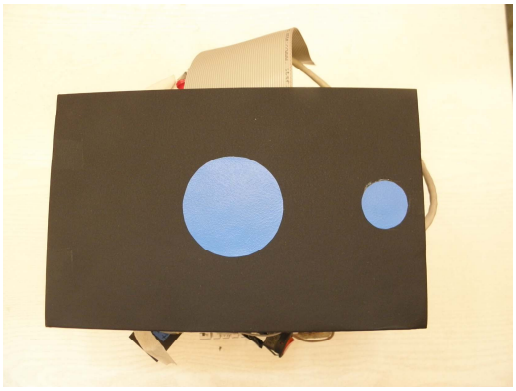

Figure 4.4: Colored circles that are pursued by camera located at the top of the set-up

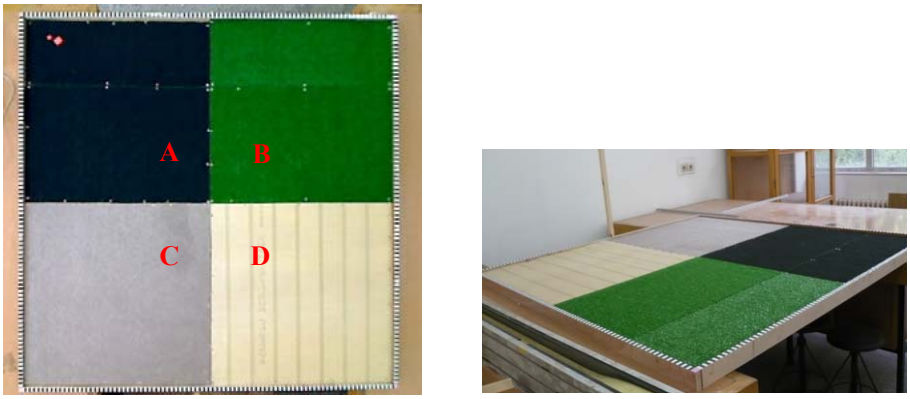

(a) (b)

Figure 4.5: Experimental surface

4.7.2 Observation of Current Drawn by the Motors

As stated above, mobile robot used in this study is suited with the current sensors shown in Figure 4.7. The current sensor gives analogue voltage between 0 and 5 V and is introduced to the I/O board of the embedded PC. In the experimental studies, the mobile robot is driven in different types of surfaces. These experiments show that the surface type can also be realized by using the current/torque information coming from the wheels actuated. The mobile robot is tested in the surfaces; smooth, carpet and soil. The results for right and left wheels are given in Figure 4.8. In these figures, the results that are obtained by lifting the mobile robot up are also given. It is described as ”free”. In this case, when the mobile robot is lifted up, the motors is commanded and no load current drawn is recorded. These current results

Figure 4.6: Experimental surface and camera located at the top of the surface

show that there is an observable difference between the current values. For instance, the left wheel's motor draws approximately 200 mA current in the lifted up position. On the other hand, the current values are 300 mA, 400 mA and 1000 mA in smooth surface, carpet and soil, respectively. Even if only current information is available, it can be useful to determine about the type of surface where the mobile robot travels. In Figure 4.9, an example related to surface determination by using current information is shown.

Same data observation approach can also be used for encoder information. As seen in Figure 4.10, the encoder pulses are recorded while the mobile robot is commanded in different surfaces. Smooth, carpet and soil surfaces, and lifted up position are used to get the encoder information. Even if only encoders are used to get the information about the surface where the mobile robot is driven, there is still chance to detect the types of surface.

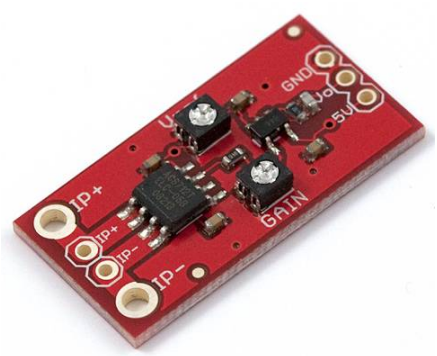

Figure 4.7: Current sensor plugged in the mobile robot

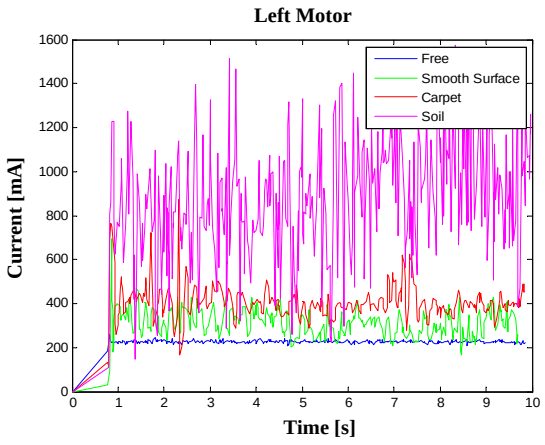

(a)

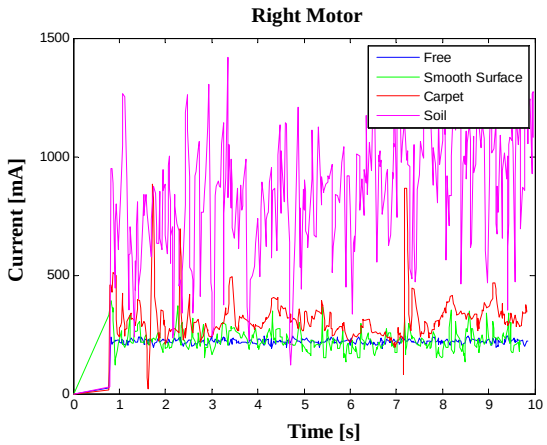

(b)

Figure 4.8: Current drawn by the left and right motors when the mobile robot is driven in different surfaces

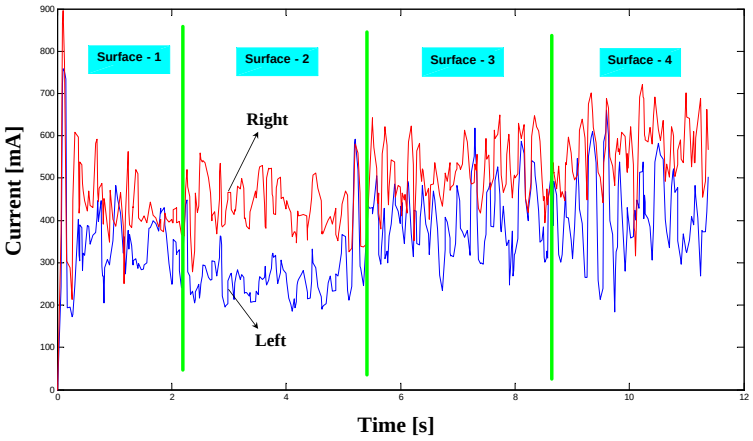

Figure 4.9: Surface determination by using current information

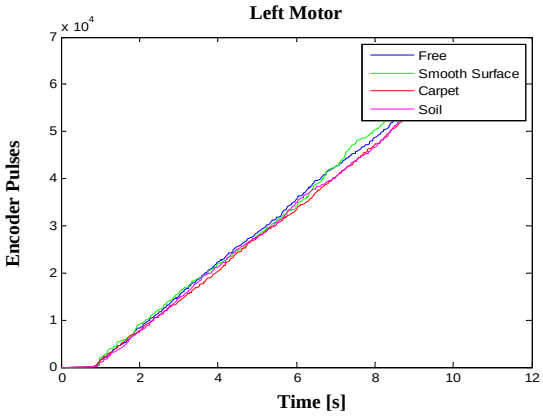

(a)

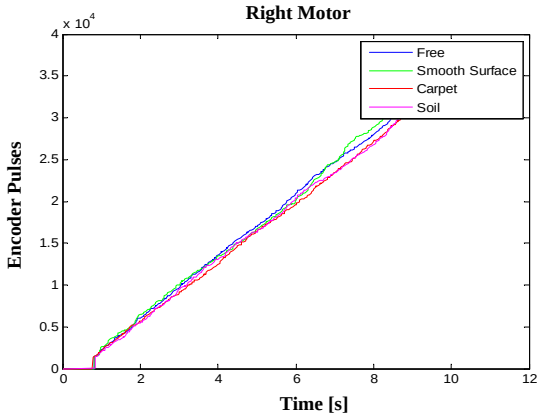

(b)

Figure 4.10: Encoder pulses coming from the left and right motors when the mobile robot is driven in different surfaces

4.7.3 Slippage Detection

The experimental studies are considered that the mobile robot should travel in three different regions and cross two transition points. It is commanded for achieving a circular trajectory having constant turning radius. The system model introduced above and the sensor information are used in order for getting the state space vector given in Equation 4.1. In Figure 4.11, the reference path and the experiment result are shown. Blue and red lines indicate the reference and actual trajectories, respectively. The mobile platform is initiated from the region indicated by letter D and it is driven through B and C. It is seen that slippage occurs when mobile robot moves and trajectory errors are happened. The slip values obtained during the experiments are given in Figure 4.12. The letters of regions (A, B, D) are indicated in this figure. The errors observed in the resultant trajectories are occurred due to the differences of interaction of the wheels and the surfaces in each region. The slippage results shown in Figure 4.12 say that the surface change can be detected by observing the slippage. The slippage characteristics of different surfaces and different transition regions can be classified by categorizing the slippage. This enables that the mobile robot can recognize the surface where it moves.

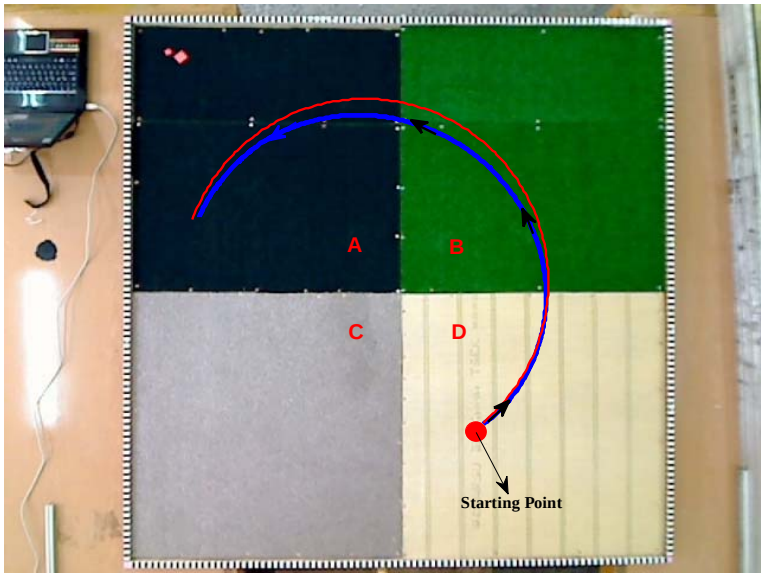

Figure 4.11: Experiment result

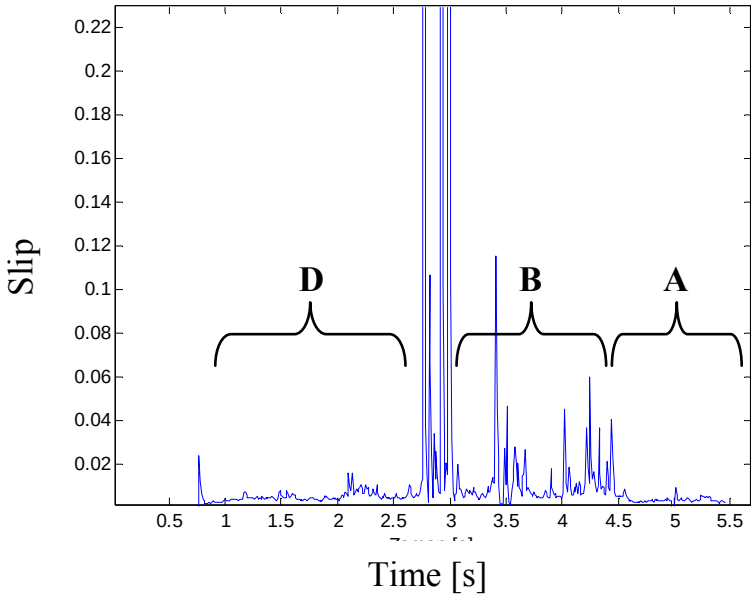

Figure 4.12: Slippage detection

4.8 Conclusion and Discussions

In this part of the thesis study it is shown that the surface changes are able to be detected via observing longitudinal slip transitions. Achieving this objective, a two wheeled differential mobile robot is modeled and the model constructed is supported by using an extended Kalman filter. The procedure is tested on a surface specially build for this application. The surface has four regions that have different surface characteristics. In the experiments, mobile robot is commanded to track a desired circular trajectory. While it moves, the surface changes is detected. In this study, it is pointed out that the procedure introduced can be used for getting the information about the surfaces and surface changes. Then this information can be fed into the control system used for tracking a desired trajectory/path.

CHAPTER 5

TRAJECTORY TRACKING CONTROL OF A MOBILE ROBOT

5.1 Introduction

Nowadays mobile robotics research area needs more autonomous solutions. Especially, including mixed terrain objectives, agricultural applications, inclined surface tasks, etc. are requiring more precision and automatic techniques. It can be seen that the motion of a mobile robot in an area having objects is limited. Moreover its motion is restricted because of the terrain whose characteristics are uncertain. This means that not only longitudinal but also lateral motion of the mobile robot is important for the autonomous drive since generally there is an objective in the mobile robotic applications that there should always be a fixed distance between the robot and the desired trajectory.

The short distance trajectory tracking has been almost achieved by using mobile robots, however the autonomous solutions for the mobile robotics missions need more attention for the long distance autonomous drives. In order to perform long distance autonomous drive in mixed terrain by using a mobile robot, a desired trajectory has to be specified. Furthermore kinematic/dynamic approaches are needed for creating a proper model and controller.

Car-like robot approach is widely used in order to develop a mobile robot motion model. Dubins curves are commonly preferred to generate curved desired trajectories. Approximate linear feedback, adaptive, robust, nonlinear and sliding mode controllers are widely used for tracking a desired trajectories. Lyapunov functions are constructed and generally used to obtain an appropriate velocity and steering controllers. These functions are also used to prove that the system with the controllers developed is stable.

5.2 Related Studies

The studies related to autonomous trajectory tracking for a mobile robot are performed in branches of research areas. Robot modeling is done by using kinematic and dynamic approaches. Desired trajectory generation is conducted according to the type of application. Longitudinal speed and orientation of the robot are controlled in order to track the desired trajectory. In a mixed terrain environment, both lateral and longitudinal errors should be compensated. More travel distance and working time should not increase the errors. At the same time, the mechanical features of the running parts of the robot's steering system should be taken into account.

In [Fang, 2004] and [Fang et al., 2005], a theoretical robust adaptive controller for autonomous guidance of farm vehicles has been proposed. Backstepping control procedure has been used to design the adaptive controller. The sliding effects are learned and compensated by parameter adaptations. Simulation studies have been provided to show the behavior of the proposed model. In [Luca and Oriolo, 1997], a feedback controller for trajectory tracking based on standard linear control theory has been presented. Car-like robot model has been used for generating the desired trajectory and appropriate controller. The procedure uses the approximate linearization of the system equations about the desired trajectory. Constant controller parameters are chosen in a way that the location of the closed loop eigenvalues are selected. It is related to find fast convergence to zero of the tracking error with a control action. In [Gu and Hu, 2002], path tracking scheme for a neural predictive control methodology has been studied. Car-like robot model for the modeling procedure has been adapted. The desired path is produced via a polynomial representation. In [Lenain et al., 2003], it has been shown that desired trajectory tracking objective could be achieved by using a nonlinear adaptive steering control law for the agricultural applications. Accuracy in vehicle localization has been the main issue. In [Lee et al., 1999], car-like robot approach related to trajectory tracking and control purposes has been used. A stability analysis procedure has been proposed to solve the desired trajectory tracking problems. The model has been controlled in order to track a desired trajectory within a certain region. In [Sotelo, 2003], the subject of developing lateral control strategy for autonomous steering of Ackerman like vehicles has been addressed. A lateral control law for adapting the steering control response has been proposed. The stability of the control law has been shown via analytical and experimental

results. In [Yang et al., 2004], nonlinear tracking control of a car-like robot via dynamic feedback linearization has been studied. The sense of nonlinear geometric control approach has been used. In [Lenain et al., 2005] and [Low and Wang, 2008], GPS-based path following control for a car-like mobile robot has been studied. Skidding and slipping issues have also been considered in the models. The proposed procedure uses real time kinematic model, GPS information and other sensors that give the posture of the robot. In order to compensate the path following error, backstepping controller has been used. In [Webers and Zimmer, 2002], a method for motion control of a mobile robot has been suggested. It claims that control parameters and the trajectory constructed are asymptotically converging. The difference between the proposed method and Lyapunov stability approach has also been discussed. In [Lee et al., 2006], an open loop path planner and a feedback tracking controller for a trajectory tracking objective has been proposed. Car-like robot model has been adapted for the modeling steps. In [Kim and Oh, 1998], the design of globally asymptotically stable tracking control law has been discussed. The stability of the controller proposed has been proved by using Lyapunov direct method. The methods have been tested in line tracking problem. In [Chen and Jiao, 2011], an adaptive path following control procedure has been focused. A nonlinear dynamic model has been explicitly combined with the kinematic constraints and car-like robot model. Sideslip friction force has also been taken into consideration. An adaptive backstepping controller has been designed to solve the path following problem in case of existing sideslip. In [Melonee and John, 2008], a robust trajectory tracking controller for an autonomous vehicle has been proposed and adapted into the overall system model.

In [Tsai et al., 2004], a hierarchical controller to point stabilization problem of a nonholonomic car-like robot has been proposed. The procedure has been called as skew-symmetry chained form. A set of sufficient condition has been introduced to determine whether a nonlinear kinematic model is converted to a skew symmetry chained form. A hierarchical controller has been developed to work with the model formed. In [Rezaei et al., 2003], the problem of on-line path following for a car-like robot working in large unstructured outdoor environments has been studied. Some path planning procedures have been followed. In [Solea and Nunes, 2007], a sliding mode control-based trajectory planning and tracking has been focused. They have used car-like robot model for their modeling and control objectives. Two sliding surfaces have been proposed such that lateral and angular errors are internally coupled with each other in a sliding surface that leads to convergence of both variables.

In [Hashim and Lu, 2009], an approach to plan the motion of a car-like robot navigating in static environment has been proposed. A multiple waypoints for trajectory generation has been introduced. The proposed approach has used cubic and quintic polynomials to obtain a smooth trajectory. In [Eaton et al., 2008], modeling and control of an agricultural vehicle has been studied. It deals with the solutions of precision of agricultural application. In [Eaton et al., 2009b], path tracking control for an agricultural vehicle has been studied. The vehicle model has been combined with the steering dynamics since it has been aimed that the force and torque inputs for the steering system could be able to control. PD and sliding mode control strategies have been implemented into the system.

In [Dolgov et al., 2009] and [Dolgov et al., 2010], the subject of proper path planning for an autonomous vehicle driven in unknown environment has been studied. They have developed a trajectory generation algorithm. In [Hoffmann et al., 2007], a controller for trajectory tracking of an autonomous automobile driven on off-road condition has been developed. In [Kuwata et al., 2008] and [Kuwata et al., 2009], a real-time motion planning algorithm with a tracking controller has been described. They have generated dynamically feasible trajectory in uncertain operating environment. They have also generated a closed loop prediction approach for motion planning. In [Hamner et al., 2011], design, control and application for an autonomous orchard vehicle for speciality crops production are presented. The work covers trajectory tracking and control of the vehicle in an orchard.

The researches related to autonomously driven mobile robot vehicles and applications are one of the popular areas in robotics. The necessity of automatic solutions in the mixed terrain environment directs the research towards autonomous vehicles. Some of the problems about autonomous motion in a filed are detection of trees, lines of trees, objects and workers, and generating and tracking of desired trajectories, controlling of heading speed and steering of the mobile robot/vehicle.

In [Ampatzidis et al., 2006], a decomposition process of autonomous navigation used in orchard applications are proposed. The procedure contains 4 stages. These are planning of field coverage, motion and action generation, motion planning and trajectory generation. The straight motion and turning strategies inside the field are discussed. In [Eaton et al., 2008], modeling and control of agricultural vehicles are focused. Precision control under slippage are investigated. In [Gonzalez et al., 2009], trajectory tracking and localization of tracked

mobile robots are addressed. Feedback linearization technique has been implemented into the overall system model with including slip definition. In [Huynh et al., 2010], path tracking problem of an agricultural vehicle has been pointed. Following the kinematic model of the farm vehicle and desired path definition, an appropriate error model has been derived. In [Lenain et al., 2010a], accurate and reliable desired path tracking are studied. A four wheeled car-like robot that moves on off-road with high speed has been focused. Kinematic and dynamic modeling procedures are studied to obtain slippage occurred during motion. Adaptive and predictive controller strategies are implemented into the system in order to achieve desired trajectory tracking tasks. In [Li et al., 2006], an extensive review study related to agricultural autonomous vehicles used for autonomous agricultural guidance applications has been done. In [Matveev et al., 2010], the autonomous path tracking problem for farming vehicles has been studied. The curved path tracking has been solved by using the proposed methods. In [Fang, 2004] and [Fang et al., 2005], a theoretical robust adaptive controller for autonomous guidance of farm vehicles in the presence of sliding has been proposed. Backstepping control procedure has been used to design the adaptive controller. The sliding effects are learned and compensated by parameter adaptations. Simulation studies are provided to show the behavior of the proposed model. In [Kim and Oh, 1998], the design of globally asymptotically stable tracking control law has been focused. The stability of proposed controller has been observed by using Lyapunov direct method. The overall system has been tested for line tracking task.

In [Bak and Jakobsen, 2004], agricultural robotic platform with four wheel steering for the application of weed detection has been studied. Row finding and guidance, and weed detection models are proposed. In [Cervantes et al., 2003], a procedure for detecting man-made roads are introduced. The methodology proposed is useful for autonomous navigation in field environment for outdoor (mixed terrain) missions. In [Libby and Kantor, 2011], a perception based GPS free approach in order to create a localization procedure for a field mobile robot in a mixed terrain has been studied. Encoders and laser range finder information are combined under an extended Kalman filter. In [Barawid et al., 2007], development of an autonomous navigation system used in an field application has been studied. 2-D laser scanning range finder has been used in order to achieve this purpose. The objective of the work is to develop an automatic guidance system which is capable of navigating an autonomous vehicle moving between rows of trees in an agricultural area for real-time agricultural applications. An autonomous tractor has been used to implement the procedures proposed and

to perform the experiments. Rows of trees are detected by using Hough transform detection algorithm. The row information has been used to correct the lateral and heading errors of the vehicle. Appropriate speed command has also been generated to meet the desired value. In [Weiss and Biber, 2011], a model for detection and segmentation of plants and ground has been proposed. The procedure that uses the information coming from Lidar has been implemented into an autonomous outdoor mobile robot to perform mapping and navigation missions.

In [Cariou et al., 2009], trajectory tracking control with high accuracy has been studied. Front and rear wheels are independently controlled. Even though there is sliding, it has been shown that the mobile agricultural vehicle could have tracked the desired trajectory in autonomous mode. The study doesn't contain the behavior of steering angle and longitudinal motion. In [Derrick and Bevly, 2009], model based adaptive control strategy has been used for controlling the lateral displacement of a farm tractor that should follow a straight desired path. The results cover the applications having short distance and short working time. In [Fang et al., 2006], trajectory tracking control of an autonomous farm vehicle despite slippage has been studied. Sliding effects are combined with the kinematic model of the system. Geometric and velocity constraints are introduced with the sliding effects of the farm vehicle while it is in motion. By using backstepping control strategy, a robust adaptive controller has been designed. The trajectory tracking accuracy has been presented by the results of simulation and experiments. In [Johnson et al., 2009], development and implementation of a team of three autonomous tractors for peat moss harvesting application are introduced. Desired trajectory tracking and turning possibilities are discussed. Different sceneries are studied and presented. In [Lenain et al., 2010a], high accuracy path tracking for a farm vehicle has been focused. The study has been addressed to the guidance for agricultural applications conducted by the autonomous farm vehicle. In [Nagasaka et al., 2009], the development of an autonomous rice transplanter has been reported. The farm vehicle has been equipped with GPS and IMU. Control issues of steering angle and heading speed are focused. Straight motion and turning strategies used for trajectory tracking of the autonomous vehicle in agricultural area are introduced. In [Ordonez et al., 2009], rut following and tracking problems by using an autonomous ground vehicle has been studied. The ruts having different shapes are studied. Reactive based approach is implemented into the system model to have the opportunity for following the ruts. In [Stentz et al., 2002], an autonomous farm tractor system is introduced.

Accurate path tracking is one of the objectives. The procedure proposed is tested in orange grove. In [Xiang et al., 2007], a suboptimal reference course for turning of a farm tractor is proposed. In order to track the reference path, a path tracking controller is designed. The performance of the methodology proposed is experimentally tested in the field.

5.3 Aim of the Study Related to Desired Trajectory Tracking of a Mobile Robot

In this part of the study, it is aimed that in order to achieve better trajectory tracking tasks for a mobile robot in the field environment, a new modeling approach should be developed. For achieving this objective, a car-like modeling procedure is used for building a new perspective for tracking a desired trajectory in outdoor environment that has the mixed terrain characteristics. Backstepping control strategy is implemented in the system which is proposed. The stability of the system is checked by using Lyapunov stability criteria. The surface effects are also introduced into the system so as to achieve better and long distance autonomous trajectory tracking tasks. Such kind of surface effects are defined by using some simple mathematical approaches. They are defined as functions of some parameters which are experimentally determined.

The outline of this chapter is as follows: The next part is related to the mathematical modeling. In this part, the motion model is constructed by using car-like robot model. In part 5, steps of desired trajectory generation are introduced. The controller developed is illustrated in part 6. The last part is composed for conclusion and discussions of this chapter.

5.4 Mathematical Modeling

Kinematic and dynamic approaches are commonly used in order to develop a motion model for mobile robots. Car-like robot approach is widely preferred to develop desired trajectory generator and controller objectives. Dubins curves are the other procedure used for generating curved trajectories. Approximate linear feedback, adaptive, robust, nonlinear and sliding mode controllers are the common trajectory tracking controllers that are implemented in mobile robots for varies applications.

The mobile robot that is considered and modeled as a test platform in this study is a four

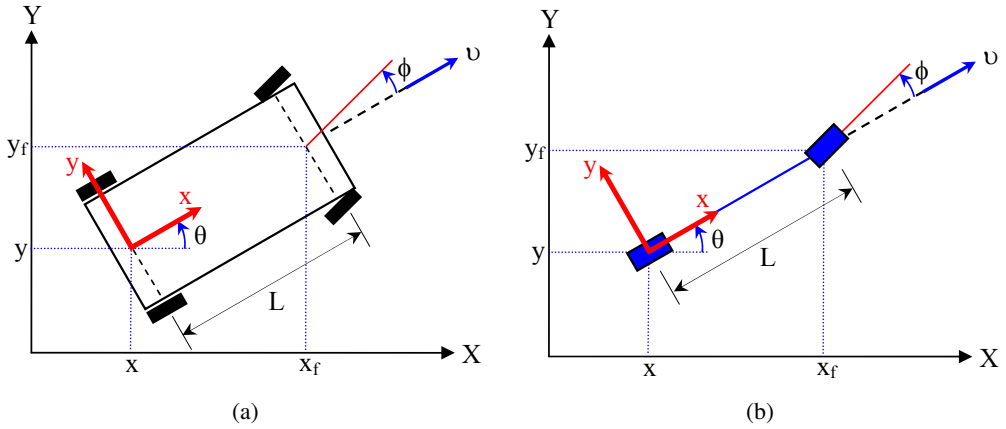

Figure 5.1: (a) Car-like robot model, (b) Bicycle model

wheeled vehicle. Here are the assumptions: Two wheels are located at the rear and motorized by an electrical motor. Two front wheels are used for steering. The steering system is Ackerman type steering. The geometric model of the mobile robot (vehicle) is given in Figure 5.1-a. In order to use car-like robot model for the modeling procedure, as usual, front and rear axles are collapsed respectively in a front and rear median wheel, reducing the model to bicycle model as shown in Figure 5.1-b. There are two frames on the model. $f(x, y)$ and $F(X, Y)$ indicate the moving frame attached to the mobile robot body and the fixed reference frame, respectively. Moving frame is attached at the rear axle of the mobile robot and its position is shown by (x,y). Position of the front axle is shown by (x_f,y_f). Longitudinal velocity of the mobile robot is specified by υ, in x-direction. Distance between the front and rear axles of the mobile robot is indicated by L. The orientation of the mobile robot with respect to fixed coordinate axes is specified by θ. Front steering angle is indicated by ϕ.

Desired motion model of the robot can be constructed in the following simplified nonholonomic system (car-like robot model).

$$\begin{aligned} \dot{x}_d &= \upsilon_d \, cos\theta \\ \dot{y}_d &= \upsilon_d \, sin\theta \\ \dot{\theta}_d &= \tfrac{\upsilon_d}{L} \, tan(\phi_d) \end{aligned} \tag{5.1}$$

where $\dot{x}_d$, $\dot{y}_d$ denote the desired velocity components of the mobile robot in x and y directions, respectively. $\dot{\theta}_d$, υ_d and ϕ_d indicate the desired angular velocity, desired heading velocity and the desired front steering angle of the robot, respectively.

In Figure 5.2, trajectory tracking errors are specified. In this figure, actual and desired locations of the mobile robot are represented by solid and dashed lines. Real position of the robot is emphasized by actual robot. The position and orientation components of the actual robot are described by (x, y, θ), and that of the desired mobile robot are presented by (x_d, y_d, θ_d). The errors in x and y directions are shown by x_e and y_e, respectively. The orientation error is indicated by θ_e.

The trajectory tracking errors can be obtained by using both Figures 5.1 and 5.2.

$$\begin{bmatrix} x_e \\ y_e \\ \theta_e \end{bmatrix} = \begin{bmatrix} cos(\theta) & sin(\theta) & 0 \\ -sin(\theta) & cos(\theta) & 0 \\ 0 & 0 & 1 \end{bmatrix} \begin{bmatrix} x_d - x \\ y_d - y \\ \theta_d - \theta \end{bmatrix} \tag{5.2}$$

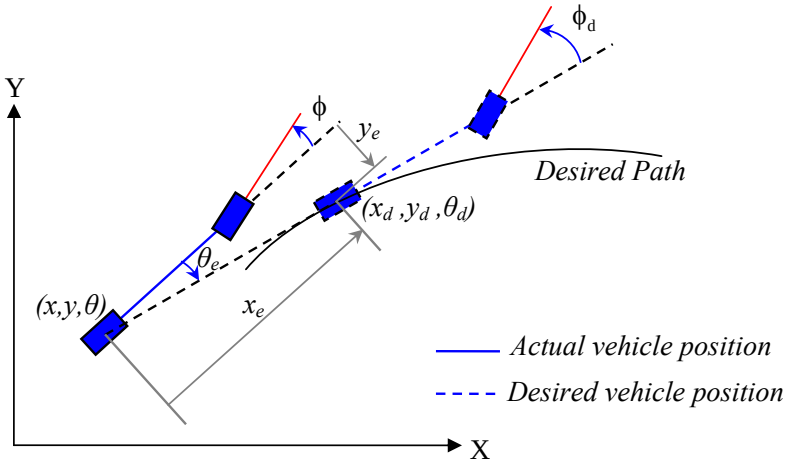

Figure 5.2: Trajectory tracking errors

The corresponding derivatives of the errors can be derived as follows.

$$\begin{aligned} \dot{x_e} &= -\upsilon + \upsilon_d \, cos(\theta_e) + y_e \, \omega + \varepsilon_1 \\ \dot{y_e} &= \upsilon_d \, sin(\theta_e) - x_e \, \omega + \varepsilon_2 \\ \dot{\theta_e} &= \upsilon_d \, C(s) \; - \frac{\upsilon_d}{L} \, tan(\phi) \end{aligned} \tag{5.3}$$

where ε_1 and ε_2 are defined to show the unknown and unmodeled parts [Eaton et al., 2009a]. This terms includes also the slippage effects that could not have been successfully modeled yet. In this study, ε_1 and ε_2 are modeled as a function of $sin(\theta)$ and $cos(\theta)$, such that $\varepsilon_1 = f(\Upsilon_1, sin\theta)$ and $\varepsilon_2 = f(\Upsilon_2, cos\theta)$. Υ_1 and Υ_2 are the controller design parameters and chosen

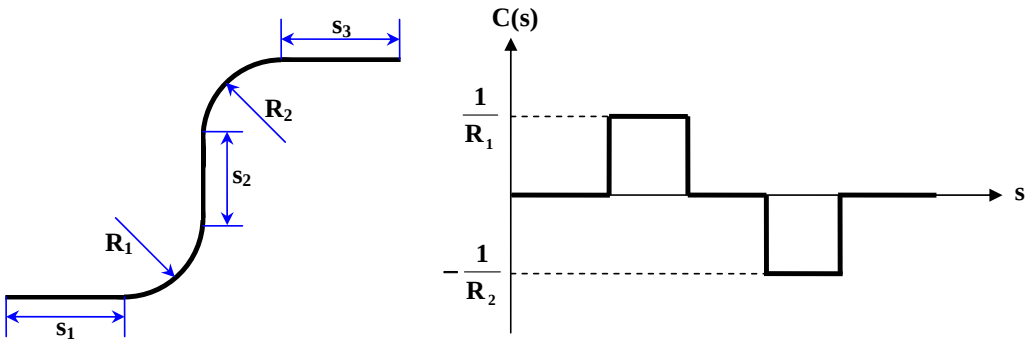

(a) (b)

Figure 5.3: Relation between C(s) and arc length

according to the experimental behavior of the mobile robot working in the field. In Equation 5.4, the definition of these functions are illustrated. Angular velocity of the mobile robot can be shown in terms of forward speed of the mobile robot and a curvature function, $C(s)$, in the form given in Equation 5.5:

$$\begin{aligned} \varepsilon_1 &= \varrho_1 sin(\kappa_1 \theta) \\ \varepsilon_1 &= \varrho_2 cos(\kappa_2 \theta) \end{aligned} \tag{5.4}$$

$$\dot{\theta}_d = \omega_d = \frac{\upsilon_d}{\frac{1}{C(s)}} \tag{5.5}$$

In order to show the relationship between the function of $C(s)$ and arc length, Figure 5.3 is given as an example. In Figure 5.3-a, a motion that is constructed via straight lines and circles is shown. In Figure 5.3-b, behavior of $C(s)$ and arc length according to this motion is given. This example briefly shows the basis of our trajectory generation procedure. Note that s_i and R_i indicate the length of straight and the radius of circular motions, respectively.

5.5 Desired Trajectory Generation

In this section, methodology of desired trajectory generation is given in detail. A smooth desired trajectory for the car-like robot model is given in the moving frame.

$$x_d = x_d(t), \quad y_d = y_d(t), \quad t \geq t_0 \tag{5.6}$$

Note that initial conditions $(x_d(t_0), y_d(t_0), \theta_d(t_0))$ and continuous inputs υ_d, and ϕ_d for $t \geq t_0$ are supplied to the system.

5.6 Trajectory Tracking Controller

It is reminded that the objective is to find the proper steering angle and forward velocity so that the robot vehicle should follow a desired trajectory. In order to construct the appropriate trajectory tracking controller, the car-like model given in Equation 5.1 is considered. The backstepping procedure is used to develop the controller to control the positional errors. Control diagram of the overall control system is given in Figure 8.9. In this figure, υ_c and ϕ_c represent controller outputs for forward speed and steering angle, respectively. $X_{desired}$, $Y_{desired}$ and $\theta_{desired}$ show the desired values of longitudinal, lateral and orientational motions, respectively. The feedback information for these terms (X_{PS}, Y_{PS} and θ_{PS}) are assumed that they are provided from a positioning feedback system.

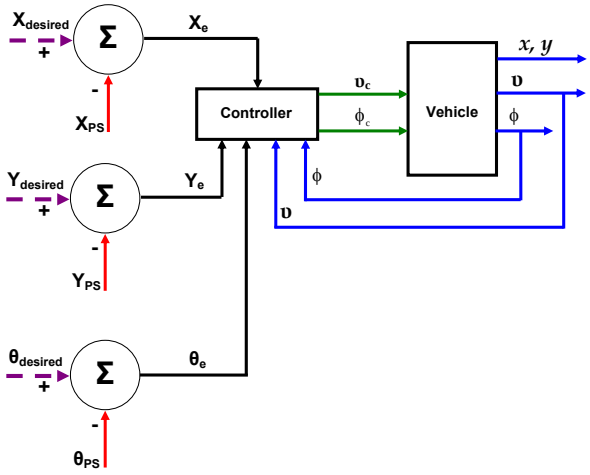

Figure 5.4: Flow chart of the control system.

Consider the following Lyapunov function which is a function of x_e, and y_e [Fang, 2004], [Fang et al., 2005], [Fang et al., 2006], [Eaton et al., 2009a]:

$$V_1 = \frac{1}{2}x_e^2 + \frac{1}{2}y_e^2 \tag{5.7}$$

Derivative of V_1 along Equation 5.3 is obtained as follows:

$$\dot{V}_1 = x_e(-\upsilon + \upsilon_d cos(\theta_e) + y_e\omega + \varepsilon_1) + y_e(\upsilon_d sin(\theta_e) - x_e\omega + \varepsilon_2) \tag{5.8}$$

where $\omega = \frac{\upsilon_d}{L}\ tan(\theta_d)$. Rearranging Equation 5.8 gives:

$$\dot{V}_1 = x_e(-\upsilon + \upsilon_d cos(\theta_e) + \varepsilon_1) + y_e(\upsilon_d sin(\theta_e) + \varepsilon_2) \tag{5.9}$$

Choose longitudinal velocity of the mobile robot υ and time-varying function Ω as follows:

$$\begin{aligned} \upsilon &= \upsilon_d cos(\theta_e) + k_x x_e + \tau_1 x_e \lambda_1^2(t) \\ \Omega &= \upsilon_d sin(\theta_e) + k_y y_e + \tau_2 y_e \lambda_2^2(t) \end{aligned} \tag{5.10}$$

where k_x and k_y are control parameters, τ_1 and τ_2 are positive parameters. $\lambda_1(t)$ and $\lambda_2(t)$ are the time-varying functions and can be chosen as $\lambda_1(t) > |\varepsilon_1|$ and $\lambda_2(t) > |\varepsilon_2|$ [Eaton et al., 2009a].

Substituting Equation 5.10 into Equation 5.9 gives the following relationship:

$$\dot{V}_1 = -k_x x_e^2 - k_y y_e^2 - \tau_1 x_e^2 \lambda_1^2(t) - \tau_2 y_e^2 \lambda_2^2(t) + x_e\varepsilon_1 + y_e(\Omega + \varepsilon_2) \tag{5.11}$$

Equation 5.11 can be defined in the following form [Eaton et al., 2009a]:

$$\dot{V}_1 \leq -k_x x_e^2 - k_y y_e^2 - \tau_1(|x_e|\lambda_1(t) - \frac{1}{2\tau_1})^2 - \tau_2(|y_e|\lambda_2(t) - \frac{1}{2\tau_2})^2 + \frac{1}{4\tau_1} + \frac{1}{4\tau_2} + y_e\Omega \tag{5.12}$$

In order to meet the Lyapunov stability criteria requirements, the following Lyapunov candidate function can be chosen.

$$V_2 = V_1 + \frac{1}{2}\Omega^2 \tag{5.13}$$

Derivative of V_2 is in the following form:

$$\dot{V}_2 = \dot{V}_1 + \Omega\dot{\Omega} \tag{5.14}$$

Derivative of Ω can be obtained as:

$$\dot{\Omega} = \upsilon_d\dot{\theta}_e cos(\theta_e) + \dot{y}_e(k_y + \tau_2\lambda_2^2(t)) + 2\tau_2 y_e\lambda_2(t)\frac{\partial\lambda_2(t)}{\partial t} \tag{5.15}$$

Combining Equation 5.14 and 5.15 gives the following result.

$$\begin{gathered}\dot{V}_2 \leq -k_x x_e^2 - k_y y_e^2 - \tau_1(|x_e|\lambda_1(t) - \tfrac{1}{2\tau_1})^2 - \tau_2(|y_e|\lambda_2(t) - \tfrac{1}{2\tau_2})^2 + \tfrac{1}{4\tau_1} + \tfrac{1}{4\tau_2} + y_e\Omega + \\ \Omega\{\upsilon_d\dot{\theta}_e cos(\theta_e) + \dot{y}_e(k_y + \tau_2\lambda_2^2(t)) + 2\tau_2 y_e\lambda_2(t)\tfrac{\partial\lambda_2(t)}{\partial t}\}\end{gathered} \tag{5.16}$$

Choose the following relationship in order to have $\dot{V}_2 \leq 0$

$$\begin{gathered}\omega \geq \tfrac{\aleph_1+\aleph_2}{\aleph_3} \\ \aleph_1 = k_\Omega\Omega + y_e + \upsilon_d^2 cos(\theta_e)C(s) + \Big(k_y + \tau_2(f(\Upsilon_2, cos\theta))^2\Big)\Big(\upsilon_d sin(\theta_e) + f(\Upsilon_2, cos\theta)\Big) \\ \aleph_2 = 2\tau_2 y_e f(\Upsilon_2, cos\theta)\tfrac{\partial f(\Upsilon_2, cos\theta)}{\partial t} \\ \aleph_3 = \upsilon_d cos(\theta_e) + x_e\Big(k_y + \tau_2\Big(f(\Upsilon_2, cos\theta)\Big)^2\Big)\end{gathered} \tag{5.17}$$

where k_Ω is the third controller parameter. Then, derivative of Lyapunov candidate function is obtained as:

$$\dot{V}_2 \leq -k_x x_e^2 - k_y y_e^2 - k_\Omega\Omega^2 + \frac{1}{4\tau_1} + \frac{1}{4\tau_2} \tag{5.18}$$

Equation 5.18 emphases that in order to meet Lyapunov stability criteria, the values of τ_1 and τ_2 should be chosen larger. In case of having zero values of x_e, y_e and Ω means the mobile robot follows exactly the desired trajectory.

Consequently, the controller outputs for longitudinal velocity and steering angle can be given as follows:

$$\begin{aligned} \upsilon_c &\geq \upsilon_d cos(\theta_e) + k_x x_e + \tau_1 x_e \Big(f(\Upsilon_1, sin\theta) \Big)^2 \\ \phi_c &= atan(\tfrac{L\omega}{\upsilon}) \end{aligned} \tag{5.19}$$

5.7 Conclusion and Discussions

In this section, a procedure to develop a trajectory for a desired task is introduced. The modeling issue for a four wheeled mobile robot is conducted. In order to track the desired trajectory, the controllers for heading speed and steering angle of the mobile robot are created. Moreover the parts, which are related to unmodeled slippage, unmodeled and unestimated parts of the overall system model, are introduced into the system so that more robust and stable trajectory tracking control can be achieved. In addition to achievement of better trajectory tracking, long distance trajectory tracking missions can be performed. The experiments related to this chapter is presented in Chapter 7.

CHAPTER 6

IMPROVING TRAJECTORY TRACKING CONTROL OF A MOBILE ROBOT WITH SLIP ESTIMATION

6.1 Introduction

As stated in the previous chapters, trajectory tracking accuracy and performance is determined by the efficiency of the modeling studies. In the mobile robot applications, especially in the field tasks, tracking a desired trajectory depends on knowledge about interaction between the wheels and surface. The most important parameters in such a case is slippage. In order to get more accurate tracking results, slippage should be estimated and fed into the system model so that the required control action to decrease the trajectory error can be activated.

In this part of the study, a slippage modeling and estimation procedure are introduced. Slippage information is combined with the system model. A backstepping-based controller, which is introduced in the previous chapters, to drive the vehicle along a desired trajectory tracking is described with combining the slippage information. These procedures can be summarized as follows: Kinematic model of the vehicle is used to derive a model-based controller, and a set of Lyapunov functions are used to guarantee (in theory) convergence of the error along the planned path to zero. Next, an estimator is used to feedback sideslip velocity information to the controller.

The methodology introduced in this chapter indicates that the combined model-based controller plus slippage estimator is expected that it improves path tracking error. The theoretical backgrounds of sideslip estimation, desired trajectory generation and trajectory tracking control methodologies are also presented in this chapter.

6.2 Related Studies

In [Grip et al., 2009], a sideslip observer for a four wheeled vehicle is developed. The proposed approach considers the nonlinearities of the system dynamics. The model developed is implemented in a vehicle and tested. In [Baffet et al., 2008], in order to enhance vehicle safety, dynamic variables of a vehicle are estimated by using a proposed estimation procedure. In addition to estimating longitudinal and lateral tire forces, the process focuses on heading velocity and sideslip angle of the vehicle. The estimation process works with the real-time sensor information. The sensor information also enables to obtain the change in the cornering stiffness values. In [Iijima et al., 2010], a new perspective for estimating sideslip angles is proposed. In the methodology, drive recorder is used to especially improve the traffic safety. The sideslip estimation process merges the information of velocity, acceleration and yaw rate of the vehicle. It doesn't need to use the steering system information during the estimation that is in progress. In [Ryu et al., 2002], vehicle sideslip angle is estimated by using an integration of GPS and INS. The method developed uses the dynamics effects of the vehicle. In [Matveev et al., 2010], autonomous path tracking for the farm vehicles which are affected by the wheel slips are focused. The proposed control algorithm is presented by the results of simulations. In [Lenain et al., 2006], an estimator for sideslip angles is introduced. The process is fed by a high accuracy positioning system namely RTK-GPS. The proposed methodology is implemented in an agricultural application covering a path tracking objective. In [Lenain et al., 2010b], an integration of backstepping kinematic and dynamic observer is introduced. This integration is used for estimating the slippage parameters. The parameters estimated are adopted in the system so as to get improvement for high speed navigation. In [Dakhlallah et al., 2008], a procedure to estimate the friction coefficient and sideslip angle is proposed. The procedure having the parameters estimated is implemented in order for achieving safe driving. In [Eaton et al., 2009a], a trajectory tracking control methodology for an agricultural tractor used in an agricultural mission is introduced. It is considered that the tractor is under the effects of slippage. In order to track the desired trajectory with minimum tracking error and maximum safety, a robust sliding model control approach is developed with inclusion of slippage effects. In [Chen and Hsieh, 2008], a sideslip estimation methodology is proposed by using the vehicle's kinematic model. In [Lindgren et al., 2002], an autonomous guided agricultural vehicle is modeled by including slippage in order to improve the positioning obtained via dead reckoning. A traction model is also adapted into the modeling studies.

It is stated that introducing slip parameters in the model enables the higher navigation accuracy than the results obtained by using only odometer. In [Anderson and Bevly, 2004], an estimation procedure for slip angles is proposed by using a model based approach together with a GPS-INS couple.

6.3 Aim of the Study Related to Improvement of Desired Trajectory Tracking

The objective of this study is to make an improvement related to the trajectory tracking control of a mobile robot by including the effects of slippage. In order to accomplish this objective, a slippage estimator is developed and adapted into the system model which is created by using the basis of car-like robot approach. Appropriate controllers for steering and driving systems are developed by using the methodology of backstepping controller. The whole system is assumed that it is to be implemented into a four-wheeled mobile robot. The front wheels of the robot are steerable. It is also assumed that a positioning system is used in order to estimate the slip velocities of the wheels in longitudinal and lateral directions.

The outline of this chapter is as follows: Kinematic modeling steps are given in the next part of the chapter. Estimation procedure of the slippage is introduced in part 5. Then desired trajectory generation and controller development steps are given in part 6. The conclusion and discussions are presented in the last part of this chapter.

6.4 Kinematic Modeling

Consider a four-wheel mobile robot given in Figure 5.1. Its goal is to follow a desired trajectory. In order to design required trajectory tracking controller, the mobile robot is modeled as a kinematic platform. The estimation process of the slippage is constructed by using this kinematic approach as well. The modeling representation without containing slippage information is given by Equation 5.1. This equation would be given to recall the system as:

$$\begin{aligned} \dot{x}_d &= \upsilon_d \, cos\theta \\ \dot{y}_d &= \upsilon_d \, sin\theta \\ \dot{\theta}_d &= \tfrac{\upsilon_d}{L} \, tan(\phi_d) \end{aligned} \tag{6.1}$$

x and y are the Cartesian coordinates of the center of the rear axle in an inertial reference frame, θ is the mobile robot orientation with respect to that frame, ω is the vehicle angular speed, ϕ is the steering angle, and υ is the forward speed (Figure 5.1). Distance between front and real axels is shown by L. Front axle coordinates are presented by x_f and y_f in this Figure.

Slippage can be included into the kinematic model given in Equation 6.1 by introducing longitudinal and lateral slip velocities. These slippage effects may be caused from due to slippery and inclined surface, unmodeled and uncertain parts. Longitudinal slip velocities at front and rear wheels are indicated by V_{LF} and V_{LR}, respectively (Figure 6.1). Lateral components of these slip velocities are shown by V_{SF} and V_{SR}, respectively. Slip angles at front and rear axles are described by β_F and β_R, respectively. Desired trajectory is illustrated by $C(s)$ (see Figure 5.3). Desired position and orientation values are defined by (x_d, y_d) and θ_d, respectively. Center of turning arc is shown by A. R is the radius of this arc. Lateral error that specifies the distance to the desired trajectory of the mobile robot is defined by y_L. The objective should always be to keep this value close to zero. Slip velocities can be inserted into the kinematic model of the mobile robot as follows ([Lenain et al., 2010b], [Fang et al., 2006], [Eaton et al., 2009a]):

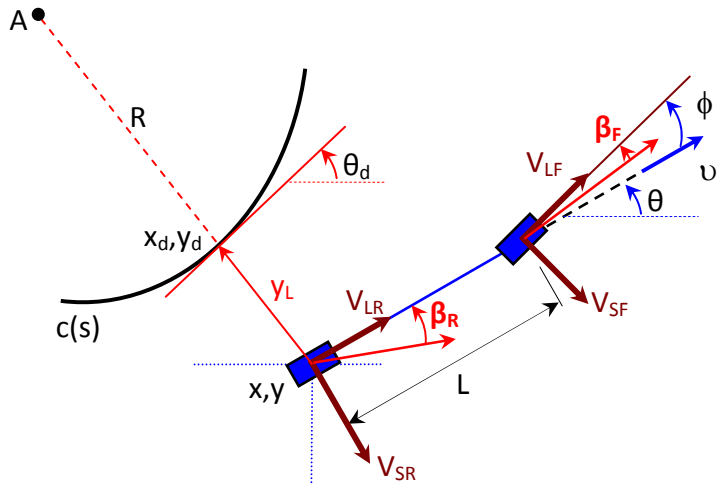

Figure 6.1: Representation of effects of slippages [Lenain et al., 2010b].

$$\begin{aligned} \dot{x}_d &= \upsilon_d \cos\theta - V_{LR}\cos\theta - V_{SR}\sin\theta \\ \dot{y}_d &= \upsilon_d \sin\theta - V_{LR}\sin\theta - V_{SR}\cos\theta \\ \dot{\theta}_d &= \frac{\upsilon_d}{L} \tan(\phi_d)\Big(\tan\beta_R + \tan(\phi - \beta_F)\Big) \end{aligned} \tag{6.2}$$

It is assumed that the mobile robot follows a desired path $q = [x_d, y_d, \theta_d]$. Considering the description given in Figure 5.2, longitudinal (x_e), lateral (y_e) and orientation errors (θ_e) are derived as given in Equation 5.2.

Error dynamics of the system can be derived as follows:

$$\begin{aligned} \dot{x}_e &= -\upsilon + \omega y_e + \upsilon_d cos\theta_e + \varepsilon_1 \\ \dot{y}_e &= \upsilon_d \ sin\theta - \omega x_e + \varepsilon_2 \\ \dot{\theta}_e &= \upsilon_d C(s) - \tfrac{\upsilon}{L} \ tan(\phi - \beta_F) + \varepsilon 3 \end{aligned} \tag{6.3}$$

6.5 Sideslip Angle Estimation

The sideslip representation is described in Figure 6.1 and Equation 6.2. Trajectory tracking accuracy, forward velocity and steering angle of the mobile robot are affected by the slippage. Whenever there is slippage, the mobile robot might move away from the desired trajectory that causes positioning error. For achieving a desired trajectory tracking, amount of slippage (sideslip angles) should be detected, estimated and fed into the system model in an ideal case (see Figure 6.2). In order to estimate front and rear sideslip angles that are indicated by β_F and β_R, respectively, longitudinal and lateral components of these angles should be obtained first. Then they are included into the system model.

Sideslip angle estimation is proposed in [Lenain et al., 2010b]. It includes an observer which is combined with the system model. The procedure uses the path tracking parameters to accomplish the estimation process. In our study, the sideslip estimation process proposed is inspired by the studies proposed in [Lenain et al., 2010b]. It is assumed that there is a positioning system located in the mobile robot which is able to give accurate position data. This system might be a high accuracy positioning system like DGPS or a dead reckoning system including high resolution encoders. In order to estimate the slippage parameters, sideslip estimation procedure is constructed according to the information coming from this position information (see Figure 6.2). In the estimation process, two variables (β_F and β_R) should be estimated. Hence two observed variables are associated with the model shown by $\prod_{obs} = (x, y)_{obs}$. It is also taken into account that the control structure is constructed to satisfy the convergence of observed values, $\prod_{obs}$ to the measured values, $\prod_{mes} = (x, y)_{mes}$. It is

assumed that as long as the positioning system continuously supplies position values, steering and odometer systems give steering angle and forward velocity of the mobile robot; the following observation system can be proposed.

$$\begin{pmatrix} \dot{x}_{obs} \\ \dot{y}obs \end{pmatrix} = \begin{pmatrix} \upsilon - \tilde{V}_{LR}cos\theta - \tilde{V}_{SR}sin\theta \\ \upsilon - \tilde{V}_{LR}sin\theta + \tilde{V}_{SR}cos\theta \end{pmatrix} \tag{6.4}$$

where $\tilde{V}_{LR}$ and $\tilde{V}_{SR}$ are the observed values of longitudinal and lateral slip velocities at the rear axel of the mobile robot, respectively. Equation 6.4 can be rearranged as follows:

$$\begin{pmatrix} \dot{x}_{obs} \\ \dot{y}obs \end{pmatrix} = \begin{pmatrix} \upsilon cos\theta \\ \upsilon sin\theta \end{pmatrix} + \begin{pmatrix} -cos\theta & -sin\theta \\ -sin\theta & cos\theta \end{pmatrix} \begin{pmatrix} \tilde{V}_{LR} \\ \tilde{V}_{SR} \end{pmatrix} \Rightarrow P = A + Bu \tag{6.5}$$

Observation of slip velocities indicated by u in Equation 6.5 can be written the following form [Lenain et al., 2010b]:

$$u = B^{-1}\Big([G][e] + [\dot{\Pi}_{mes}] + [P] - [A]\Big) \tag{6.6}$$

where e represents the observation error defined by $e = \Pi_{obs} - \Pi_{mes}$. Error dynamics of the estimation process is specified by $[\dot{e}] = [G][e]$. G is a (2x2) matrix and considered as a Hurwitz matrix that determines the observer gain regulating the settling time. Matrix G is set up as a diagonal matrix so that the convergence of two variables observed can be decoupled. In this study it is assumed that the sideslip angle at the front is negligible ($\beta_F \approx 0$) since the mobile robot runs at low speed, the steering system is controlled efficiently and does not have any mechanical defects.

6.6 Design of Desired Trajectory and Controller

Remember that in Chapter 5 in addition to development steps of desired trajectory, the model based controller design strategy is introduced. To make a refreshment about the controllers for the heading velocity and steering angle of the mobile robot, the followings have been designed and given in Equation 5.19:

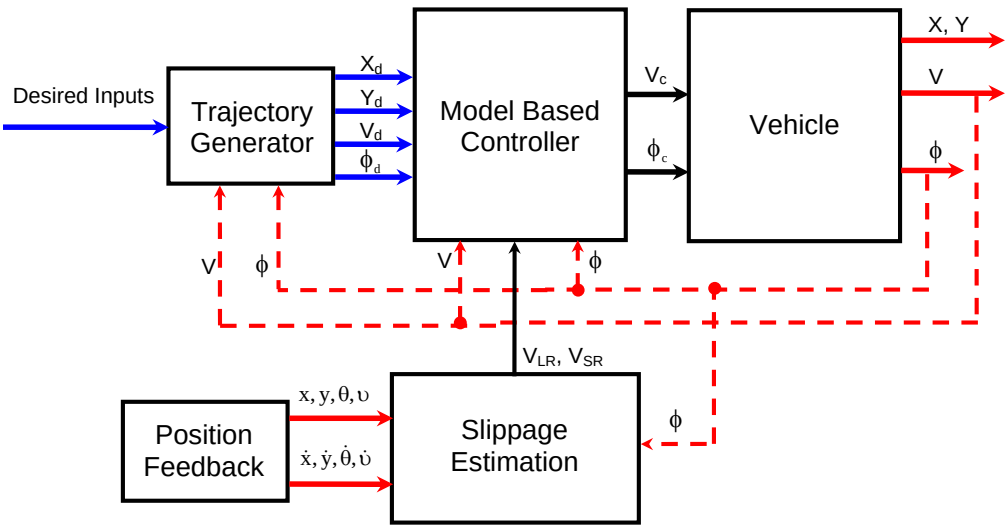

Figure 6.2: Control system chart

$$\upsilon_c \geq \upsilon_d cos(\theta_e) + k_x x_e + \tau_1 x_e \Big(f(\Upsilon_1, sin\theta) \Big)^2$$
$$\phi_c = atan(\tfrac{L\omega}{\upsilon}) \tag{6.7}$$

where ω is illustrated in Equation 5.17. In Chapter 5, turning strategy, which is simple to implement and yields natural looking turns is also mentioned and given in detailed steps. The control chart of the system is given in Figure 6.2. In this chart, it is shown that trajectory generator block works according to the desired inputs. Model based controller block uses the feedback coming from slippage estimation block.

6.7 Conclusion and Discussions

In this part of the study, the four wheeled mobile robot system is introduced with a system that contains the slippage information. The trajectory development procedure is updated according the information about slippage. Slippage is described in terms of front and rear wheel slip velocities. In order to obtain these slip velocities, an estimation procedure is proposed. This process is also combined with the overall system model. The trajectory tracking control strategy is adapted into this system as well. The experimental studies about the procedure introduced in this chapter are to be given in Chapter 9.

CHAPTER 7

FIELD STUDY-1: TRAJECTORY TRACKING CONTROL OF A MOBILE ROBOT FOR AN ORCHARD APPLICATION USING A HIGH ACCURACY POSITIONING FEEDBACK

7.1 Problem Statement

This field study is a part of autonomous orchard application project. Desired trajectory tracking objective has been previously performed by using a non-model based approach in this project. Long distance autonomous drive has been achieved, however the results haven't met the expectations of the project requirements. In order to provide these requirements, this study is conducted. In this study, long distance autonomous trajectory tracking for an orchard vehicle is studied. Besides longitudinal motion, lateral motion of the vehicle is also considered. The longitudinal and lateral errors are objected to keep into a region of less than 10 cm. The details of the modeling studies are given in chapter 5. Here are the reminders; Car-like robot kinematic modeling approach is used to create desired trajectory. In order to control longitudinal velocity and steering angle of the vehicle, a controller methodology is proposed. Stability of the controller proposed is shown by using Lyapunov stability approach. The proposed model is adapted into a four-wheeled autonomous orchard vehicle and tested in a nursery for long distance autonomous drives. More than 15 km autonomous drive is successfully achieved and the details are presented in this chapter.

In agricultural areas, autonomous orchard applications have been gained in the last decade because the needs have been increasingly changing. This brings necessity of new autonomous orchard solutions. Autonomous orchard navigation is one of the main concern in the agricul-

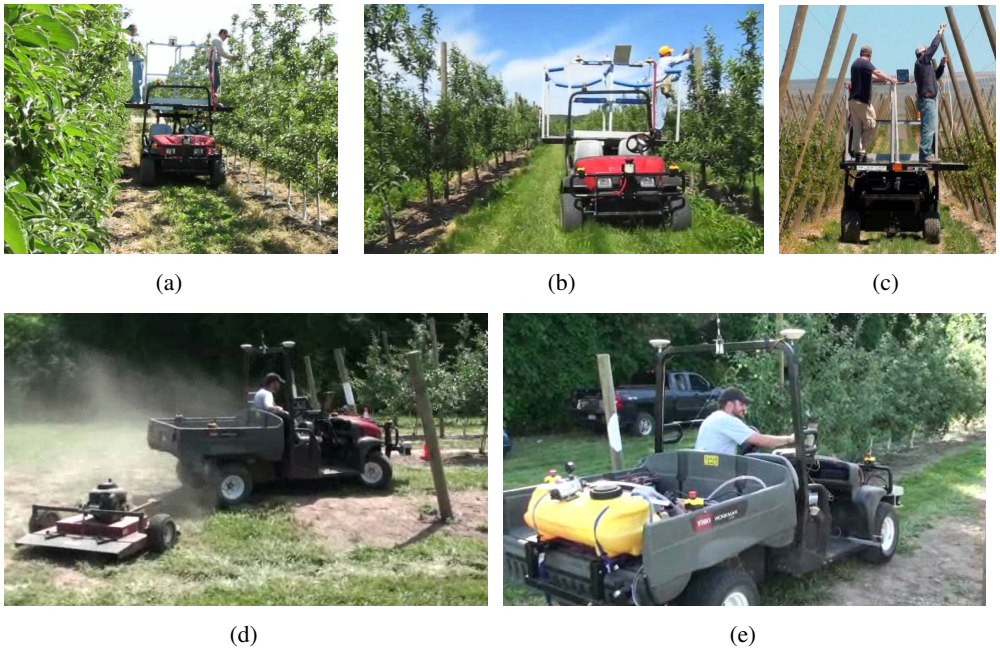

(a) (b) (c)

(d) (e)

Figure 7.1: Some examples for autonomous orchard navigation, (a) Harvesting, thinning, (b) Pruning, (c) Tree tying, (d) Cover crop mowing, (e) Spraying. In (d) and (e), the human is onboard for safety reasons and is not driving the vehicle

tural area. It can be considered into two subgroups. The first group is automated operations like mowing (7.1-d), spraying (Figure 7.1-e), etc. The second group is augmented operations like pruning (Figure 7.1-b), thinning (Figure 7.1-a), harvesting (Figure 7.1-a), tree tying (Figure 7.1-c), etc. In order to perform these operations, the autonomous vehicle should be able to follow a desired trajectory into a predefined error region. The studies related to autonomous orchard applications are generally conducted for short distance autonomous drive. However, long distance autonomous drives are needed into the orchard having long length rows of trees.

In this stıudy, APM based autonomous vehicle is aimed that it has to follow a desired trajectory in an orchard. The autonomous vehicle should move on a center line that shows the line between two consecutive rows of trees. In order to achieve this objective, two solutions have been targeted. One of them is detecting the trees and rows of trees by using laser scanning range finder. The second solution is performing a mapping operation to get the earth positions of the rows of trees, creating a desired trajectory and tracking by using an appropriate controller. In this solution position feedback is taken from a positioning system.

One of the solution for such a study is pure pursuit methodology. In [Hamner et al., 2011], [Singh et al., 2009], [Singh et al., 2010], the autonomous orchard tasks are achieved by using

the sensors like laser scanning range finder, odometer and steering encoder. Long distance trips have been performed. The solution covers detecting of rows of trees by using a particle filter and tracking the desired path by using simple pure pursuit controller. Pure pursuit controller controls only steering angle. It is not be able to control the forward velocity of the vehicle. Lateral error, distance between the vehicle and the center line, could have been achieved in a range more than 10 cm. This amount of error causes sharp turning of steering system and more steering angle error than desired.

One of the most challenging issue of autonomous driving in an orchard is turning between two center rows. In the first solution described just above, turning operation has been performed by using K turn (three point turn) strategy. This strategy doesn't contain any information related to the characteristics of the steering actuator and system. Unfortunately, this can easily cause to give damage to the steering system since the methodology used in the first solution does't control the change of steering angle speed.

In order to make enhancement over the first solution, this study, second solution, is conducted. In this study, a new model based trajectory generation algorithm is proposed, which is introduced in Chapter 5. The controllers for adjusting heading velocity and steering angle of the vehicle are developed by using backstepping approach. The stability of the overall system is observed by using Lyapunov stability theory. In order to achieve a natural turning operation in the orchard, a circular bulb turning methodology is proposed. It is created according to the characteristic information of the steering system containing steering actuator. In the processes of desired trajectory generation, tracking and control, the characteristic of the steering system is taken into consideration in order not to give any damage to the steering system.

The earth positioning information of the rows of trees are firstly obtained by using a mapping stuff. According to this mapping results, desired trajectory is created. In the experimental site where all the experiments have been conducted, there are 8 rows of trees and 7 center lines (rows). It is aimed that the vehicle should move on the center rows. At the end of each center row, it should perform the turning operation to pass the neighbor center row. At the end of the seventh row, the vehicle should continue its trip without stopping and pass the next row. This autonomous trip should continue until the desired trip distance is covered.

The following objectives are aimed in the solution procedure:

- Long distance autonomous drive should be performed in the experimental orchard. The longitudinal error should be less than 10 cm.
- On the other hand, the lateral error (distance between the vehicle and the center row) should be less than 5 cm.
- A natural turning operation between two center rows should be achieved.
- The steering angle speed should be under control during turning operation.

In this study, long distance autonomous desired trajectory tracking experiments are conducted in an experimental nursery located in Robot City area of Pittsburgh, PA, USA. The nursery has 8 rows of trees that are in line (and 7 center rows). Each row has a length of about 53 m. The width between two rows of trees is nearly 4 m. As the aim of long distance autonomous drive, the vehicle should move in the center row, which indicates the center line between two parallel rows of trees, and enter the next row. At the end of the last row (7^{th} row), it should continue its motion by entering the neighbor row so that the autonomous motion should continue infinitely. A bulb turn strategy that is constructed by using three tangent circles is used for turning between the rows.

Figure 7.2: Toro MDE eWorkman based autonomous vehicle

The experiments are performed by using a Toro MDE eWorkman based autonomous vehicle shown in Figure 7.2. High resolution encoders are attached to the steering and the driving systems of the vehicle. A high accuracy Applanix PosLV positioning system is also mounted to the vehicle in order to provide the ground truth. Steering system is controlled by using a

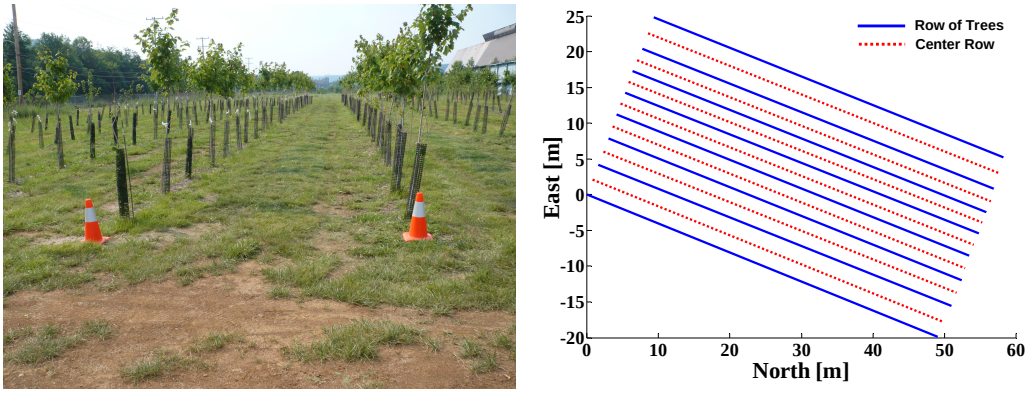

(a) (b)

Figure 7.3: Test field (a) a scene from the field, (b) structure and orientation of the field

stepper motor connected to the steering axle by a chain. The vehicle uses a electrical motor, which is originally placed at the rear axle of the vehicle, and its controller. The speed control is achieved by commanding this controller. All the computational and communication works are performed under the Linux-ROS (Robot Operating System) platform.

7.2 Desired Trajectory Generation for Autonomous Drive in the Orchard

In this work, the aim is achieving long distance autonomous drive in an experimental nursery. The nursery shown in Figure 7.3-a has 8 line of trees (each line has nearly 35 trees) and 7 center rows to be autonomously covered. Figure 7.3-b shows the earth positioning of the nursery. As seen in this figure, solid and dashed lines show the rows of trees and center lines (rows), respectively. Each row has nearly length of 53 meters and width of 4 meters. However row lengths and row widths are not same in each line.

In order to drive the vehicle autonomously in this nursery, a desired trajectory has to be constructed. Straight line and circular motion velocities (V_1, V_2) should also be specified. They are set as 1 m/s and 0.5 m/s, respectively in this study. There are four steps for designing the desired trajectory. The first step is designing the path crossing the rows. Second step is generating the suitable steering angle for the vehicle. In Figure 7.4-a, desired path representation is given. In order to generate this path, the steering angle is obtained as given in Figure 7.4-b (dashed line). As seen in this figure, the change of steering angle between different motions are dangerously sharp. This kind of steering behavior can't be acceptable. Because of that,

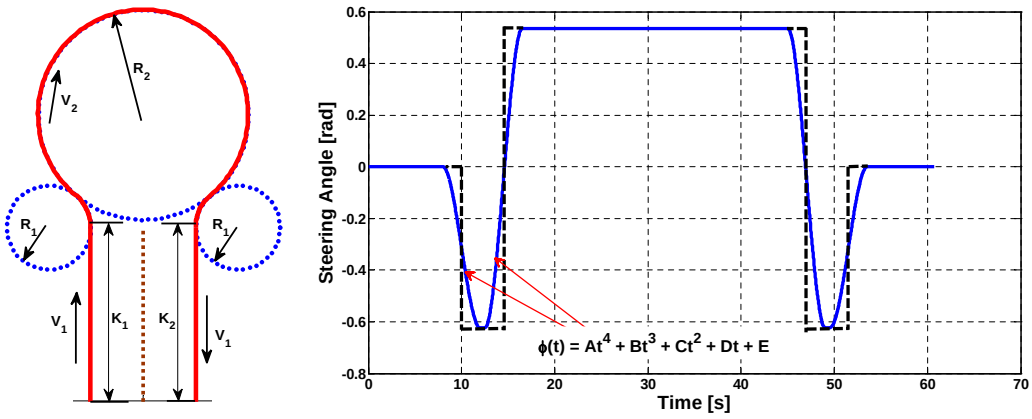

(a) (b)

Figure 7.4: Desired trajectory (a) and steering angle (b)

such sharp changes of steering is not preferable for the actuator lifetime, and can break down the actuator easily. In order to solve this problem, a polynomial representation that is a fourth order polynomial is adapted to the steering change as shown in Figure 7.4-b (solid line). This representation is shown as:

$$\phi(t) = At^4 + Bt^3 + Ct^2 + Dt^2 + E \tag{7.1}$$

where t and ϕ denote axes of time and steering angle, respectively. Coefficients of the polynomial A, B, C, D, and E are determined according to the steering system characteristics. In addition to give safe steering motion to the steering system during turning, the steering speed can also be controlled by using this mathematical representation. This steering angle definition can be used in both straight and turning motions. In the steering angle design process, it is the most significant requirement that $max(\dot{\phi}_d(t)) \leq \Gamma$ where Γ is the steering motor rating.

As introduced in the control diagram of the overall control system given in Figure 8.9, the control system chart of this study is illustrated in Figure 7.5. The feedback information shown in this figure (X_{PS}, Y_{PS} and θ_{PS}) are coming from a high accuracy positioning system, called RTK-GPS (real time kinematic-GPS).

In order to achieve desired trajectory tracking objective into the predefined error regions, desired trajectory is divided into three regions (see Figure 7.4-a). These regions are straight parts, presented by K_1 and K_2 (*Part-1*), small angle circular parts, shown by R_1 (*Part-2*), and

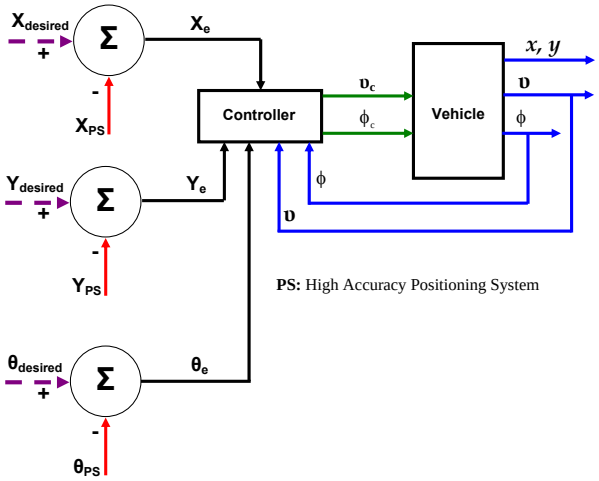

Figure 7.5: Control system of desired trajectory tracking task

large angle circular part, indicated by R_2 (*Part-3*). Development steps of the controller are given in chapter 5 in detail. All the details and information can be found in that chapter. As given in chapter 5, appropriate functions for $\lambda_1(t)$ and $\lambda_2(t)$ are chosen according to the characteristics of the vehicle used in the experimental side. (Note that sets of controller parameters (k_x, k_y, k_Ω) are chosen according to the definition introduced in Equation 5.9.) The values of τ_1 and τ_2 are also selected in agreement with the system behavior.

7.3 Experimental Studies

In order to perform desired trajectory tracking task in an experimental orchard, first a mapping study has been conducted. Mapping study has been given the position and orientation information of the experimental field. Then desired trajectory has been constructed by using this information. The detailed experimental results illustrating the desired trajectory tracking performance are given in the following sections.

7.3.1 Mapping Study

As stated above, the experiment site shown in Figure 7.3 locates at the robot city area in Pittsburgh, PA, USA. The surface is a mix-type terrain and includes some inclined parts. In order to find the exact lengths and widths of each row, a mapping work is conducted. In order

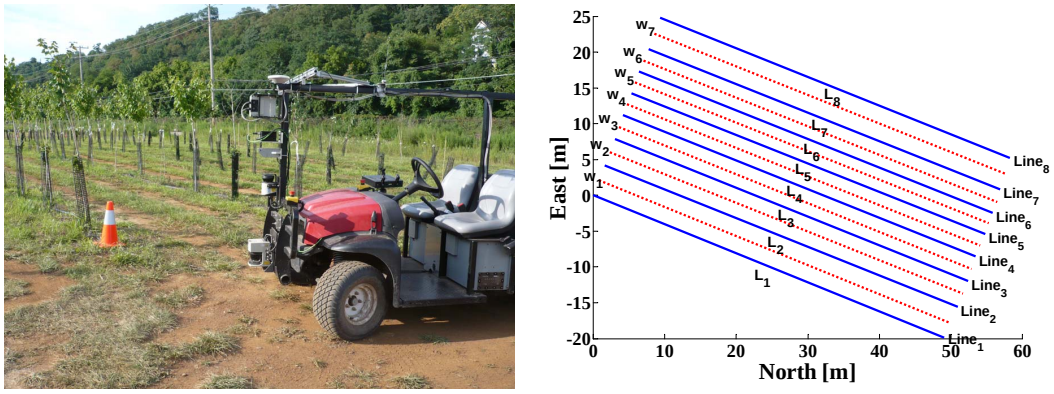

(a) (b)

Figure 7.6: Mapping study conducted in the orchard

Table 7.1: The real values of length and width of each rows

	L_1	L_2	L_3	L_4	L_5	L_6	L_7	L_8
Row Length [m]	52.95	53.15	53.14	53.16	53.22	53.27	52.93	53.11
	w_1	w_2	w_3	w_4	w_5	w_6	w_7	
Row Width [m]	4.44	3.98	3.51	3.24	3.19	3.39	4.72	

to perform mapping stuff, reflected cones, which are used for getting reflection through laser scanner, are located at the beginning of each tree lines (see Figures 7.3 and 7.6). Reflection amount of laser scanner and position information coming from positioning system are used together to complete the mapping stuff. The resulting mapping of rows of trees is shown in Figure 7.6-b. In Figure 7.6-b, rows of trees are shown by blue solid lines. The centers of two consecutive tree lines (rows) are indicated by red dashed lines. Length of each tree row is denoted by L_i, $i = 1, 2, ..., 8$. Width of each consecutive tree rows is presented by w_j, $j = 1, 2, ..., 7$. The numerical vales of lengths and widths are given in Table 7.1. Length of the center lines (indicated by red dashed line in Figure 7.6-b) can be easily calculated by using the numerical information given in this table.

7.3.2 Orchard Experiments

In this nursery, more than 15 km autonomous drive have been achieved. In this part of the study, results of 5 runs of autonomous drives are given. These runs are 0.5 km, 2.5 km, 3.5 km, 4 km and 4.2 km. They are completed without stopping and human intervention. The

total driving distance of the 5 runs including the turnings is about 14 km. Note that desired speeds in straight and circular parts of the desired trajectory are set to 1.0 m/s and 0.5 m/s, respectively.

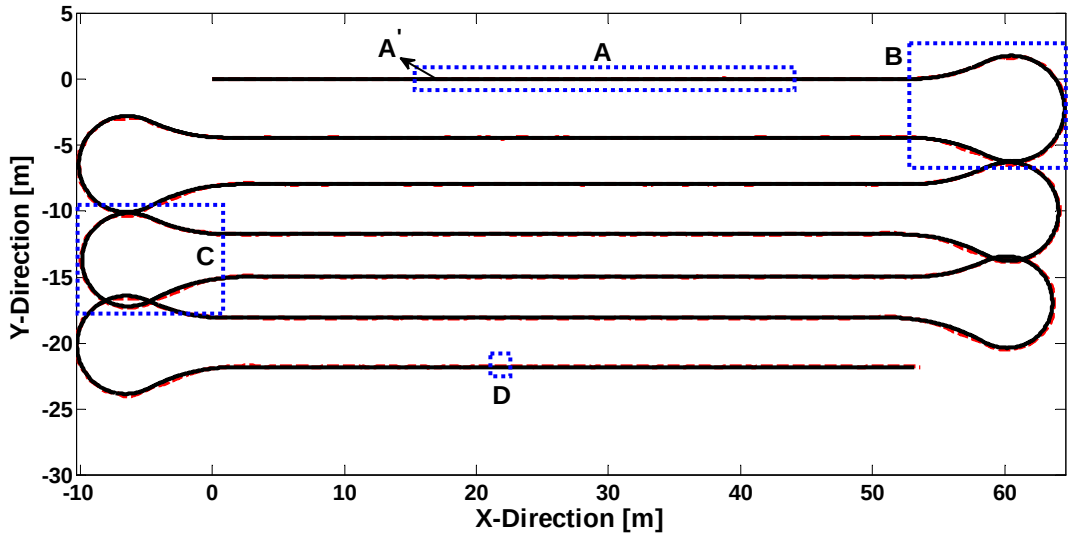

Figure 7.7: 0.5 km autonomous drive in the orchard

The first autonomous drive results are related to 0.5 km distance. It is not a long distance autonomous drive. However, it is given that the details of the motion can be easily realized. The desired and experimental trajectories are shown in Figure 7.7. They are indicated by solid and dashed lines, respectively. In order to show the details, four subregions are specified. They are shown by dashed boxes and letters, A, B, C, D. The regions A and D present the straight motions. The turning motions are specified by letters B and C.

The zoomed in views of the specified regions A$'$, B, C, and D are presented in Figures 7.8-a, 7.8-b, 7.8-c, and 7.8-d, respectively. Note that dimensions are given in meters in these figures.

The error values in x and y directions that are the differences between the desired and actual trajectories are given separately. In Figure 7.9, error values related to straight motion (specified by region A in Figure 7.8) are presented. On the other hand, error values obtained in turning motion (specified by region B in Figure 7.8) are indicated in Figure 7.10. In these two figures, x and y represent longitudinal and lateral motions, respectively (Figure 5.1 may be seen for recalling the coordinate axes set).

In Figure 7.11, desired and actual steering angles, which generate the trajectories shown in

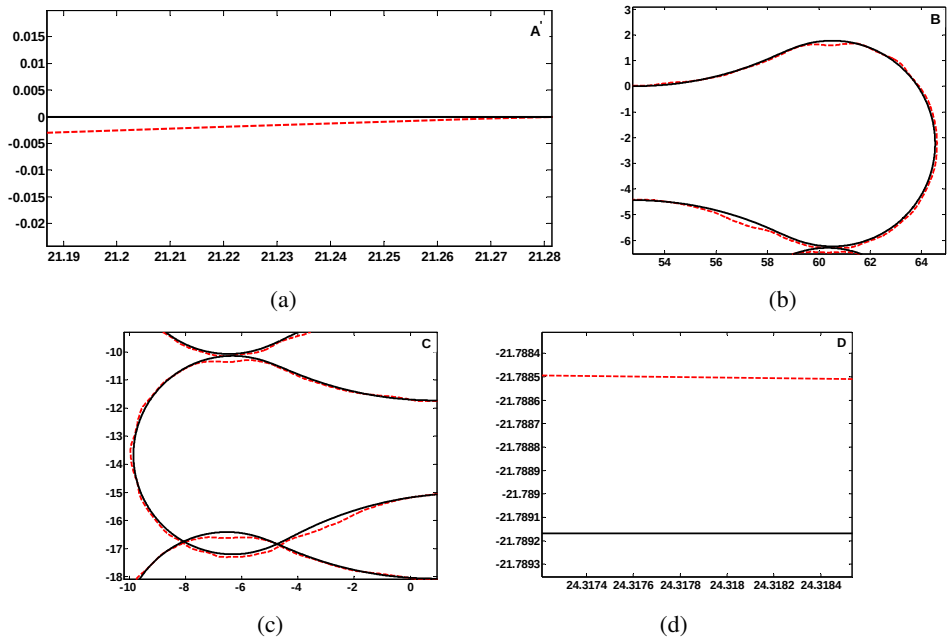

Figure 7.8: Zoomed in views of the regions ($A^{'}$, B, C, D) of 0.5 km autonomous drive. Desired and experimental trajectories are specified by solid and dashed lines, respectively.

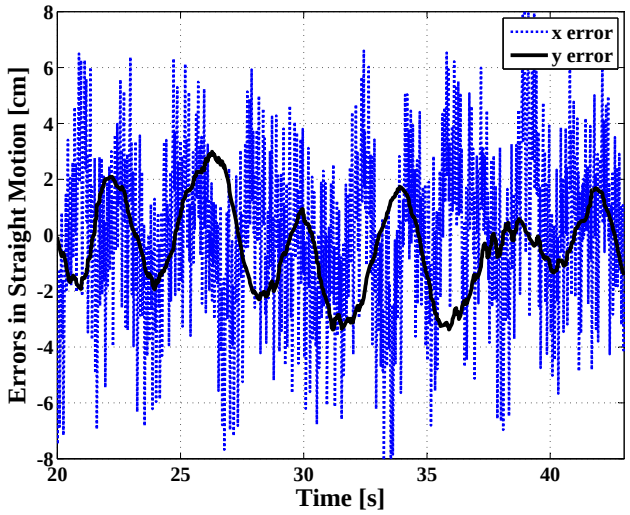

Figure 7.9: Errors in straight motion for 0.5 km autonomous drive - Region A

Figure 7.7, are represented. They are specified by using solid and dashed lines, respectively. In order for a clear view, results containing first 200 seconds (two completed rows (straight) and turning motions) are given. Steering angles, shown in this figure, command the vehicle to complete straight lines and turning motions.

Another experimental result related to 4 km autonomous drive completed in the orchard is

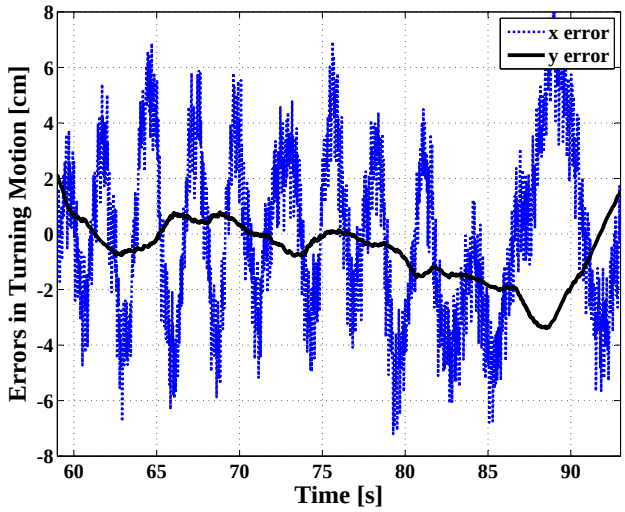

Figure 7.10: Errors in turning motion for 0.5 km autonomous drive - Region B

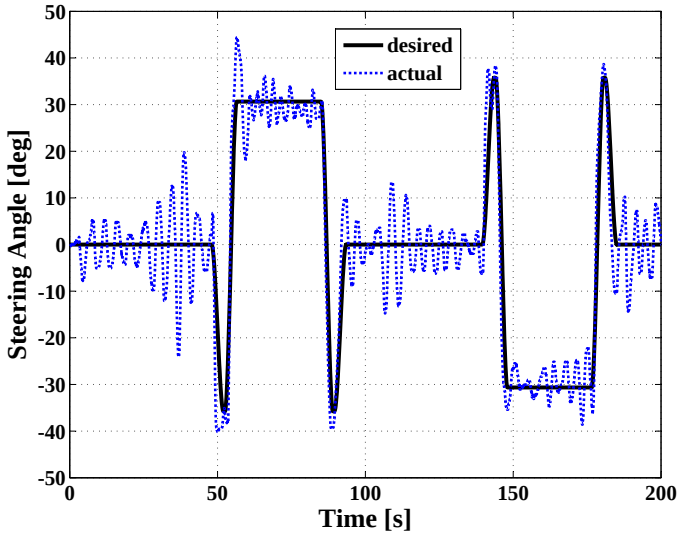

Figure 7.11: Steering angles obtained in the first 200 seconds for 0.5 km autonomous drive

presented in Figure 7.12. Desired and experimental trajectories are presented by dashed and solid lines, respectively. Both trajectories start from point (0,0). This trip takes nearly 1.3 hours in autonomous drive mode. The desired and actual steering angles, which produce these trajectories, are shown in Figure 7.13. Steering angle values which are obtained in the first 600 seconds are given in a zoomed view in order for creating a clear and detailed view.

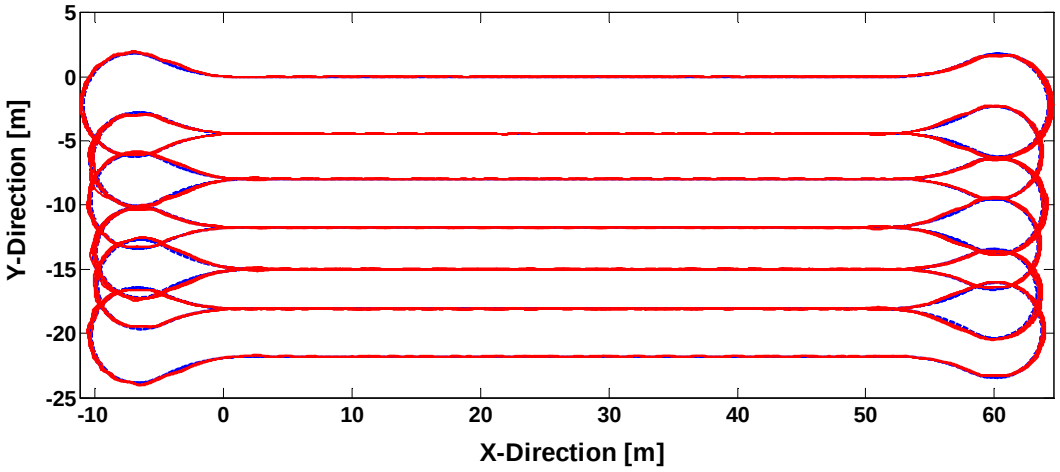

Figure 7.12: 4 km autonomous drive achieved in the orchard. Red and blue lines indicate actual and desired trajectories, respectively

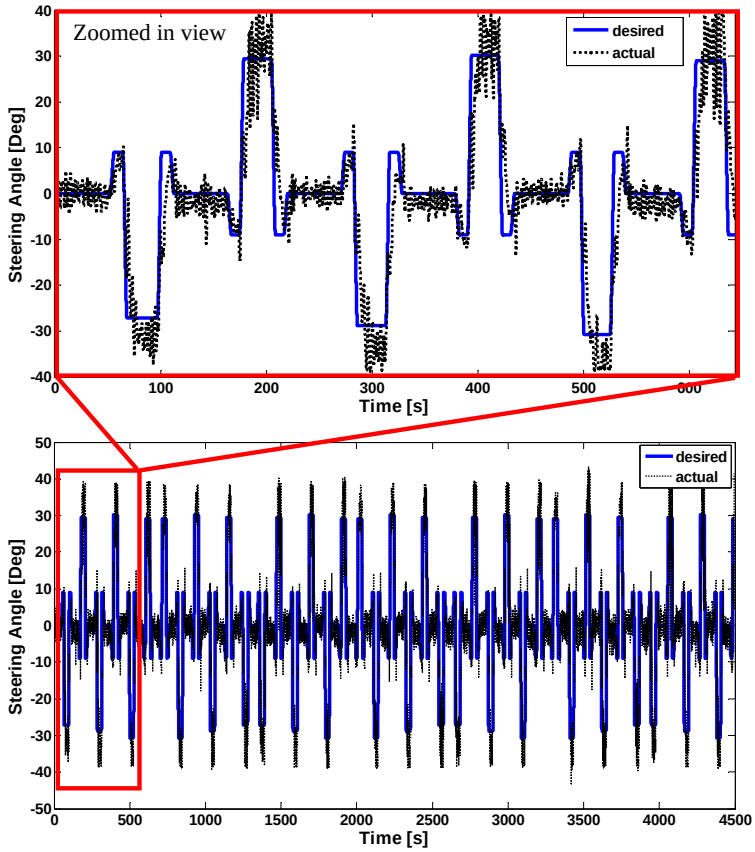

Figure 7.13: Desired and actual steering angles for 4 km autonomous drive (First 600 s time line is zoomed for a detailed view)

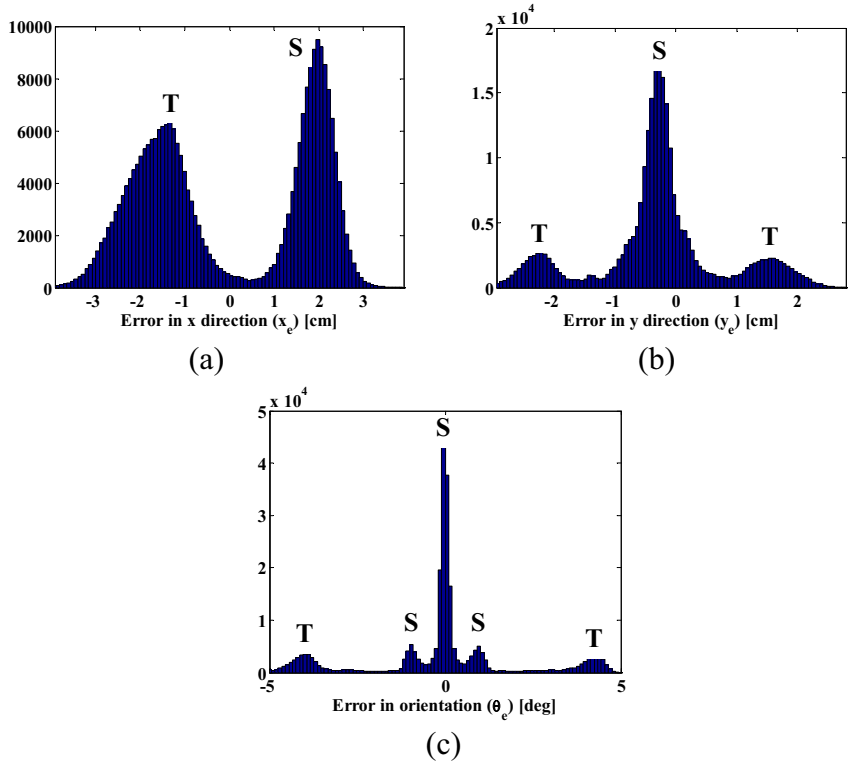

Figure 7.14: Positional and orientational errors for 4 km autonomous drive. S and T represent straight and turning motions, respectively

In order to show the position and orientation errors in 4 km autonomous drive, histogram plots are prepared. In Figure 7.14-a, error values for longitudinal motion, x_e, are presented. As seen in this figure, there are two peaks. The bigger peak represents the straight motion errors specified by S and the other peak specified by T is related to the errors of turning motion. Error values for straight motion are in the region of 0.5 and 4 cm. On the other hand that for turning motion are between -5 and 0.5 cm. Lateral errors, y_e, for 4 km autonomous drive are shown in Figure 7.14-b. The figure contains 3 peaks. The biggest peak indicates the straight motion errors indicated by S and the others specified by T are related to the errors obtained in turning motion. As indicated, the lateral errors are walking in the region of -4 and +4 cm. Figure 7.14-c is prepared to show the orientational errors, θ_e, for this autonomous drive. The error region is between -5 and 5 degrees. Orientational errors are observed in the region of -2, +2 degrees in the straight motion highlighted by S. The rest of the errors pointed by T shows the errors measured during the turning motion.

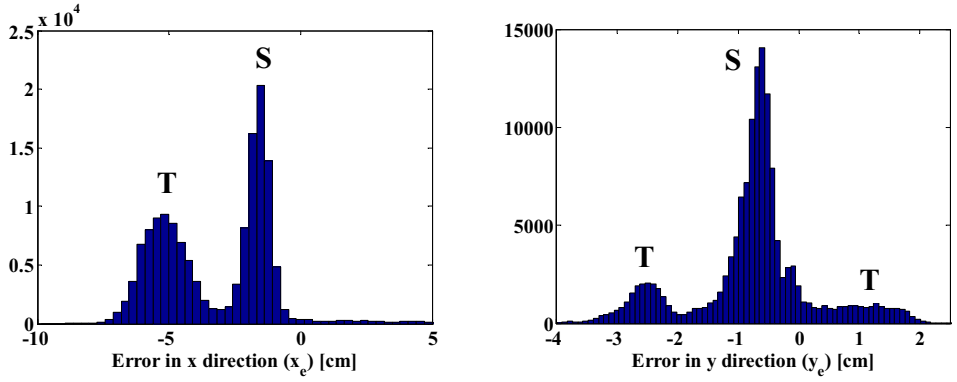

(a)

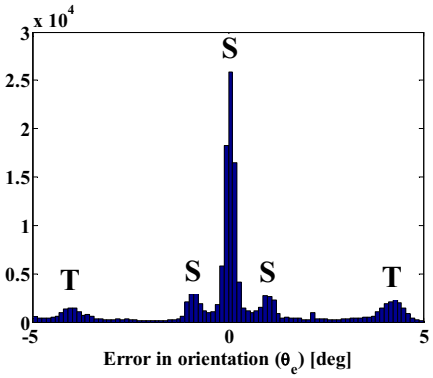

(b)

Figure 7.15: Positional and orientational error histograms showing 2.5 km autonomous drive. S and T represent straight and turning motions, respectively

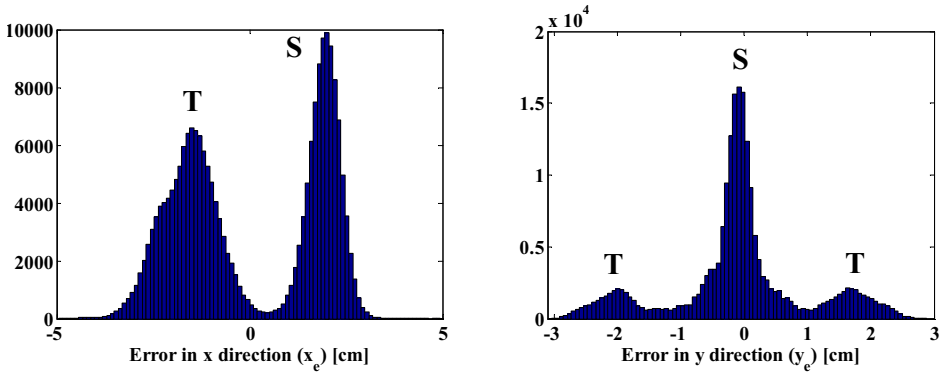

(a)

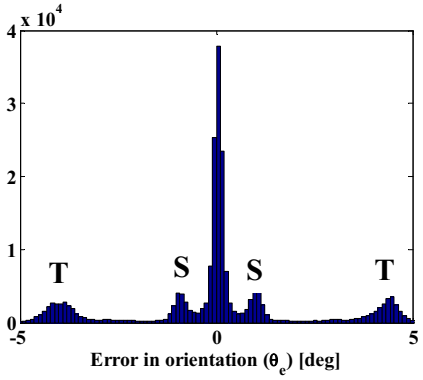

(b)

Figure 7.16: Positional and orientational error histograms showing 3.5 km autonomous drive. S and T represent straight and turning motions, respectively

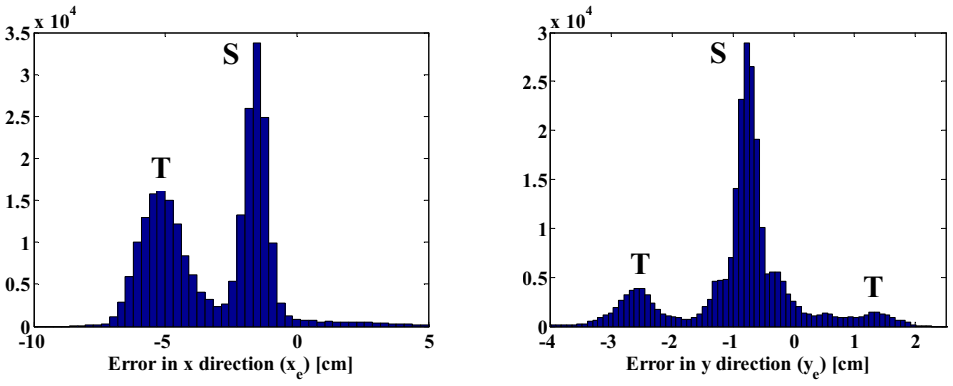

(a)

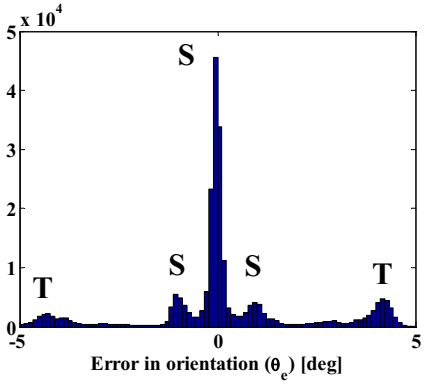

(b)

Figure 7.17: Positional and orientational error histograms showing 4.2 km autonomous drive. S and T represent straight and turning motions, respectively

Apart from 4 km long distance autonomous drive in the orchard, in the other three autonomous drives, 2.5 km, 3.5 km and 4.2 km distances are autonomously traveled. Error results associated with x-direction, y-direction and orientation (x_e, y_e and θ_e) are shown in Figures 7.15, 7.16 and 7.17. Figure 7.15-a and Figure 7.15-b are related to 2.5 km autonomous drive. Longitudinal errors of 2.5 km drive are presented in Figure 7.15-a, left. Lateral and orientational errors are given in Figure 7.15-a, right and 7.15-b, respectively. The error results related to 3.5 km autonomous drive are shown in Figure 7.16-a and Figure 7.16-b. Figure 7.17-a and 7.17-b are placed to indicate the errors obtained in 4.2 km autonomous drive. In all these figures, **S**traight and **T**urning motions are indicated by letters **S** and **T**, respectively.

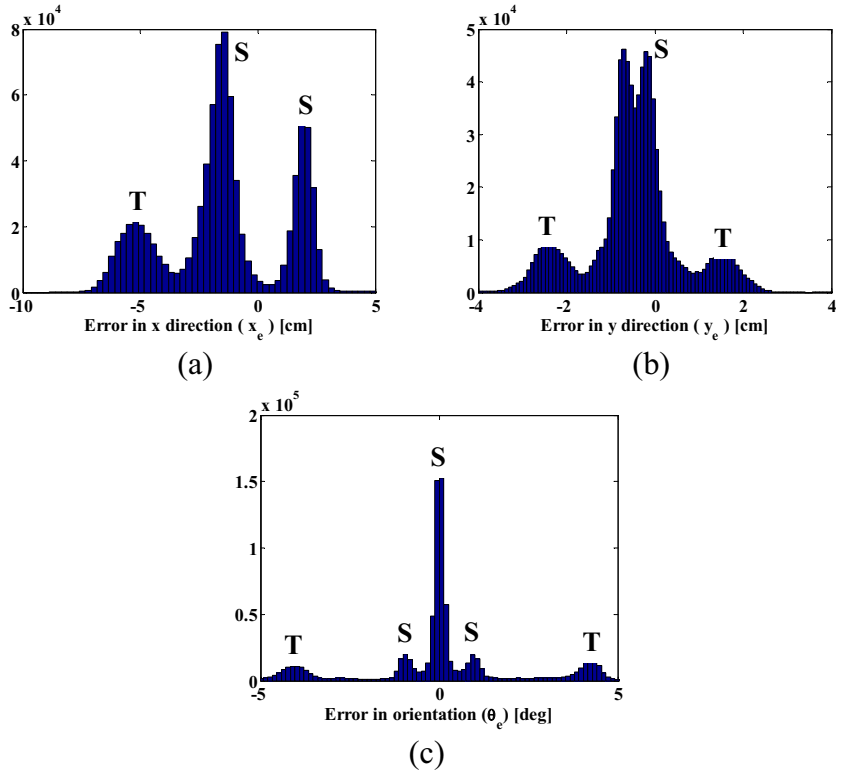

Figure 7.18: Positional and orientational error histograms showing 14.2 km autonomous drive. S and T represent straight and turning motions, respectively

In Figure 7.18, the results of all autonomous drives (0.5 km, 2.5 km, 3.5 km, 4 km and 4.2 km) are collected. They show the 14.2 km long distance driving results. Longitudinal, lateral and orientational errors (x_e, y_e and θ_e) are given in Figure 7.18-a, 7.18-b, 7.18-c, respectively. These results show the maximum and minimum error regions. It is observed that lateral errors, especially, are inside a desired error region that is less than ± 5 cm. This error region

is an objective outcome. Interpreting the lateral error results, the vehicle can follow a desired trajectory inside a safe region. In the straight part, it can be able to move on the center row (line). The sharp change of orientation is not observed since steering angle is always produced in a region of desired steering angle. The steering angle controller proposed can be able to steer the steering system so that the possibility of having any mechanical harm on the steering mechanism including steering actuator is decreased. This expands the usable life of steering mechanism. Longitudinal errors are also inside a desired error region. Velocity controller proposed controls the driving motor of the vehicle in an effective way. The maximum longitudinal error is observed less than 10 cm. This enables the safe motion of the autonomous vehicle in the agricultural area. The longitudinal velocity of the vehicle has to be inside a predefined region in the orchard because it is thought that people are going to be working around and/or on the vehicle. The less longitudinal and lateral errors produces less orientational errors (see Figure 7.18-c). In the straight part of the trip, the vehicle's orientation is always in a region of ± 3 degrees. The maximum orientation error is observed at ± 5 degrees in the turning motion of the vehicle.

7.4 Conclusion and Discussions

In the long distance autonomous orchard applications, accuracy of the resultant motion is so important. It is the main objective that the autonomously driven vehicle in an orchard should follow a desired trajectory in a admissible error region. For such an application, lateral error is the biggest concern. In order to perform the long distance autonomous drive in an orchard area, a strategy is developed in this study. The autonomous vehicle is commanded to keep its motion in the center line, which describes the middle line between two parallel rows of trees. In order to accomplish the objectives, model based control procedure introduced in chapter 5 in detail is adapted into the vehicle. For this purpose, a high accuracy positioning system is installed to the vehicle. As well as modeling the vehicle's motion, an appropriate trajectory tracking methodology is proposed. In order to achieve this tracking objective, controllers for steering angle and forward velocity of the vehicle are developed. The stability of the system proposed is observed by using Lyapunov functions defined. A turning strategy, which is created according to the mechanical limitations of the steering system and actuator, is developed. This kind of information of the steering system is also used in the straight motion of the

vehicle. More than 15 km autonomous drive is performed in an experimental orchard. Less lateral, longitudinal and steering angle errors with respect to the desired values are obtained. The steering angle speed are controlled during turning so that the problem related to damaging of steering actuator could have been solved. As a conclusion, the experimental results show that an autonomous orchard vehicle can be safely driven for long distance driving purposes by using the methodology introduced in this thesis study.

CHAPTER 8

FIELD STUDY-2: TRAJECTORY TRACKING CONTROL OF A MOBILE ROBOT FOR AN ORCHARD APPLICATION USING INFORMATION COMING FROM A LASER SCANNING RANGE FINDER

8.1 Problem Statement

This field study is a part of autonomous orchard application project which is about developing autonomous agricultural technologies for the apple and orchard tree industries. The objective of this study is to develop an autonomous guidance of rows of trees and autonomous desired trajectory tracking in real-time orchard applications. New approaches for detecting the trees, rows (lines) of trees and creating desired trajectory that lies on the center line between two consecutive tree lines are focused. In order to track the desired trajectory, a control procedure for heading speed and steering angle of the vehicle is proposed. Design of two detectors (high and low level) used for detecting trees and rows of trees are introduced. High level row detector is developed for detecting the rows of trees. On the other hand low level row detector is developed to detect the trees close to the vehicle in motion. Both ends of the rows are also detected via low level row detector. Furthermore, the missing trees (caused from implanting), which may be at both ends of tree rows or in anywhere inside the row, are detected by using low level row detector. In order to achieve turning between two center lines, circular type turning strategy is used. According to the information which are heading speed of the vehicle, row width coming from row detectors, safe turning length and safe turning width, the steering angle is generated in the turning motion. It is also focused that the change of steering angle speed is adjusted according to the characteristic information of the

steering system. The speed adjustment of the steering system are performed in both straight and turning motions. It is shown that the speed control of the steering system prevents the possible damages to the steering actuator which can be caused by sharp change of steering angle. The proposed procedures are implemented into an autonomous orchard vehicle. The orchard experiments are conducted in an experimental side and the results are exhibited in this part of the thesis study.

Autonomous solutions in the orchard area have been gaining interest since the needs of agricultural products are rapidly increased due to worldwide growth in population. While the orchards are heavily used, they should be saved for the future. In this contradictory circumstance, autonomous farm vehicle approach brings solutions to solve some of the problems encountered in the field of orchards. Including cropping, seeding, cleaning, harvesting etc. which require attention, precision and automatic farming techniques can be done by using autonomous farm vehicles as well.

Motion of a farm vehicle used in an orchard having trees is limited because of trees. Trees can be placed in a line or randomly placed. In order to perform a desired trajectory tracking task in an orchard, trees have to be firstly recognized. According to the place of trees and the desired task, the reference trajectory should be generated. Then steering and velocity commands are to be produced. All these operations should be done in real-time. Not only longitudinal motion but also lateral motion of the farm vehicle has to be controlled. Because it is desired that there should always be a fixed distance between the vehicle and trees during the operation of vehicle in an orchard. Note that the modeling strategy used in this field study is given in chapter 5 in detail. All the details and information about the design steps can be obtained there.

In this study, it is aimed that the mobile farm robot should perform a desired trajectory tracking task autonomously in an orchard. The experimental orchard has 8 rows of trees that are in line (and 7 center rows). Each row has a length of about 53 m. The width between two rows of trees is nearly 4 m. The robot vehicle should move in the center line (row), which indicates the line between two parallel rows of trees, and enter the next row.

A circular type turning strategy is used to do turning between the rows. The parameters of this turning are calculated in real-time according to the information, which are heading speed of the vehicle, maximum steering angle allowed, row width, safe turning length and safe turning

width. The proper circular type turning geometry is created and required steering angle is produced.

(a)

(b)

Figure 8.1: Autonomous orchard vehicle used in this study

The experiments are performed on a Toro MDE eWorkman vehicle shown in Figure 8.1. To be able to drive the vehicle at low speeds, a gear-chain couple is placed at the rear shaft of the vehicle as seen in Figure 8.1-a. High resolution encoders are attached to the steering and the driving systems of the vehicle. A laser scanning range finder shown in Figure 8.1-b (highlighted by the blue rectangle) is located at front of the vehicle. Steering system is controlled by using a stepper motor attached to the steering rod. The vehicle uses a electrical motor, which is originally placed at the rear axle of the vehicle, and its controller. The speed control is achieved by commanding this controller. All the computational and communicational works have been done under Linux-ROS (Robot Operating System) platform.

8.2 Desired Trajectory Generation for the Mobile Robot Used in the Orchard

Methodology of generating of desired trajectory is given in this section. A smooth desired trajectory for the vehicle model is given in the moving frame in the following form:

$$x_d = x_d(t), \quad y_d = y_d(t), \quad t \geq t_0 \tag{8.1}$$

with the initial conditions ($x_d(t_0)$, $y_d(t_0)$, $\theta_d(t_0)$). Continuous inputs that are supported are υ_d, ϕ_d for $t \geq t_0$.

In this work, the objective is to accomplish autonomous driving of the orchard vehicle in an experimental orchard. The experimental orchard shown in Figure 7.6-a has 8 lines of trees and 7 center rows (lines). Each row of trees has nearly 35 trees. Figure 7.6-b shows the earth positioning of the nursery. As seen in this figure, solid and dashed lines show the lines of trees and center rows, respectively.

Desired trajectory and desired steering angles are generated to drive the vehicle autonomously in this nursery. In Figure 8.2, an example related to construct the desired trajectory for an orchard is presented. As seen from this figure, there are 7 rows having 25 m length (L) and 3.3 m width (w). Turning between the rows are achieved by using a circular shape. Circular shapes are constructed by using three circles. The radius of this circles are determined by the information of safe turning area. This area is specified by S_L and S_w shown in Figure 8.2. Vehicle heading velocities for straight and turning motions are also specified for generating the desired trajectory. They are indicated by V_1 and V_2, respectively.

After constructing the trajectory, suitable steering angles for the vehicle are generated. Desired trajectory and steering angle representations are given in Figure 8.3-a and 8.3-b (dashed line), respectively. In order not to damage the steering system and actuator, the sharp change of steering angle is replaced with a curved representation of steering angle. This kind of representation is developed by using a fourth order polynomial as shown in Figure 8.3-b (solid line) (see Equation 7.1).

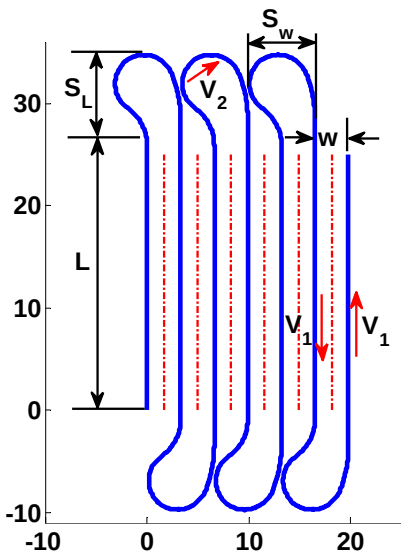

Figure 8.2: An example for creating a desired path having 7 rows (dimensions are in meters)

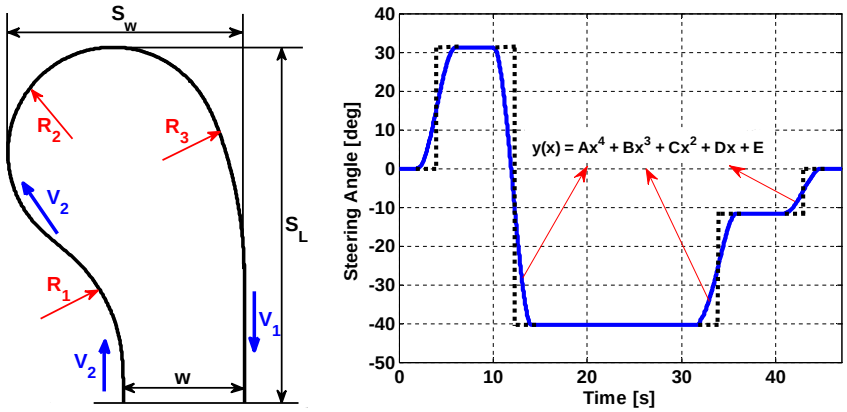

(a) (b)

Figure 8.3: (a) Desired trajectory, (b) steering angle

8.3 Row Detection

A laser scanning range finder is located at the center of the vehicle's front frame about 30 cm off the ground as seen in Figure 8.1-b. The laser is able to scan 270^0 in a horizontal plane and provide distance information about the objects that are placed in front of the laser. Maximum scanning range of the laser is about 20 m. Angular resolution and scanning frequency that we've used are 0.5^0, 50 Hz, respectively. This laser setup allows the vehicle to see the surroundings of it. It can see the objects having height of 30 cm relative to the ground. The

world around the vehicle is not only the objects placed in front of the vehicle, but also the tree trunks, canopy, weeds and furthermore the terrain itself when it has an upward slope.

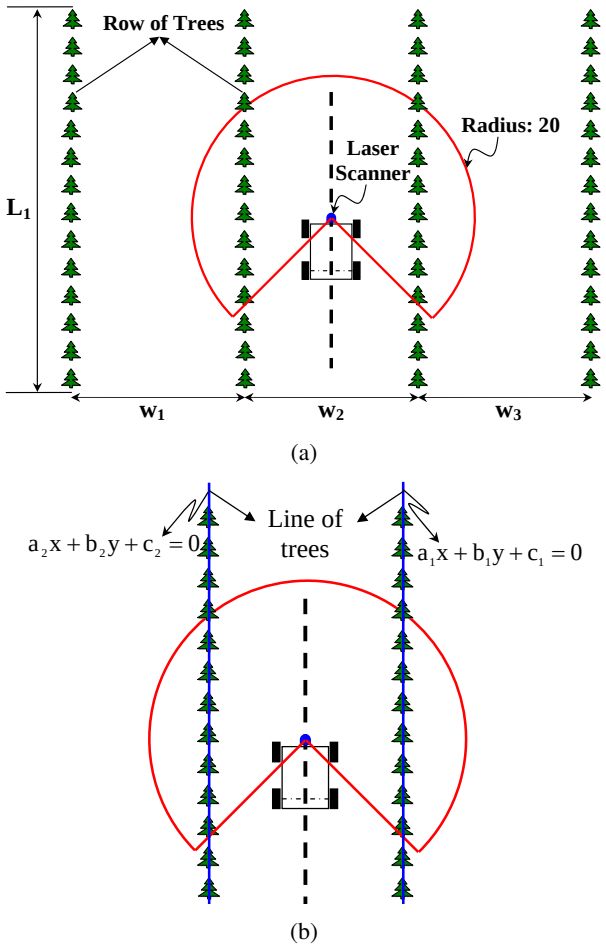

Figure 8.4: Schematic view of the experimental side. (a) Rows of trees and vehicle donated with laser scanner, (b) Created line functions showing the lines of trees

General schematic of the experimental area is shown in Figure 8.4-a. Each row of trees has different lengths (L_1, L_2, etc.) and distance between two consecutive rows (w_1, w_2, etc.) are also different. In this representation, the trees are shown in an exact line however, they are not fit in an exact line in a real orchard.

There are two row detectors developed in this study. One of them is called as high level row detector. High level row detector creates lines for rows of trees. As seen in Figure 8.4-b (blue line), the trees seen in the rage of laser scanner are first recognized. A particle filter [Hamner et al., 2011] is run in order to create a line representing the row of trees. It uses the methodology that tries to guess the location of row of trees [Dellaerty et al., 1999],

[Gustafsson et al., 2002]. The methodology used gives a first order line equation that describe the line (row) of trees. This equation is given as follows:

$$ax + by + c = 0 \tag{8.2}$$

where x and y show longitudinal and lateral movement of the coordinate axis located at the center of rear axel of the vehicle, respectively. a, b, and c values are produced by using particle filter. These variables are obtained in every time instant. As seen in Figure 8.4-b, right and left rows have own line functions with different variables. a_1, b_1 and c_1 indicate the values of right row. The variables of a_2, b_2 and c_2 belong to line of left row.

The second row detector is called as low level row detector. Low level detector observes the surrounding of the vehicle and creates center line. It is also responsible for finding the exact location of the trees which are the nearest trees to the vehicle. Furthermore, the missing trees caused from wrong tree planting are recognized by using low level row detector. The missing tree status can be encountered at both ends of the rows of trees. They can also be randomly placed inside the rows.

While high level row detector is run for detecting rows of trees, trees which are close to the vehicle are recognized by using low level row detector. By this way, the faults caused by particle filter are able to be corrected. The brief summary of the methodology of low level row detector is given in Figure 8.5. In this figure, the vehicle orientation angle relative to the center line is indicated by θ. This angle can be thought as orientation error as well. The trees detected at the right and left sides are shown in Figure 8.5-a. Distance between the laser scanner and the trees detected are specified by D_{R1}, D_{R2}, D_{R3} and D_{R4} at the right side. These distance values obtained at the left side are indicated by D_{L1}, D_{L2}, D_{L3} and D_{L4}. The angle information related to the trees detected are given in Figure 8.5-b. They are obtained relative to the vehicle orientation angle, θ. The angles at the right side are specified by α_{R1}, α_{R2}, α_{R3} and α_{R4}. The angles associated with the vehicle orientation angle and the distance vectors at the left side are shown by α_{L1}, α_{L2}, α_{L3} and α_{L4}. Both row detectors are used not only finding the line of trees but also calculating the position of the vehicle relative to the center line. This gives the ability to find both lateral and orientational errors of the vehicle according to the desired trajectory. The procedure of how to obtain the vehicle position inside the row can be summarized as follows:

1. High level row detector creates right and left lines showing row of trees and a_1, b_1, c_1 and a_2, b_2, c_2 parameters are determined. These gives an opportunity to have a general idea about the line of trees. Moreover, the shape of the row can be recognized by using the high level row detector.

2. Low level row detector observes the near surrounding of the vehicle and creates lines by determining the parameters of D_{L_i}, D_{R_i}, α_{L_i} and α_{R_i} $(i = 1, 2, 3, 4)$. A simple first order line fitting approach is used, and lateral and orientation errors are calculated.

3. An observer continuously works to observe the behavior of the lines created by high and low level row detectors. It interprets the lateral and orientation errors that are calculated by both row detectors in every time instant. The observer also uses the previous data coming from row detectors to make interpretation about how the errors and line behaviors are changed. High level row detector is not always able to give stable distance information between the vehicle and row of trees since it uses a particle filter which can possibly give sharp change in the values of a_i, b_i and c_i $(i = 1, 2)$. This means that vehicle can jump in lateral direction in a short time instant which is not possible in reality. This jump can also cause unstable orientation information. On the other hand, low level row detector is capable of giving more reasonable data for lateral distance and orientation of the vehicle when there is no missing tree case. Consequently, the observer is able to determine reliable lateral and orientation information of the vehicle running inside the row.

4. Low level row detector is capable of determining the missing tree cases which cannot be specified by using high level row detector. In this case, the observer enables to run the sub-algorithm that determines the vehicle position inside the row.

5. In order to accomplish a good turning from one row to another, in addition to row width the information about where the end point of row is important. High level row detector is able to give approximate row width information however it hasn't got the ability to say the end position of row. Fortunately low level row detector is intelligent enough to say more accurate row width and alert about the end point of row.

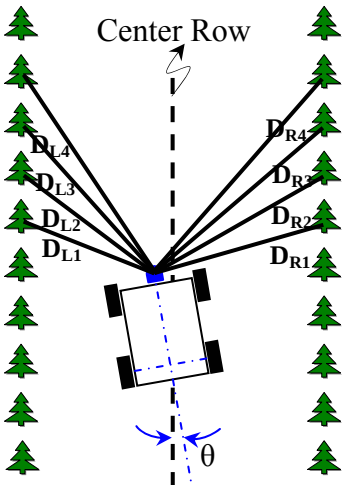

(a)

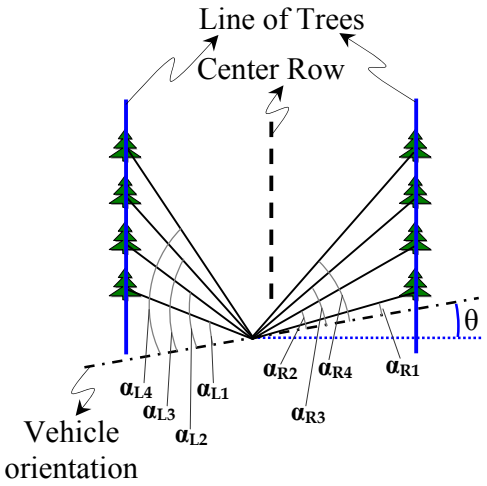

(b)

Figure 8.5: Schematic representation of working principle of low level row detector. D_{Li} and D_{Ri} indicate the distance information coming from the laser scanner. They show the trees placed near surrounding of the vehicle. α_{Li} and α_{Ri} present the angles. Vehicle orientation shown by θ can also be considered as orientation error

8.4 Turning

When the robot vehicle is at the end of the row, it attempts to turn into the neighbor row. Because of the inconsistencies in the planting of trees, missing trees and inaccurate position estimation of robot, the row width is not same in every row. Inside the row, robot can predict its position by using odometer, steering encoder and laser scanner. However, at the outside of the row laser scanner is out of use. The couples of odometer and steering encoder can only be the sensors for estimating position of the vehicle.

There are some ways to achieve turning. One of them is sharp turn towards the next row. The method of sharp turn is easy to build and implement, however there are couple of problems related to use it. Sharp turn is not good for the steering actuator. It may be harmful for it (a motor failure due to this reason has been reported in [Hamner et al., 2011]). Another problem related to use of sharp turn can be difficulty about row finding when the vehicle is pointed perpendicular to the row. In this case, the distance between the vehicle and the nearest row is so close and row detection may not work properly. Because the canopy of the nearest trees can block the good estimation of row, having not enough data to work with the autonomous system.

Other turning method is ”K” turn also called as three point turn. In this turning strategy, vehicle turns to past the row first, then comes back and position itself until it points towards the row, drives the row, at the final stage. In this method, the dead reckoning should supply enough accurate information about location of the vehicle, otherwise there is no enough safe space to find the row exactly and enter. One of the difficulties of using this method is that creating of turning points of K turn does not follow a functional basement so that the speed of steering angle change cannot be adjusted.

In order to create a proper turning and control the steering speed, three same kind of turning strategies are created. These are bulb, clothoid and circular turnings. Examples for these 3 same kind of turning strategies are shown in Figure 8.4. These results are obtained by using the following criteria; The width of the row is 3.3 m. Safe turning width and safe turning length (see Figure 8.3-a) are 6 m and 9.5 m, respectively. Longitudinal velocity of the vehicle is 0.5 m/s. The desired trajectories developed by using bulb, clothoid and circular methods are shown in Figure 8.4-a, 8.4-d, 8.4-g, respectively. The steering angle representations for these methods are indicated in Figure 8.4-b, 8.4-e, 8.4-h, respectively. The steering angle speeds are presented in Figure 8.4-c, 8.4-f, 8.4-i for bulb, clothoid and circular turnings, respectively.

Bulb, clothoid and circular turning methods are compared in terms of natural row entry and fast online computation. Natural row entry means that the vehicle should turn and enter row as if it was driven by a human. This enables the natural steering speed. These three turning methods need to be optimized so that the turning parameters should be estimated. Heading velocity of the vehicle, row width, safe turning length and safe turning width information are the inputs for the estimation process. All these processes should be done in real time. The

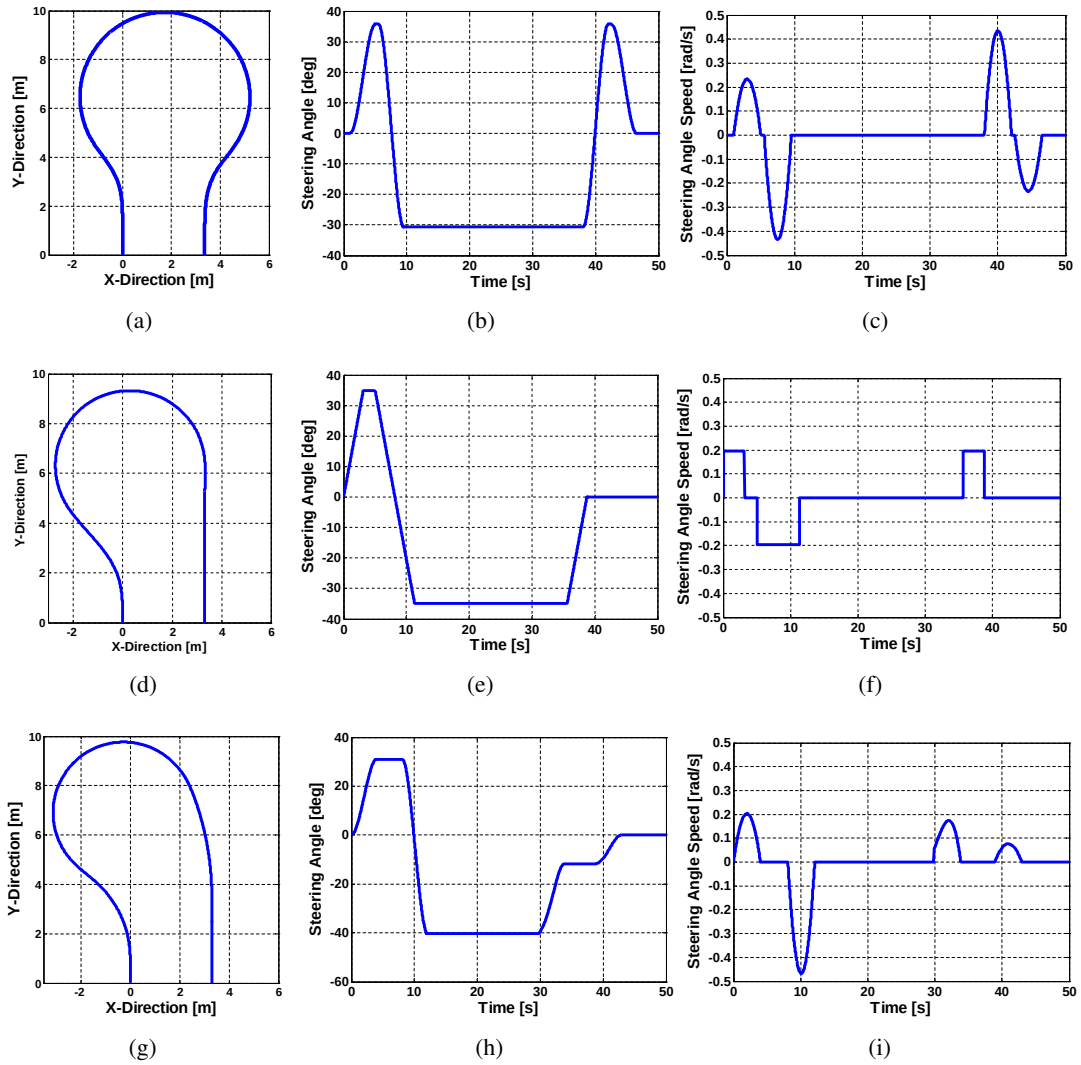

Figure 8.6: Desired trajectory generation: (a) Bulb turn, (b) Steering Angle for bulb turn, (c) Steering angle speed for bulb turn, (d) Clothoid turn, (e) Steering Angle for clothoid turn, (f) Steering angle speed for clothoid turn, (g) Circular turn, (h) Steering Angle for circular turn, (i) Steering angle speed for circular turn

speed of process of the estimation depends on both the simplicity of the methodology and hardware. They have been experienced that estimation of parameters of bulb turning method is fast enough in real time, however it provides unnatural row entry sometimes. Clothoid turning model creates the best steering angle representation, but the estimation process needs more time than the others. The turning trajectory created by using clothoid turning method is natural. The last method, circular turning, shows a natural drive for row entry. It does not need so much time for estimation as well. These requirements are compared in Table 8.1. In this table, ”Yes” represents that methodology used meets the expectations and ”No” indicates

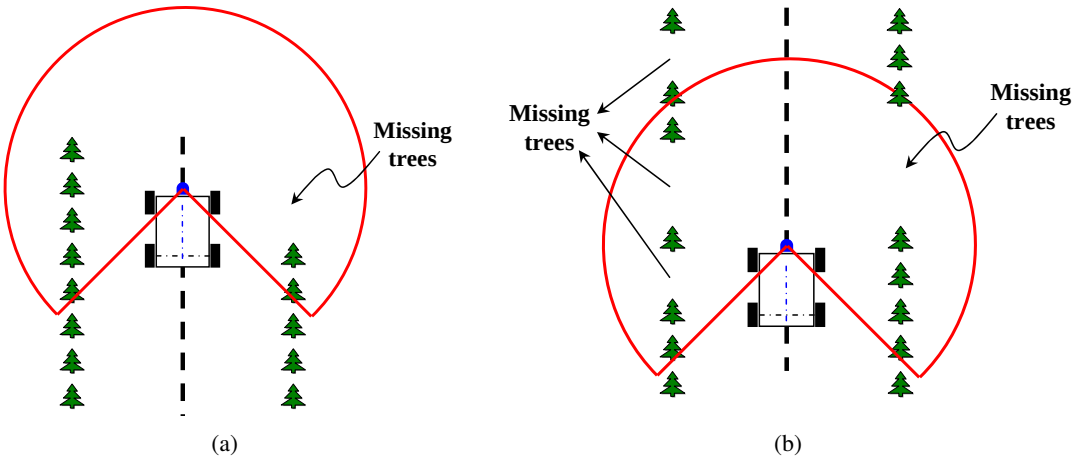

Figure 8.7: Missing tree status in a line of trees. (a) Missing tree(s) are placed at the end of the line of trees, (b) Missing tree(s) are randomly placed inside the line of trees

that the method used does not provide desired behavior. Since it is the best option, we have used circular turning method in our studies.

Table 8.1: Comparison of turning methods

	Bulb Turning	Clothoid Turning	Circular Turning
Natural Row Entry	No	Yes	Yes
Fast Online Computation	Yes	No	Yes

8.5 Finding End of the Row, Start Turning and Row Entry

As mentioned above, row finding procedure uses two row detectors which are high and low level row detectors. High level row detector creates lines for rows of trees. The limits of this detector is related to the maximum scan range of laser scanner. Low level detector looks the surrounding of the vehicle and generates center line between two lines of trees. It is liable for finding the exact location of the trees which are close to the vehicle. By using the row detectors, both ends of the row can also be detected. Moreover, row detectors enable to realize the missing trees inside the rows. Due to inconsistencies in tree plantings, trees can be missing in the line of trees as seen in Figure 8.7. Trees can be missing at the end of the rows (Figure 8.7-a) or they can be missing randomly in the line (Figure 8.7-b). Use of row detectors brings away these missing tree conditions.

In the turning operation it is assumed that the neighbor row's width is same as with the row which is travelled by the vehicle. The row width is calculated by the low level row detector. According to the safe turning information including heading velocity of the vehicle (V_2), safe turning width (S_w), safe turning length (S_L) and safe forward distance (S_s) (see Figure 8.8-a), the steering angle is calculated (see Figure 8.3-b). Finding end of the row, turning and entering the new row are depicted in Figure 8.8. As seen in this figure, the vehicle follows the desired trajectory and enters the next row. In reality, this case is hard to be seen. First of all, row widths are not same in a real orchard. Even if the orchard is professionally built, there are some differences about row widths and lengths. Secondly, terrain is not flat in every part of the field. It may have different slopes in different regions and different surface characteristics like soil, grass, mud, etc. Thirdly, the only feedback related to position of the vehicle comes from dead reckoning at the out of the row since we don't use GPS, IMU or any other sensors giving position information.

The robot vehicle may have possibly positioning errors at the outside of the row because of the following reasons: tires of the vehicle slip during the turning operation, information coming from the encoder of odometer contains errors and there are numerical errors caused by dead reckoning. As seen in Figure 8.8-b, these create a lateral error (y_e) between the vehicle and the center line. This lateral error can be compensated by using the controller to be mentioned in the next section.

During the turning operation, the vehicle follows the desired circular trajectory until it's orientation is parallel to the row. When the orientation of the vehicle is parallel to the row, the row detectors provide enough data to detect the trees and create line of trees. From this point forward, the vehicle is able to point towards the row. When the vehicle enters the row, turning motion is completed and straight motion starts. This turning story is graphically summarized in Figure 8.8-a.

8.6 Controller Design for Tracking Desired Trajectory

8.6.1 Controller Design

In this study, forward velocity and steering angle of the vehicle is controlled by using the procedure proposed in chapter 5. The control structure introduced is called as model based

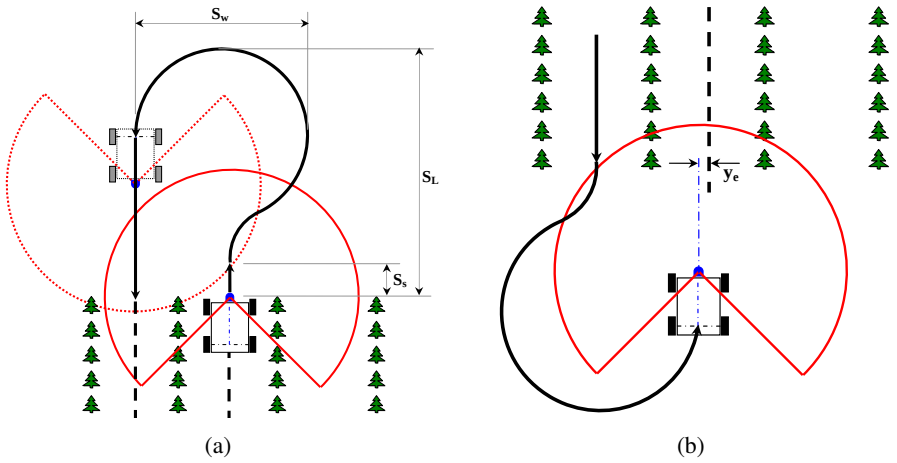

Figure 8.8: Finding the end of the row, turning and entering the next row

controller. Recall that the control procedure is developed by using the methodology of back-stepping approach. It is the objective that the controller keeps the vehicle inside the desired trajectory when the vehicle is in motion (straight motion inside the row and turning motion outside the row). In addition to control forward velocity of the vehicle, a new approach to make enhancement on steering control is proposed in this study. As presented in Figure 8.3, the change of steering angle speed is arranged according to the mechanical characteristics of the steering system of the vehicle. Steering angle speed information is introduced into the system model and desired trajectory is generated by using it. The overall control system accomplishes the control objective by using the feedback information coming from row detectors, odometer and steering encoder. Control chart of the system is presented in Figure 8.9. In this figure, V_c and ϕ_c represent controller outputs for forward speed and steering angle, respectively. V and ϕ are the velocity and steering angle read from odometer and steering encoder, respectively. X_d and Y_d are x and y components of desired trajectory, respectively. V_d and ϕ_d represent desired forward velocity and steering angle, respectively. As mentioned above, high and low level row detectors use the data coming from laser scanner. They feed the system blocks of trajectory generator and model based controller. Trajectory generator block is also fed by real values of forward velocity and steering angle of the vehicle. The inputs to generate the control commands (V_c and ϕ_c) are supplied to the model based controller block. High and low levels row detectors that use laser information are presented in a flow chart shown in Figure 8.10.

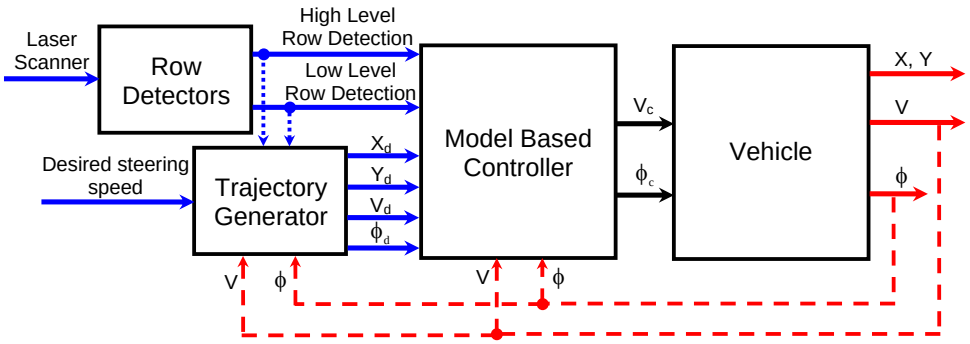

Figure 8.9: Flow chart of the control system.

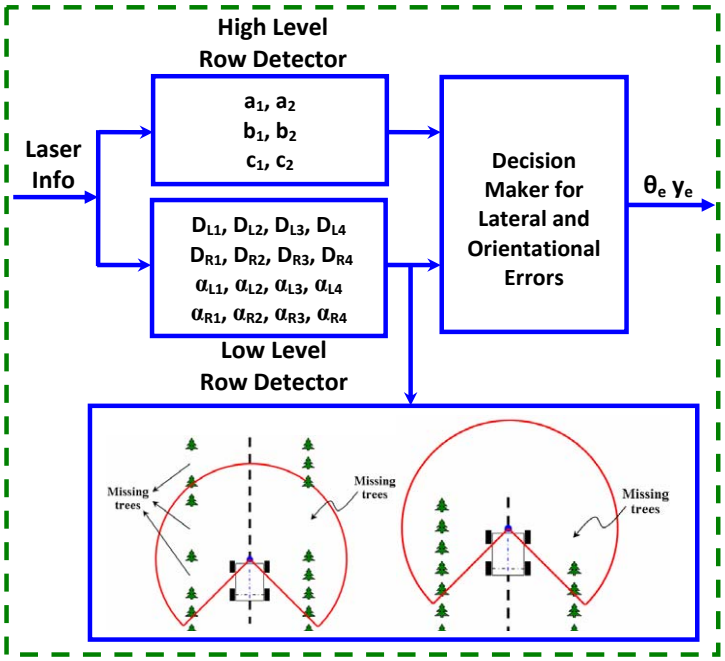

Figure 8.10: Flow chart of the control system.

8.6.2 Pure Pursuit Controller

In order to show the usability of the control procedure introduced in chapter 5, another controller strategy that is commonly used for the autonomous vehicle applications is also adapted into the vehicle. In the autonomous orchard applications, desired trajectory tracking is achieved by the extensively usage of pure pursuit control strategy [Hamner et al., 2011]. The basic representation of pure pursuit control strategy is given in Figure 8.11. The objective in this method is to reach the goal points shown by (G_x,G_y).

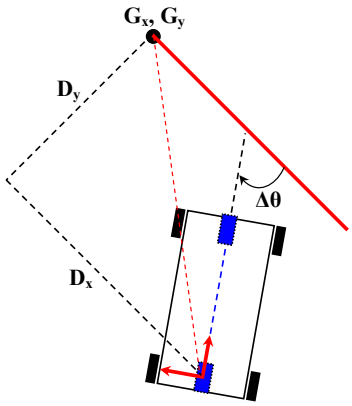

Figure 8.11: Graphical representation of pure pursuit control

Pure pursuit control strategy is used to convert base goal positions into velocity command. By using this control approach, angular velocity of the vehicle can be controlled and directed to the goal position as given in Equation 8.3 [Hammer et al., 2009].

$$\begin{aligned} V_t &= K_x D_x \\ \dot{\theta} &= K_\theta \Delta\theta + K_y V_t sin(\Delta\theta) D_y \end{aligned} \tag{8.3}$$

where V_t is the translational velocity that is generated. D_x and D_y show the translational and perpendicular distance to the goal point, respectively. Angular velocity is indicated by $\dot{\theta}$. $\Delta\theta$ emphasis the angle difference which is between the actual orientation angle of the vehicle and the goal angle. K_x, K_y and K_θ express the proportional gains which are experimentally determined. There is linear relationship between the translational velocity and the goal point. Angular velocity of the vehicle depends on the heading difference. It also contains the term which tries to push the vehicle to a line extending from the goal angle. In this relationship, it is seen that while the vehicle closes to the desired trajectory, the sine term goes to zero.

Successful experiments have been done by using pure pursuit control strategy in an orchard environment [Hamner et al., 2011]. However, there are still problems with using this method. The method is a non-model based approach so the characteristics of the working parts of the vehicle cannot be combined with this approach. Moreover, the speed of the change of steering angle information cannot be introduced in this strategy. In an orchard field, steering angle speed is so important. Surface of the orchard is not always flat, generally it is mixed. There may be some holes on the ground. The tires can easily fall into them. Furthermore

slippage is one the biggest issue that causes trajectory tracking errors in an orchard field. In such cases, the vehicle can be out of the desired trajectory and can produce sharp steering angle to catch it. In order not to have any mechanical problem with the steering system, steering actuator should be commanded according to its healthy working range.

In this part of the study, the experiments are performed by using both model based control strategy which is proposed in this study and pure pursuit control methodology which is commonly used for the autonomous vehicle applications. The results obtained by using both control strategies are given together so that a comparison can be easily done.

8.7 Experimental Studies

The experiment site shown in Figure 7.6 locates at the robot city area in Pittsburgh, PA, USA. It has 8 parallel tree rows. The surface is a mix-type terrain. The real values of lengths and widths of the rows are given in Table 7.1 and Figure 7.6-b.

In this experimental orchard, autonomous row detection, desired trajectory following and autonomous drives are achieved. The autonomous drives are completed without stopping and human intervention. Desired speed in straight and circular motions is set to 0.5 m/s. As previously mentioned, the robot vehicle has the sensors like laser scanner, odometer and steering encoder. It hasn't got a ground truth like a GPS or an IMU (inertial measurement unit). The experimental results are presented for 7 center rows. The distances (lateral errors) between the vehicle and the row center are shown for each row. Besides lateral errors, steering angle results are given. In order to show the improvements obtained by using the procedures proposed in this study, the results are compared with the method of pure pursuit controller. The lateral error results are obtained by using the strategy introduced in Equation 8.2. Note that model based control (MBC) strategy uses both high and low level row detectors, whereas Pure Pursuit Control (PPC) procedure uses only high level row detector.

In Figure 8.12, the experimental results obtained in the first center row of the experimental field are shown. The width and the length of the first center row are 4.44 m and 52.95 m, respectively. First and second lines of trees are not straight so the center row is not a straight line. The steering angle results obtained by using PPC and MBC methods are given in Figure 8.12-a. The distance between the vehicle and the center row is given in Figure 8.12-b. These

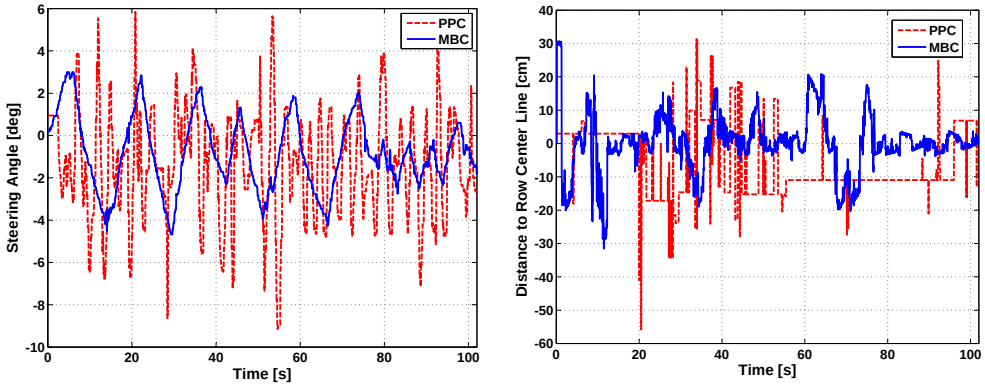

(a) (b)

Figure 8.12: Experimental results obtained in Row-1. Width = 4.44 m, Length = 52.95 m. (a) Steering angles, (b) Lateral errors

distance results are also called as lateral error since the task is always to keep the vehicle on the center line inside the row. As seen in Figure 8.12-b, there are sharp and instant jumps. Lateral errors are obtained according to the axis location (see Figure 5.1). It is located at the center of rear axel of the vehicle. In reality, it is impossible to have such jumps. However, lateral errors are obtained by using the first order line equation (see Equation 8.3). This line equation is produced via a, b, c values that are calculated in every time instant. a, b, c values for right and left lines of trees are shown in Figure 8.13-a and 8.13-b, respectively. As seen in these figures, these values do sometimes sharp jumps which cause jumps on the results of lateral errors.

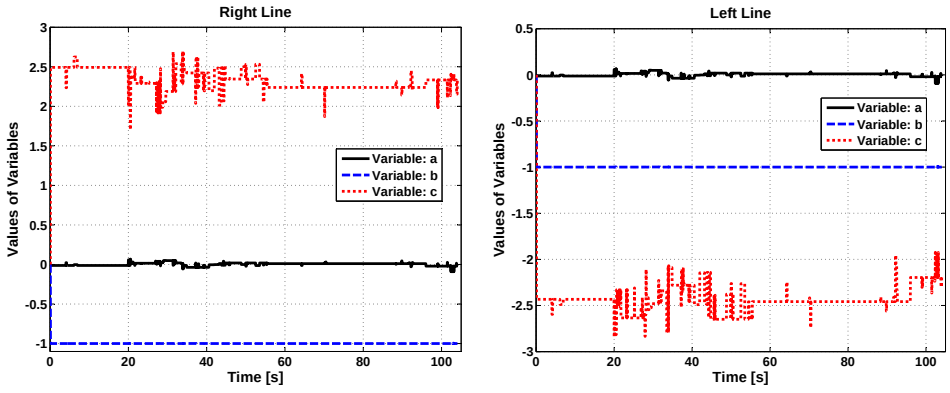

(a) (b)

Figure 8.13: The values of first order line equation that describes the line for the rows of trees

As mentioned above, the vehicle doesn't have a ground truth and laser scanner cannot provide any positioning information at outside of the rows. By this reason, the turning results are

presented by using the video frames as given in Figure 8.14. In this figure, there are 16 successive frames of the turning motion. It briefly summarizes that the vehicle comes to the end of the center row and it starts turning. Then it does the turning operation described in Figure 8.2. Whenever it's orientation is parallel to the row of trees, row detectors start to work to detect the rows and center line.

Figure 8.14: Video frames showing turning procedure of the vehicle (the human is walking near by the vehicle for safety reasons and is not interfering the vehicle)

Experimental results obtained for the second row through fifth row are given in Figure 8.15. The results related to second row are given in Figure 8.15-a and 8.15-b. Length and width of second row are 3.98 m, 53.15 m, respectively. Second row is slightly narrower than the first row. The length is almost same as with the first row. Steering angle results obtained by using two methods are given in Figure 8.15-a. Lateral errors are presented in Figure 8.15-b. As seen from these figures, the speed of steering angle is successfully controlled. Steering angle is gradually changed as designed. The procedure doesn't allow sharp jump of steering angle that may damage the steering system. The control of the steering system performed by using MBC creates less lateral error than the procedure of PPC.

At the end of the second row, there is missing tree case. This case is similar to the one graphically shown in Figure 8.7-a and shown in Figure 8.17-a. Even though this missing tree case is a problem in case of using only high level row detector and pure pursuit controller, it is not a problem in the case that both high and low level row detectors with model based control strategy proposed are in use.

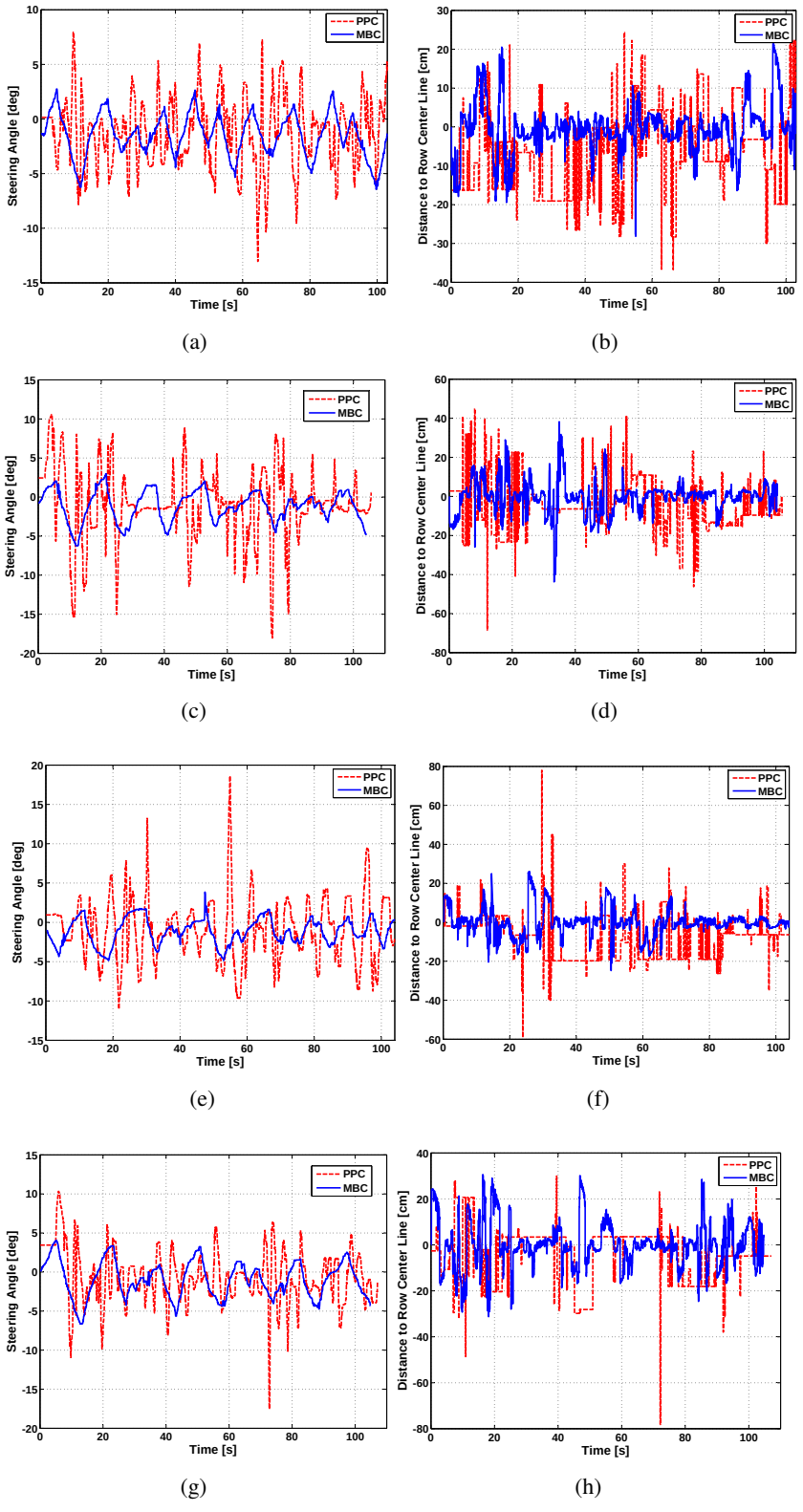

Figure 8.15: Experimental results of steering angles and lateral errors obtained for Row 2, 3, 4 and 5: (a-b) Steering angles and Lateral errors of Row-2: Width = 3.98 m, Length = 53.15 m, (c-d) Steering angles and Lateral errors of Row-3: Width = 3.51 m, Length = 53.14 m, (e-f) Steering angles and Lateral errors of Row-4: Width = 3.24 m, Length = 53.16 m, (g-h) Steering angles and Lateral errors of Row-5: Width = 3.19 m, Length = 53.22 m

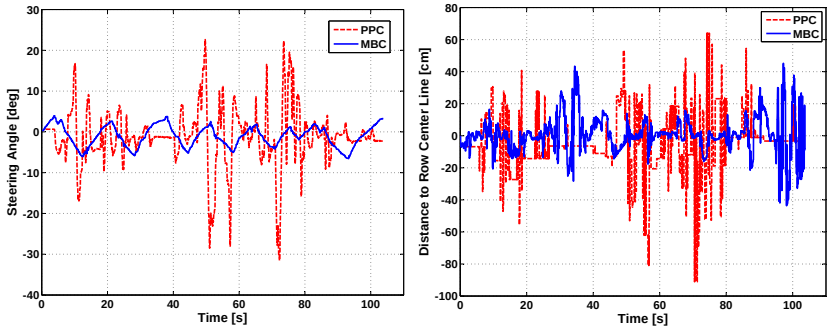

(a) (b)

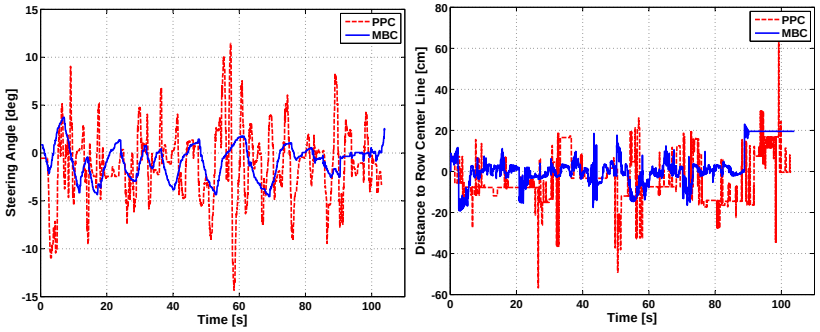

(c) (d)

Figure 8.16: Experimental results of steering angles and lateral errors obtained for Row 6 and 7: (a-b) Steering angles and Lateral errors of Row-6: Width = 3.39 m, Length = 53.27 m, (c-d) Steering angles and Lateral errors of Row-7: Width = 4.72 m, Length = 52.93 m

(a) (b)

Figure 8.17: Missing trees due to inconsistencies in tree plantings. Missing trees exist both at the ends and along rows

Experimental results for steering angle and the lateral errors are presented in Figure 8.15-c, 8.15-d and 8.15-e, 8.15-f for row 3 and row 4, respectively. Widths of these rows are 3.51 m and 3.24 m, respectively. The lengths of them are 53.14 m and 53.16 m, respectively. As seen in these figures, the proposed methodology makes improvement for the lateral movement of the vehicle and the steering angle. It can be said that the results are in the desired error region.

Steering angle and lateral error results for fifth and sixth rows are shown in Figure 8.15-g, 8.15-h and 8.16-a, 8.16-b, respectively. In a similar manner, the results obtained by using PPC and MBC methods are presented together in these figures. Width and length of row 5 are 3.19 m and 53.22 m, respectively. Those values of row 6 are 3.39 m and 53.27 m, respectively. Sixth row has missing tree case as shown in Figure 8.7-b and 8.17-b. Missing trees are randomly placed inside the row. Use of proposed methodology solves this inconsistency in tree planting and gives opportunity to complete the desired trajectory tracking in the experimental area.

The experimental results for seventh row are given in Figure 8.16-c and 8.16-d. The row has a width of 4.72 m and length of 52.93 m. It is the widest row in the experimental area. In this row, trees haven't been planted into a line so the lines of trees are not exact lines. The last row has missing tree case at its end as well. It has also missing trees inside the row. These cases are shown in Figure 8.17-c and graphically presented in Figure 8.7-b. The methodology proposed is even successfully used in this disorganized row. The problems caused by implanting in trees could be solved by using two levels row detectors. The model based control strategy can produce proper command so that the vehicle is kept inside the desired trajectory.

Table 8.2: Comparison of pure pursuit control (PPC) and proposed methods. PPC method uses high level row detector whereas proposed method uses high and low level row detectors

	PPC Method	Proposed Method
Row Width Definition	Manual Input	Laser based
Row Length Definition	Manual Input	Laser based
Starting Point Definition	Manual Input	Laser based
Steering Speed Control	Not Applicable	Applicable

The comparison of both methods (PPC and proposed methods that is called as model based control, MBC) are shown in Table 8.2. The behaviors of lateral motions and steering angles of the vehicle obtained using two procedures are given in detail above. In this table, other comparisons are emphasized. While row width and length definitions have to be specified in the PPC method, there is no need to specify them in the new method. When PPC method is in use, the vehicle has to be placed at the starting point of the first row before autonomous motion is started. Luckily, it is not required in the new method. Although there is no chance to perform the steering speed control in the PPC method, the new method gives ability to con-

trol the speed of steering angle's change. Presented results and comparisons are highlighted that the row detection and trajectory tracking control in an orchard by using an autonomous orchard vehicle are improved by using the new method.

8.8 Conclusion and Discussions

Automatic farming necessity for agricultural applications have been rapidly increasing. In order to make a contribution to this necessity, this study is conducted. A new perspective to autonomous orchard applications is proposed in this work. Two levels of row detectors are declared to detect the trees and create a line showing line (row) of trees. Furthermore these row detectors are used for detecting the missing trees that are caused from implanting of trees in the orchard. A desired trajectory generator, which follows the requirements of the steering system's characteristics, is proposed. In order to achieve turning between two consecutive center lines of trees, a circular type turning strategy is introduced. Besides this turning strategy, other two turning methods are discussed. Backstepping procedure is used to be able to propose the controllers for heading velocity and steering angle of the orchard vehicle. The controllers developed are applied in both straight and turning motions of the vehicle for an orchard task. The whole system model is tested in an experimental orchard. The experimental results show that an autonomous orchard vehicle having sensors like laser scanner, odometer and steering encoder can be effectively controlled inside an orchard for agricultural applications by using the models and procedures discussed in this study.

CHAPTER 9

FIELD STUDY-3: TRAJECTORY TRACKING CONTROL OF A MOBILE ROBOT FOR AN ORCHARD APPLICATION WITH INCLUDING SLIPPAGE ESTIMATED

9.1 Problem Statement

Mobile robots have been started to use extensively in the field for agricultural applications. In the orchard environments, especially fruit production like apple, orange, grape, etc., these robots are becoming the main labors. They are the potential mobile robotic solution for transferring issues of tree fruit production. They can be used for automating some important key operations like mowing, spraying, etc. Moreover they can be operated to augment the workers who conduct pruning, thinning, tree maintenance, and harvesting.

In this study, we focused on the mobile autonomous vehicles that can work in an orchard environment having trees planted in a line. Trajectory tracking inside the rows and turning outside the rows are addressed. While performance when driving down the row is satisfactory, there is room for improvement during turns. The main reason is the sensing suite adopted for vehicle navigation. The vehicle used in this study relies on one laser rangefinder installed on the hood and steering and wheel encoders to navigate. While in the row the system uses the laser to find the trees to follow; outside the row, however, the system can only count on the encoders, at least until the vehicle is facing the next row and the laser can see trees again. Especially if the soil is wet, muddy, snowy and/or the surface is inclined, wheel slippage causes odometry errors, occasionally preventing the vehicle from completing the turn. This requires manual intervention to reposition the vehicle.

The vehicle used in this study (see Figure 7.2) is capable of following an orchard row, turning at the end of the row, and entering the next one using only the hood-mounted laser rangefinder and a steering and wheel encoders. It is suited also with a RTK-GPS receiver as a ground truth.

There are two main field tasks for the autonomous orchard vehicle. The first one is related to the row detection and moving inside the row. The general orchard view is given in Figure 9.1-a. The motion task in such an orchard is to detect the trees, create tree rows, develop a desired trajectory and then control forward velocity and steering system of the vehicle (see Figure 9.1-b). As seen in Figure 9.1, the widths and lengths of each row can be different from each other. The laser scanner located at the front-middle of the vehicle can see the surrounding of the vehicle in a range having 20 m radius.

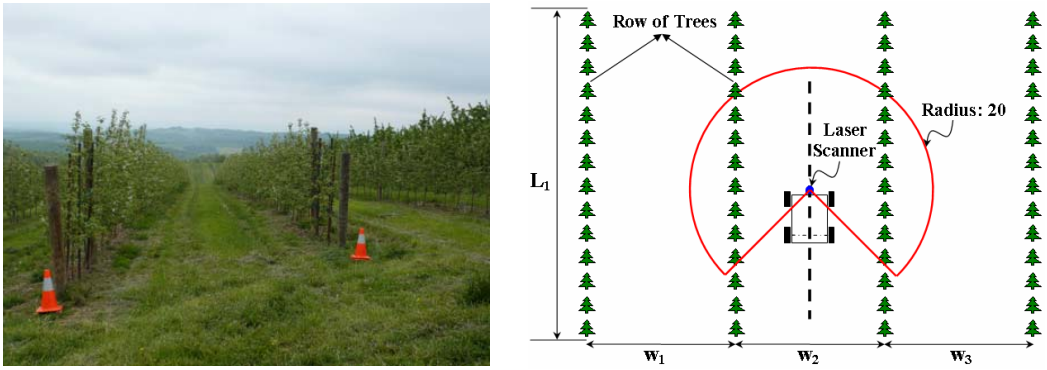

Figure 9.1: (a) View from an orchard, (b) Indicating of row detection

The second main field task of the autonomous orchard vehicle is turning from one row to another. This objective is described in Figure 9.2. The vehicle follows the desired line that is the center row between two neighbor rows of trees. The row detection system alerts the vehicle when the vehicle reaches at the end of the row. Then the desired turning trajectory development system creates a desired path according to the safety parameters that are indicated in Figure 9.2 by S_L, S_w, S_s and S_F. These four parameters are the inputs and introduced to the system before the real-time operations. They depend on the physical properties of the orchard field. As seen in Figure 9.2, there is a target region. This region shows that during the journey of the orchard vehicle from the point at which the vehicle starts the turning operation to the target region, it is almost blind (i.e. laser scanner cannot see any tree). The vehicle is able to use only its distance and steering encoders for the localization feedback (dead-reckoning).

In order to detect the rows safely after completing the turning, the vehicle should be able to locate itself inside the predefined target region. The vehicle inside the target region and having the correct heading angle can easily enter the next row as shown in Figure 9.2. This story is valid only if there is no slippage. If the surface is slippery, muddy, snowy or inclined, achieving turning operation by using the dead-reckoning approach may not be possible.

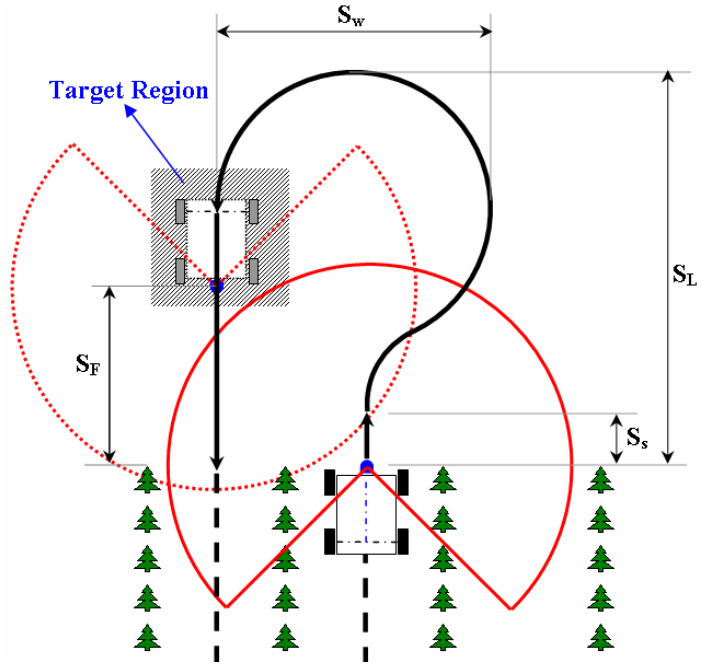

Figure 9.2: Row following, turning and accessing through the target region

All the details about the modeling structure about this study is given in chapter 6. The details and modeling information can be seen in that chapter. In this study, in order to achieve row following and turning operations successfully in case of slippery, snowy or inclined surface conditions, a slippage estimation procedure is proposed. The estimated values are fed into the system model and the controller takes action to perform the required corrections to track the reference trajectory. In order to test the proposed methodologies which are trajectory generation, turning operation, steering angle and forward speed adjustment, the experiments are performed in two different fields. The first experimental area is an open space without trees. The experiments conducted in this field are ”flat-dry surface” and ”inclined surface (covered with snow)” tests. This field tests make sure to see the accuracy of slippage estimation procedures. The second field tests are conducted in an experimental orchard. In this area, row following and turning from one row to the next row operations are performed on a muddy

surface. Slippage effects are observed and able to be fed into the overall system model. The improvements on trajectory tracking are illustrated with the experimental results of both field tests.

9.2 Development of Trajectory for Turning

The navigation strategy of the orchard vehicle used in this study includes two main issues; tracking the desired trajectory inside the rows and turning from one row to another. The turning strategy starts at the end of the row which is recognized via the row detectors. After this point, the turning strategy produces the necessary turning control commands until the point where the vehicle's heading is parallel to the row that is to be entered. During turning, there are two main concerns that should be focused: the first concern is related to the location of the vehicle (where the vehicle is) and the second one is vehicle should be placed inside a predefined region at the end of the turn (Figure 9.2). According to our experiences, the following points provide information about these concerns before the vehicle attempts to drive to the next row:

- At the end of the turn, the vehicle should be placed inside the target region where the vehicle is as centered with respect to and pointed as parallel to the row as possible (see Figure 9.2). This enables the row detection system to work better since the detection faults caused by the trees located in neighboring rows are minimized.
- The other point is related to the "natural-looking". This issue is similar to how a human drives the vehicle manually to move from one row to other (turning between the rows). The term, "natural-looking" gives the necessary information about time, space, safe turning angle and safety for the turning task. Furthermore it gives one of the most important information about the limits and behavior of steering speed.

In this study, these concerns are focused and implemented into the system model. The turning procedures used in this study are shown in Figure 7.4 and Figure 8.3. They are stated in the previous chapters as bulb and natural-looking turnings. In order to see the steering system's behavior, these turning methods are adapted into the vehicle to conclude this study. The bulb turning approach is easy to create and simple to adapt. It is an useful turning strategy in an open space however may not be a good choose in an orchard environment due to

unnatural-looking behavior. This problem can be solved by developing a natural-looking turning procedure that it is called circular turn. The procedure combines the bulb turn's simplicity and usability in real time and clothoid turning [15, 16] approach's natural-looking behavior. Circular turn is basically similar to bulb turn's approach. The biggest difference is that change of steering angle can be controlled by using thumb method.

9.3 Slippage Estimation

As stated in the previous chapters, the slippage estimation procedure is one of the contributions in this thesis study. Trajectory tracking control study is combined with the slippage estimation procedure which is introduced in chapter 6. The control chart of the overall system including slippage estimation block is shown in Figure 6.2. In this study, in order to show the usability of the estimation procedure, it is tested by using two different types of feedback sources. The system is tested by high accuracy positioning feedback system (RTK-GPS) first so that the capability of the estimator could be able to be seen. Then the system is tested by the feedback system including odometer, and steering information system. The control charts including RTK-GPS and odometer-steering information system are shown in Figure 9.3 and Figure 9.4, respectively.

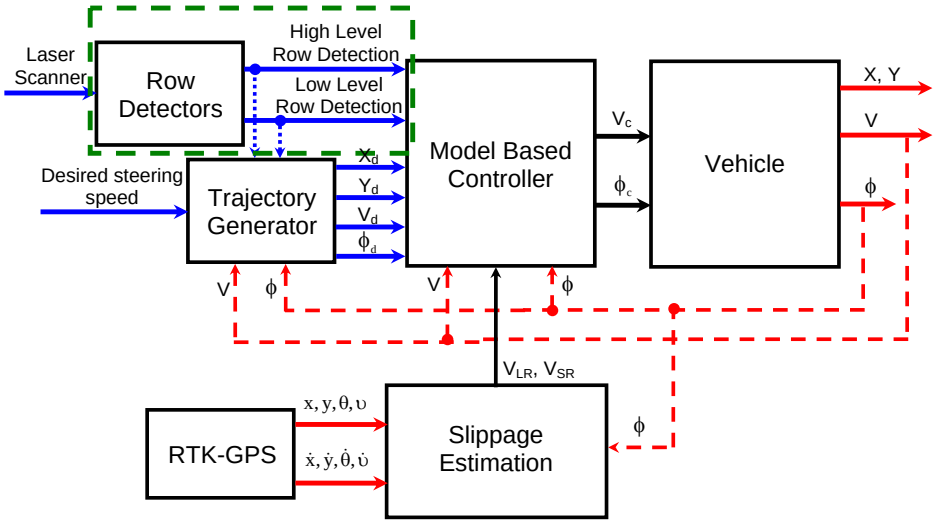

Figure 9.3: Control chart that includes slippage estimation procedure fed by the high accuracy positioning feedback (RTK-GPS).

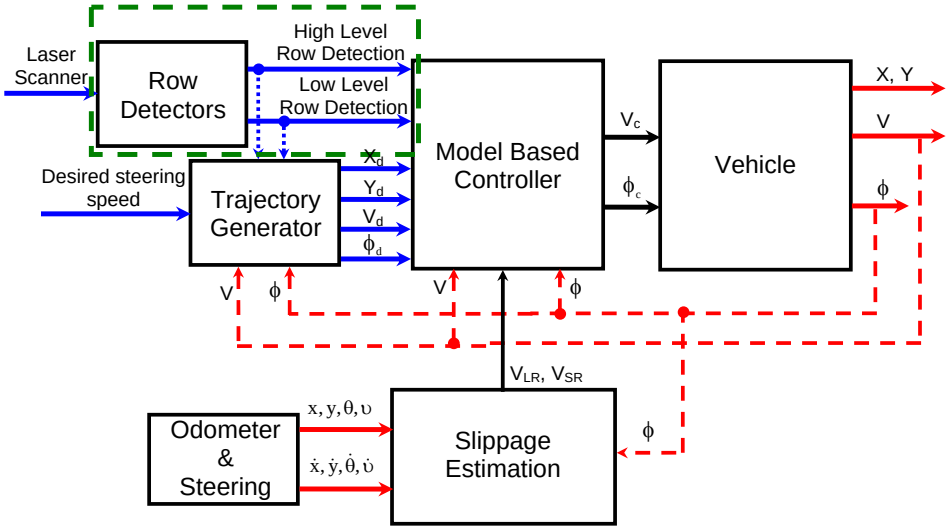

Figure 9.4: Control chart that includes slippage estimation procedure fed by the odometer and steering information system.

9.4 Experiments

In order to show the effects of slippage and emphasize getting benefit from slippage estimation, the following experimental studies are conducted. Dry, snowy and inclined surface experiments are conducted in the Schenley Park area of Carnegie Mellon University campus (Figure 9.5-a). Muddy surface experiments are conducted in an experimental orchard located in Robot City area of Pittsburgh, PA, USA. Dry, snowy and inclined surface experiments are performed by using bulb turn. On the other hand, circular turn is used in the orchard environment which is muddy. Hence there are a lot of experimental data obtained to make a comparison related to different types of surface conditions and turning strategies.

9.4.1 Open Space Experiments

Dry surface experimental studies were conducted in July. In this month of the summer season, the surface is almost dry and there is no slippage occurred and observed during the experiments. Hence during the experiments, it is assumed that there is no slippage and motion model of the vehicle is developed regardless of slippage information. The results are shown in Figure 9.5-b. In this figure, reference trajectory is indicated by blue lines as real position of the vehicle is presented by red lines.

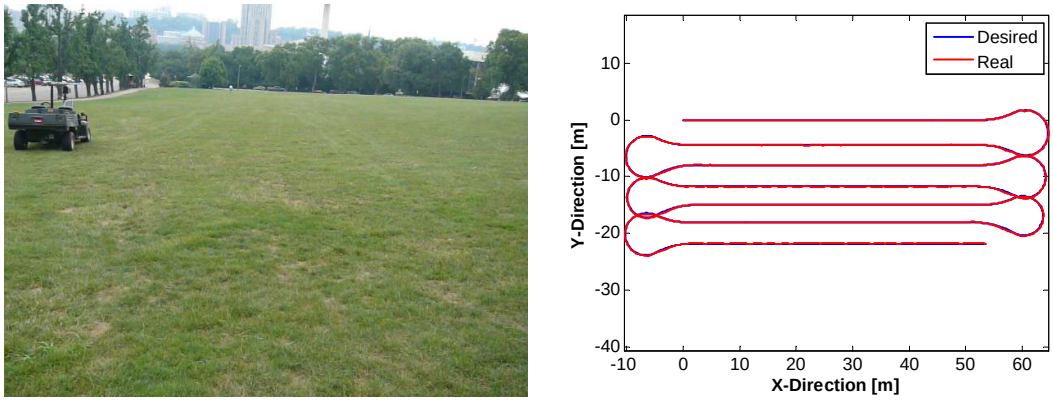

(a) (b)

Figure 9.5: (a) Dry surface experimental area, (b) Experiment results

Dry surface experimental field (Schenley Park area of Carnegie Mellon University campus) was also used to perform the snowy surface tests. The experiments were done in March of winter season. The area covered by snow is shown in Figure 9.6. During the snowy surface experiments, the same desired trajectory input, which is used in dry surface experiments, are sent to the vehicle. The study doesn't contain any slippage estimation process as well. The experimental results are shown in Figure 9.7. Desired and real trajectories are shown by blue and red lines, respectively. As seen in the figure, the experiment is interrupted during the second turning operation since the steering system behavior is not healthy at that time due to slippage. This experiment emphasizes the importance of slippage inclusion in the model.

In the next experimental studies, the slippage estimation procedure presented in chapter 6 is introduced into the system model. The vehicle is let to follow autonomously the desired trajectory in the same experimental area shown in Figure 9.6. In addition to snowy surface, experiments are hold in the inclined part of the area. The area having slope is shown in Figure 9.8-a. As seen in this figure, it can be considered that the surface has two-dimensional inclinations. These inclinations are presented in Figure 9.8-b where inclination angles are shown by δ_1 and δ_2. In this case the vehicle should follow the desired trajectory under the following effects: slippage caused from not only because of snow but also due to the inclined surface covered with snow.

The results of experiments conducted in the inclined surface covered with snow are illustrated

Figure 9.6: Experimental area covered by snow

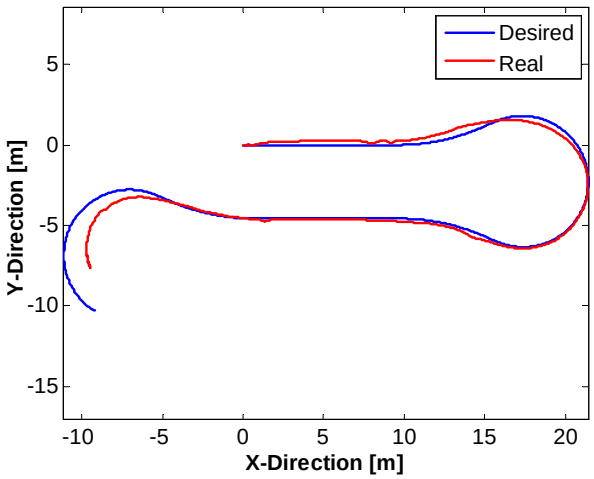

Figure 9.7: Snowy-flat surface experiments

in Figure 9.9. The experiments are performed for two cases. The first case is related to the trajectory tracking without including the estimation procedure. In the second case, slippage estimation procedure is included in the overall system model. The position results are given

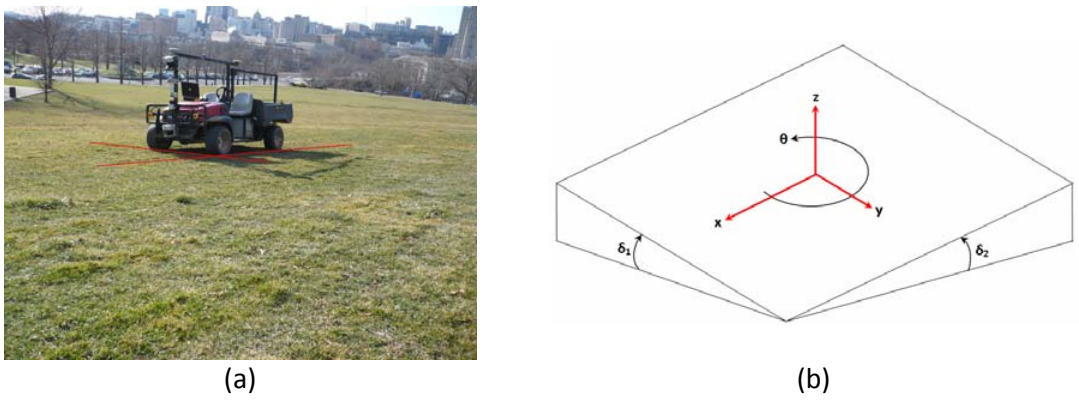

(a) (b)

Figure 9.8: (a) Inclined surface, (b) Representation of 2-D inclination angles

Figure 9.9-a. Desired trajectory is shown by blue lines. The resultant trajectories obtained without slippage estimation and with slippage estimation cases are indicated by black and red lines, respectively. In Figures 9.9-c and 9.9-d position values for X and Y directions are given, respectively. In these figures, the notations wo/S and w/S specify without slip and with slip estimation. The inclination angles of the terrain, which are specified in Figure 9.8 by δ_1 and δ_2, are shown in Figure 9.9-b. As seen in this figure, the inclination angles are not constant, change while the vehicle is in motion.

Longitudinal and lateral slip velocities that are estimated at the rear wheels of the vehicle are shown in Figure 9.10-a. Slip angle values estimated at the rear of the vehicle are shown in Figure 9.10-b.

While the vehicle is in autonomously trajectory tracking motion, the controller generates the steering angle and forward velocity command for the vehicle as shown in Figure 9.11. As seen in Figure 9.11-a, inclusion of the slippage information into the model enables to generate more stable steering angle command. Especially, the steering command used for turning operation becomes smoother when the slip information is fed into the control system. Same behavior is observed in the heading velocity results as illustrated in Figure 9.11-b.

The inclined and snowy surface experiments show that slippage estimation procedure enables to achieve better trajectory tracking. After getting good results with using slippage estimation procedure, the 6-turns experiment is conducted on the same area shown in Figure 9.8. The

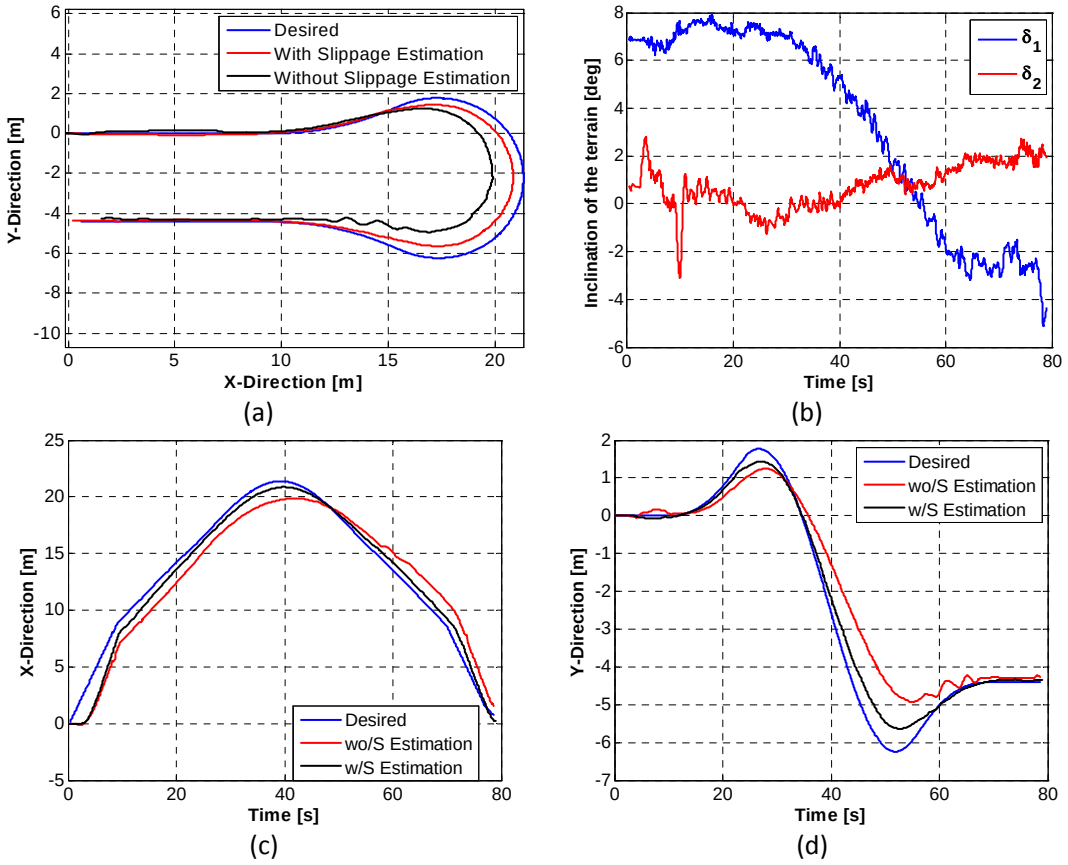

Figure 9.9: Trajectory tracking experiment results performed in the inclined surface covered with snow

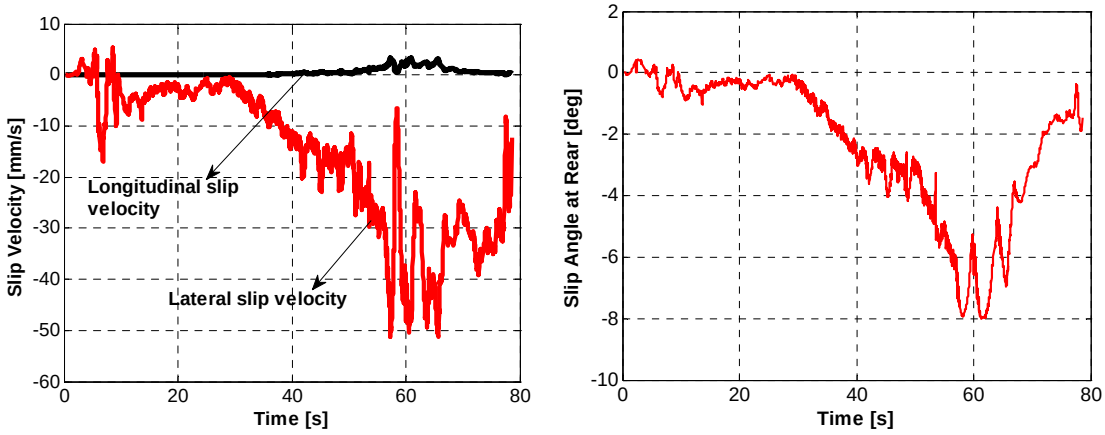

Figure 9.10: (a) Longitudinal and lateral slip velocities estimated at the rear of the vehicle, (b) Slip angle estimated at the rear of the vehicle.

desired and actual trajectories are shown by blue and red lines in Figure 9.12-a, respectively. The results are obtained by adding the slippage information into the overall system model. Starting position is point (0, 0). Green arrow shows the uphill drive while pink arrow indicates

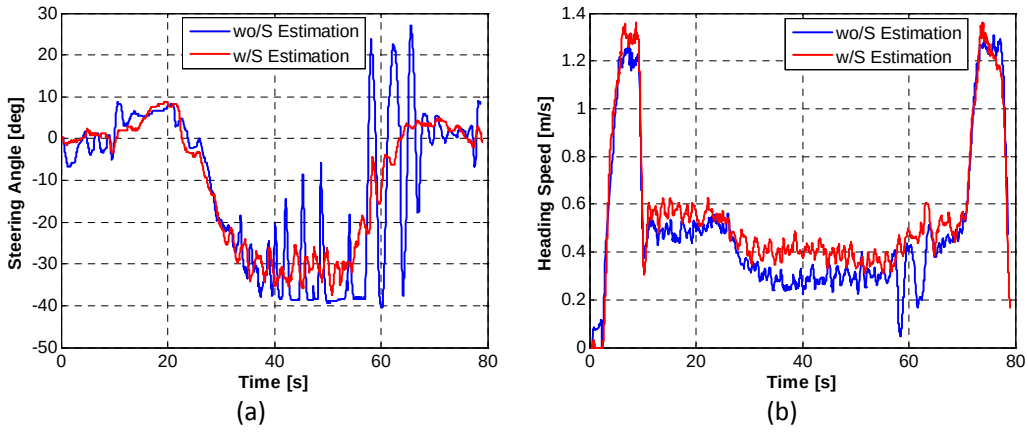

Figure 9.11: (a) Steering angle, (b) Heading velocity of the vehicle

downhill motion of the vehicle. The slope angles of the test area can be seen in Figure 9.12-b. As shown in this figure, the slope angles, δ_1 and δ_2, are not constant.

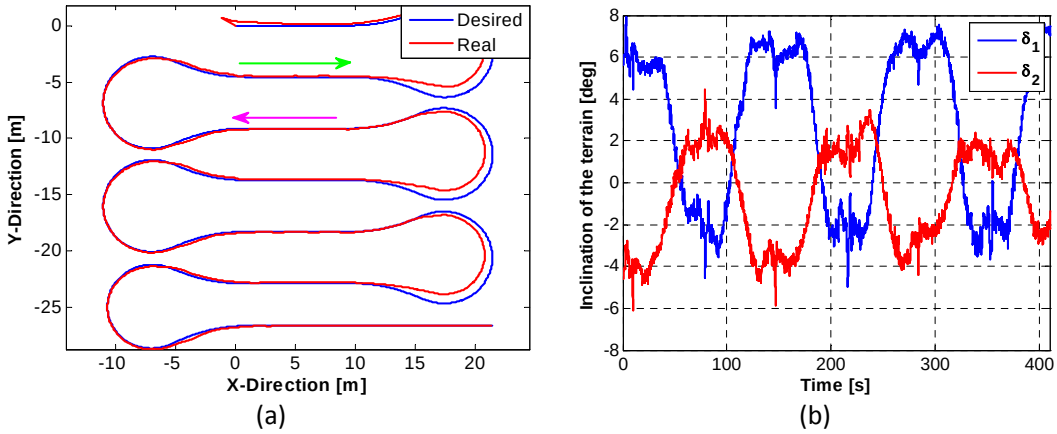

Figure 9.12: Trajectory tracking on the inclined surface covered with snow

Desired and experiment values of X and Y positions are shown in Figure 9.13-a and Figure 9.13-b, respectively.

Longitudinal and lateral slip velocities are presented in Figure 9.14-a. These values are fed into the system model so that the controller can take the required action to overcome such a slippage effect. Side slip angle occurred at the rear axle of the vehicle is shown in Figure 9.14-b. During the desired trajectory tracking task in the inclined part of the test area covered with snow, the vehicle is commanded by the controller in terms of its steering angle and forward

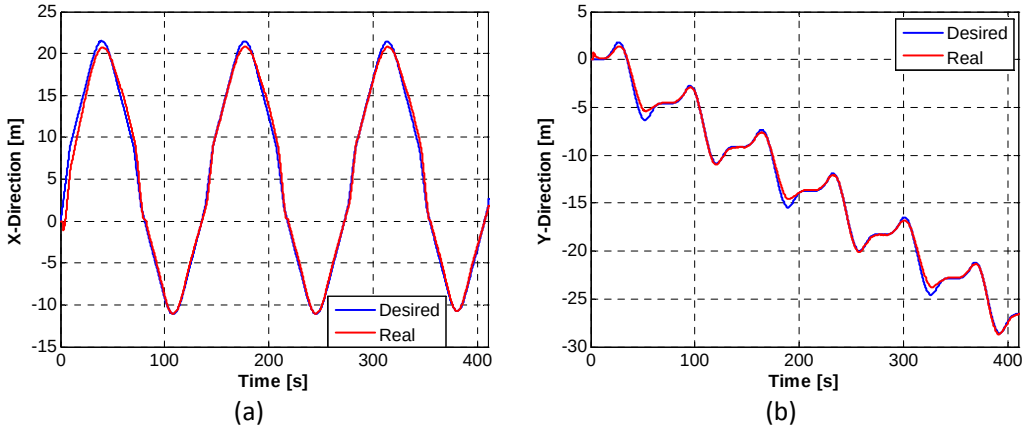

Figure 9.13: Position values in X and Y directions

velocity. These results are shown in Figure 9.15.

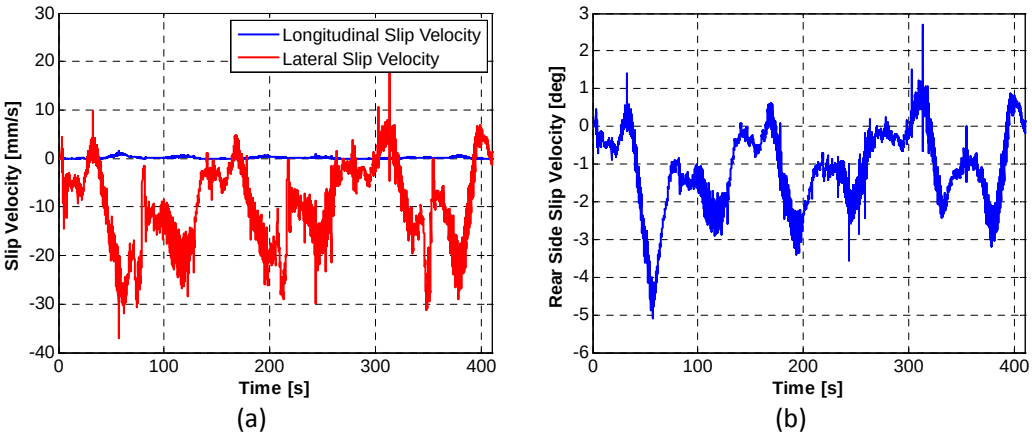

Figure 9.14: (a) Slip velocities, (b) Side slip angle during the motion

9.4.2 Orchard Experiments

As stated above, orchard vehicle uses a laser scanning range finder to detect the trees and specify the rows of trees. For these tasks, a set of row detection procedure is developed and briefly introduced above. In addition to detect the trees and create lines that describe the rows for the trees, the row detectors are able to detect the end of each row. This gives the ability to vehicle to start and continue turning until the row detectors emerges the vehicle about end of turning. Inside the row, the vehicle is always able to see the trees, in other words it has eyes.

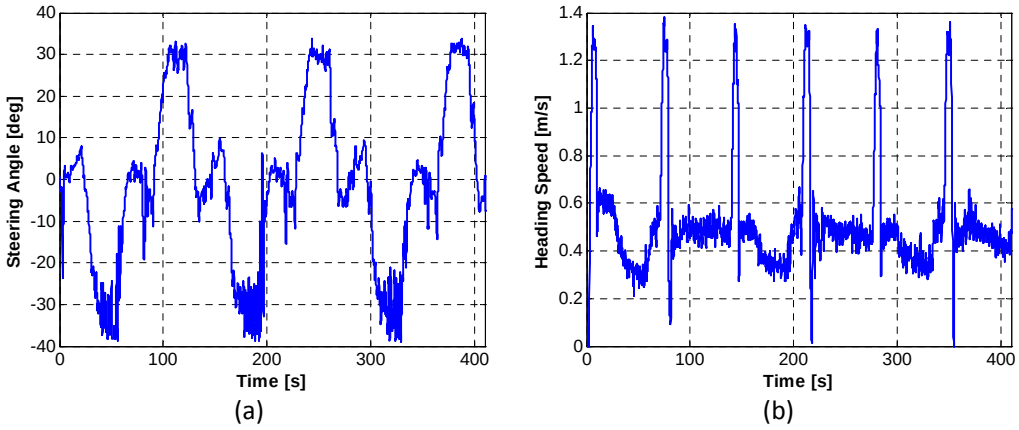

Figure 9.15: (a) Steering angle, (b) Heading velocity

This lets the vehicle position itself and track the desired trajectory. On the other hand, the vehicle is almost blind at the outside of rows. It cannot see any tree until it reaches the target box shown in Figure 9.2. From beginning of the turning to the target box, the vehicle can be able to use only steering system and odometer as sensing devices. The amount of slippage inside the row is reasonable to overcome due to the facts mentioned just above. In contrast, the slippage is generally more than reasonable amount at the outside of rows when the surface is muddy, snowy or slippery. These surface conditions develop slippage and prevent the vehicle to follow the desired trajectory, and access to the target box. When the vehicle is not able to locate itself inside the target box, the following events may occur:

- Row detector may give wrong information about the next row; this causes the vehicle to enter the wrong row of trees.
- The vehicle outside of the target box should do a sharp steering angle change; this can be harmful for the steering actuator.
- The location of the target box is calculated according to the turning trajectory generator which uses optimum arc characteristics (distance, radius, time, power, etc.); the vehicle, which is outside of the desired turning trajectory and target box, has to spend more effort to do necessary corrections.

The orchard environment which has muddy surface is illustrated in Figure 9.16. The surface creates a sticky condition with the tires due to its clay feature therefore the vehicle is faced

Figure 9.16: Experiments conducted in the orchard having muddy surface

with large amount of slippage. As stated above, the parameters of slippage that occur during turning from one row to another are estimated by using estimation procedure. The procedure can be run using two different feedback information systems in this study; RTK-GPS and odometer-steering information systems. The estimated values are fed into the system model and the required actions are created. The turning geometry is developed by using circular turning approach of which definitions are given above. The experiments are conducted for two cases; with including slippage estimation and without including slippage estimation procedures. The results are given in Figure 9.17. In this figure, E_1 shows the trajectory tracking result obtained by using RTK-GPS feedback without using slippage estimation. E_2 represents the trajectory tracking control result obtained by using the slippage estimation procedure that uses RTK GPS feedback. E_3 indicates the trajectory tracking control result gotten access to feedback information coming from odometer-steering information system. No slippage estimation procedure is adapted into the system model during obtaining this result. E_4 illustrates the trajectory tracking result achieved by using the slippage estimation process that uses the odometer-steering feedback information.

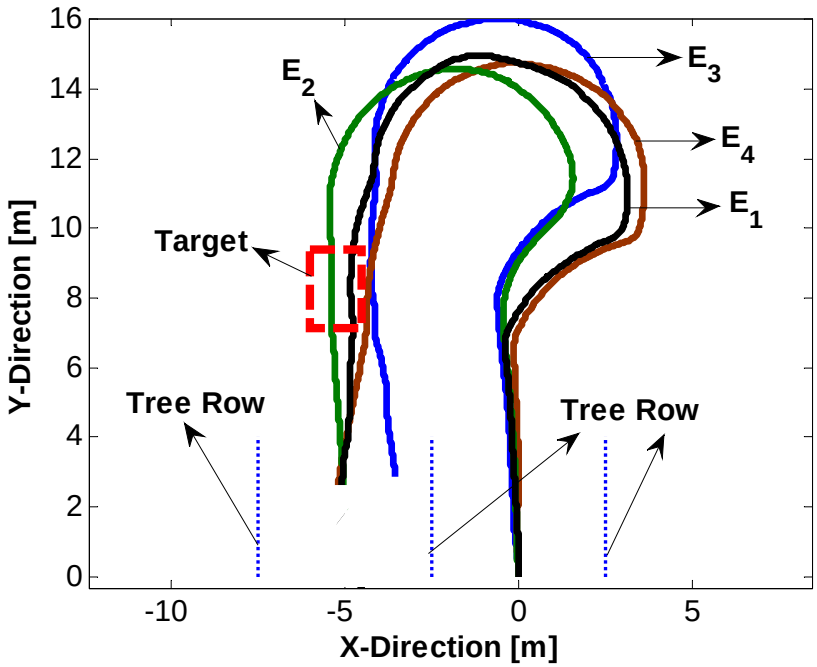

Figure 9.17: Desired trajectory tracking control in slippery surface. E_1 shows the trajectory tracking result obtained by using RTK GPS feedback without using slippage estimation. E_2 represents the trajectory tracking control result obtained by using the slippage estimation procedure that uses RTK GPS feedback. E_3 indicates the trajectory tracking control result gotten access to feedback information coming from dead reckoning algorithm. No slippage estimation procedure is adapted into the system model during obtaining this result. E_4 illustrates the trajectory tracking result achieved by using the slippage estimation process that uses the dead reckoning feedback information.

The slip velocities in longitudinal and lateral directions are illustrated in Figure 9.18-a and 9.18-b respectively. The side slip angle at the rear axle of the vehicle is also shown in Figure 9.18-c. These figures emphasize that slippage prevents the vehicle to track the desired trajectory and access in the target box. The system that is fed by the slip information can be able to generate the required commands to give ability to the vehicle to accomplish the desired task. The vehicle can locate itself inside the target box. Furthermore the heading angle of the vehicle is parallel to the next row of trees as objected.

In order to see the repeatability and reliability of the methodology proposed, the orchard experiments are conducted for so many times. Ten experimental results are shown in Figure 9.19. Five experiments are performed by using the method in which the slippage estimation procedure is included (”w/o” notation is used in the Figure. The results are shown by blue color). The other five experiments are conducted by using the method that slippage estimation procedure is not used (”w/” notation is used in the Figure. The results are shown by red color).

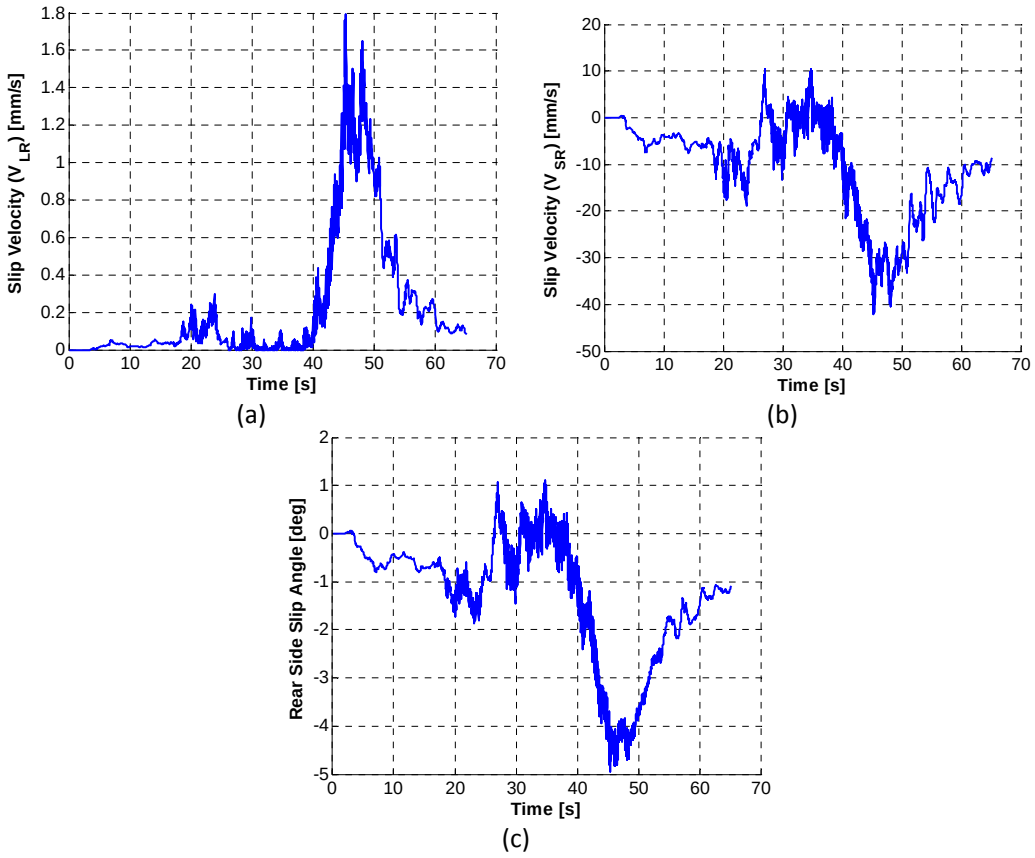

Figure 9.18: (a) Slip velocities in longitudinal direction, (b) Slip velocities in lateral direction, (c) Side slip angle at the rear of the vehicle

In addition to heading angle of the vehicle, its end position according to the turning trajectory is shown in Figure 9.19-a. The end positions and orientations of the vehicle with respect to the row center that is to be driven are indicated. As seen in this figure, the vehicle is in the desired region if the slippage estimation procedure is used. Otherwise, the vehicle is located at the out of desired region (see circles filled by blue color). The summary of these experiments are done in Figure 9.19-b. In this Figure, δ_D indicates the lateral distance (in meter) between the vehicle and the row to be traveled. δ_θ shows the vehicle heading angle (in degree) with respect to the row center. The results are shown into four regions. By following these results, it can be said that region 1 and region 2 can be the best regions for achieving a good row entry.

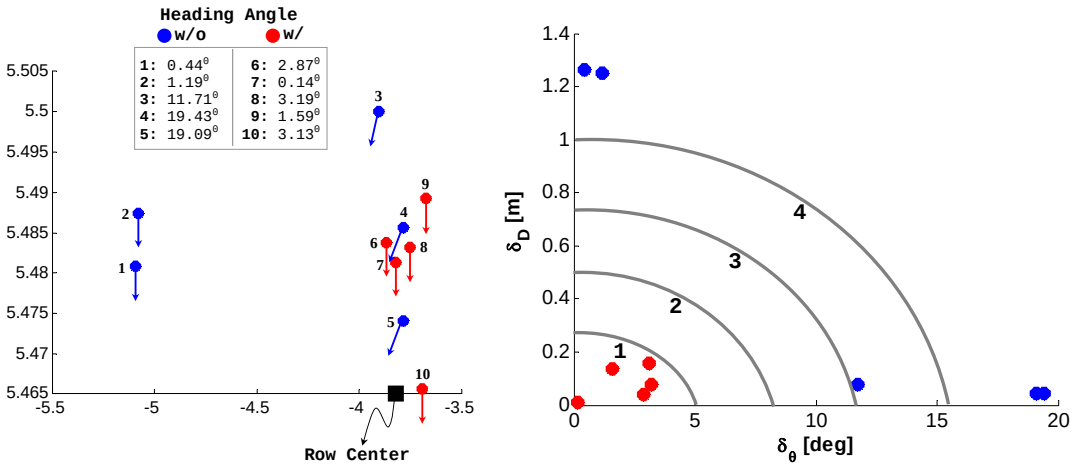

(a) (b)

Figure 9.19: Orchard experiments performed by using the methodologies in which the slippage estimation procedure is included (indicated by notation "w/o" and blue color) and not included (indicated by notation "w/" and red color).

9.5 Conclusion and Discussions

In this study it is aimed that trajectory tracking control of an orchard vehicle can be achieved in an orchard in case of having slippage. In order to accomplish this objective with minimum positioning errors, slippage is taken into account that it produces positioning errors and keeps the vehicle away from the desired trajectory. A model based slippage estimation and control methodology are proposed and implemented in an orchard vehicle. The proposed procedures are tested on different types of surface; flat, inclined, snowy and muddy. They are also examined in an orchard environment for an application that covers row following and turning from one row to another. It is observed that there is a big slippage occurred during turning between rows in an orchard field covered with mud. The experimental results show that the orchard vehicle can be positioned with less positioning errors by implementing the procedure that includes the observation and estimation of slippage and feeding the slip information into the system model. By this way the required compensation to decrease the trajectory error is able to be activated.

CHAPTER 10

CONCLUSION AND FUTURE WORKS

Because of the behaviors of ground-wheel interaction that can show difference characteristics in different terrains, a predefined tracking performance for a mobile robot cannot be achieved by using a set of constant controller parameters and a motion model that follows the simple assumptions. The simple assumption approach is widely used in mobile robotic researches for performing indoor tasks and short run outdoor gaols. In order to get a better trajectory tracking performance for a mobile robot, new modeling approaches are introduced in this thesis study. In the literature, wheel forces, traction and rolling, are modeled in a solution procedure defined by using parametric equations. However, there is no lateral force representation which is easy to implement and adapt into a system. In order to find a solution in this subject, a lateral wheel force representation is constructed by using a parametric equational form. The motion model of the differential drive mobile robot is combined with these three external wheel force representation. These wheel force representation have parameters that should be estimated. In order for achieving this objective, a parameter estimation methodology is also proposed so that the parameters could be able to estimated. It is also shown that the estimation procedure can be adapted into a mobile robotic system easily. By estimating the parameters, the effects of wheel forces could be indicated via the results of simulation and experiments. It can be emphasized that the desired trajectory tracking performance and accuracy can be improved by introducing the system with the external wheel forces. This can be able to achieve better trajectory tracking tasks in outdoor environment having mixed terrain characteristic.

In addition to introducing the motion model of the mobile robot with the external wheel forces, the effects of inclination of the surface should be taken into account to get better accuracy and

performance for trajectory tracking tasks. In this study, a method that takes into account of the effects of inclination of the surface is developed and adapted into the overall system dynamics. In this modeling study, the effects of wheel forces are also considered. The methodology is tested on a specially constructed surface which is inclined. The experimental results show that the motion model of a mobile robot can be enhanced by including the inclination information. This enhancement can also provide to achieve better performance and accuracy for a given reference trajectory.

A trajectory generator which takes into account the steering system's working characteristic is developed in order for achieving a trajectory tracking control with having minimum tracking errors. In this study, car-like robot modeling approach is used to create the desired trajectory. The modeling structure is also introduced with a part which is related to the surface effects. Surface effects is defined by using a parametric representation whose parameters are obtained according to the experimental behavior of the mobile robot. In addition to desired trajectory generator and controllers for heading velocity and steering angle of the mobile robot, a slippage estimator is developed and adapted into system model. The slippage estimated is based on the slip velocities of front and rear wheels. The proposed modeling study is tested in outdoor field environment to show the improvements related to trajectory tracking control task. Performing the outdoor field experiments, a four-wheeled mobile robot is used in different terrain conditions. The procedures proposed are tested in smooth, rough, mixed, dry, snowy, muddy and inclined terrain conditions. The experimental results show that performance and accuracy of a desired trajectory tracking task can be achieved by using the methodology developed in this thesis study. The methodology can also provide to perform long distance autonomous drive in field. The experimental studies also indicate that performance and accuracy of the trajectory tracking goal can be managed to do in case of slippage. The methods contributed in this study are successfully tested for different objectives and in different terrain conditions and it can be concluded that the procedure can be adapted into the different mobile robotic systems running for different applications.

As the future works, the procedures used in this study can be implemented into a mobile robotic platform equipped with different sensors network and used for different real-field applications. Furthermore, the trajectory tracking control structure developed can be run into a mobile robot which has the differential drive capability at its rear and steering system at its front. In such a platform, it is thought that more accurate and more robust trajectory track-

ing might be achieving. The future works that can be implemented in several mobile robotic platforms can be listed as follows:

- The parameters of wheel forces can be estimated on-line and implemented into the overall system model.
- The desired trajectory generation procedure that is used for a mobile robotic platform for a specific application can be updated according to the information coming from the subsystem running to obtain the effects of wheel forces.
- The parameter estimation procedure can also be implemented into a four-wheeled mobile robot that uses a steering system at its front.
- The inclination information can be used in real-time operations for achieving better trajectory tracking tasks. Especially this will be useful for long distance trajectory tracking goals.
- The inclination information can be combined with the controller sub-algorithm that is shown in chapters 5 to 9. It can be useful for both differential drive mobile robot and the mobile robot that uses ackerman steering system.
- Surface change detection can be implemented into the procedure of desired trajectory tracking control. This will enable to get better trajectory tracking.
- The trajectory tracking control procedure proposed in this thesis study can be implemented into any autonomous mobile robotic platform that does not use any high accuracy positioning system. This proposed strategy can also be implemented into a mobile robotic platform which uses a differential drive system.
- The proposed slippage estimation procedure can be used in a robotic platform having differential drive system. The estimation procedure can be run by using the sensors except odometer and high accuracy positioning system. If the procedure can be run by using the slippage estimation system that uses laser scanning range finder information, it will be an eligible contribution in the autonomous ground vehicle research area.
- The trajectory tracking control procedure proposed in this thesis study has been implemented in an autonomous ground vehicle that is constructed for orchard applications.

This procedure can be implemented for any other applications so that the usability in different areas would be seen.

- Simple dubins curves and lines are used for creating desired trajectory. Other mathematical approaches like clothoids may be used for this aims so that more complicated geometries would be created.

- In this study, desired trajectory tracking controller is compared with only pure pursuit control strategy. The controller can also be created by using the other control procedures so that a comprehensive comparison can be done.

- The modeling structures of trajectory tracking control, wheel forces' effects, inclination effects and slippage effects can be combined under a unique model and implemented into different mobile robots which have different drive capabilities. One of them may have a driving system such that it uses a steering system at its front and is motorized differentially at its front and rear.

REFERENCES

[Ampatzidis et al., 2006] Ampatzidis, Y., Vougioukas, S., and Bochtis, D. (2006). A decomposition framework for the autonomous navigation of agricultural vehicles. In *International Conference HAICTA (Information Systems in Sustainable Agriculture, Agroenvironment and Food Technology)*, Greece.

[Anderson and Bevly, 2004] Anderson, R. and Bevly, D. M. (2004). Smooth local path planning for autonomous vehicles. In *American Control Conference*, Boston, Massachusetts, USA.

[Baffet et al., 2008] Baffet, G., Charara, A., and Lechner, D. (2008). Estimation of tire road forces and vehicle sideslip angle. *Advances in Robotics, Automation and Control, book in a book edited by: Jesus Aramburo and Antonio Ramirez Trevino*.

[Bak and Jakobsen, 2004] Bak, T. and Jakobsen, H. (2004). Agricultural robotic platform with four wheel steering for weed detection. *Biosystems Engineering*, 87.

[Balakrishna and Ghosal, 1995] Balakrishna, R. and Ghosal, A. (1995). Modeling of slip for wheeled mobile robots. *lEEE Transactions on Robotics and Automation*, 11:126–132.

[Barawid et al., 2007] Barawid, O., Mizushima, A., Ishii, K., and Noguchi, N. (2007). Development of an autonomous navigation system using a two-dimensional laser scanner in an orchard application. *Biosystems Engineering*, 96.

[Bekker, 1956] Bekker, M. G. (1956). *Theory of land locomotion; the mechanics of vehicle mobility*. University of Michigan Press, Ann Arbor, USA.

[Caracciolo et al., 1999] Caracciolo, L., Luca, A. D., and Iannitti, S. (1999). Trajectory tracking control of a four wheel differentially driven mobile robote. In *IEEE International Conference on Robotics and Automation*, Detroit, Michigan.

[Cariou et al., 2009] Cariou, C., Lenain, R., Thuilot, B., and Berducat, M. (2009). Automatic guidance of a four-wheel-steering mobile robot for accurate field operations. *Journal of Field Robotics*, 26.

[Cervantes et al., 2003] Cervantes, G. A., Devy, M., and Hernandez, A. M. (2003). Lane extraction and tracking for robot navigation in agricultural applications. In *The 11th International Conference on Advanced Robotics*, Coimbra, Portugal.

[Chen and Jiao, 2011] Chen, B. and Jiao, Z. (2011). Adaptive path following control of car-like mobile robot using dynamic model. In *6th IEEE Conference on Industrial Electronics and Applications*, Beijing, China.

[Chen and Hsieh, 2008] Chen, B. C. and Hsieh, F. C. (2008). Sideslip angle estimation using extended kalman filter. *Vehicle System Dynamics*, 46:353–364.

[Dakhlallah et al., 2008] Dakhlallah, J., Glaser, S., Mammar, S., and Sebsadji, Y. (2008). Tire-road forces estimation using extended kalman filter and sideslip angle evaluation. In *American Control Conference*, Seattle, Washington, USA.

[de Wit, 1999] de Wit, C. C. (1999). Dynamic tire friction models for vehicle traction control. In *38th IEEE Conference on Decision and Control*, Phoenix, AZ, USA.

[Dellaerty et al., 1999] Dellaerty, F., Foxy, D., Burgardz, W., and Thruny, S. (1999). Monte carlo localization for mobile robots. In *IEEE International Conference on Robotics and Automation (ICRA99)*, Detroit, Michigan.

[Derrick and Bevly, 2009] Derrick, J. B. and Bevly, D. M. (2009). Adaptive steering control of a farm tractor with varying yaw rate properties. *Journal of Field Robotics*, 26.

[Dolgov et al., 2009] Dolgov, D., Thrun, S., Montemerlo, M., and Diebel, J. (2009). Path planning for autonomous driving in unknown environment. *Experimental Robotics, Springer Tracts in Advanced Robotics*, 54:55–64.

[Dolgov et al., 2010] Dolgov, D., Thrun, S., Montemerlo, M., and Diebel, J. (2010). Path planning for autonomous vehicles in unknown semi-structured environments. *The International Journal of Robotics Research*, 29:485–501.

[Eaton et al., 2009a] Eaton, R., Katupitiya, J., Pota, H., and Siew, K. W. (2009a). Robust sliding mode control of an agricultural tractor under the influence of slip. In *IEEE/ASME International Conference on Advanced Intelligent Mechatronics*, Singapore.

[Eaton et al., 2008] Eaton, R., Katupitiya, J., Siew, K. W., and Howarth, B. (2008). Autonomous farming: Modeling and control of agricultural machinery in a unified framework. In *15th International conference on Mechatronics and Machine Vision in Practice*, Auckland, New-Zealand.

[Eaton et al., 2009b] Eaton, R., Pota, H., and Katupitiya, J. (2009b). Path tracking control of agricultural tractors with compensation for steering dynamics. In *Joint 48th IEEE Conference on Decision and Control and 28th Chinese Control Conference*, Shanghai, China.

[Fang, 2004] Fang (2004). *Automatic guidance of farm vehicles in presence of sliding effects*. A scientific report for the post-doc research project of all-terrain autonomous vehicle control.

[Fang et al., 2005] Fang, H., Lenain, R., Thuilot, B., and Martinet, P. (2005). Robust adaptive control of automatic guidance of farm vehicles in the presence of sliding. In *Proceeding of the 2005 IEEE International Conf. on Robotics and Automation*, Barcelona, Spain.

[Fang et al., 2006] Fang, H., Ruixia, F., Thuilot, B., and Martinet, P. (2006). Trajectory tracking control of farm vehicles in presence of sliding. *Journal of Robotics and Autonomous Systems*, 54:828–839.

[Gonzalez et al., 2009] Gonzalez, R., Rodriguez, F., Guzman, J., and Berenguel, M. (2009). Localization and control of tracked mobile robots under slip conditions. In *IEEE International Conference on Mechatronics*, Malaga, Spain.

[Grip et al., 2009] Grip, H. F., Imsland, L., Johansen, T. A., Kalkkuhl, J. C., and Suissa, A. (2009). Vehicle sideslip estimation design, implemanttaion and experimental validation. *IEEE Control Systems Magazine*, 29:36–52.

[Gu and Hu, 2002] Gu, D. and Hu, H. (2002). Neural predictive control for a car-like mobile robot. *Int. Journal of Robotics and Autonomous Systems*, 39:1–15.

[Gustafsson, 1997] Gustafsson, F. (1997). Slip based tire road friction estimation. *Automatica*, 33:1087–1099.

[Gustafsson et al., 2002] Gustafsson, F., Gunnarsson, F., Bergman, N., Forssell, U., Jansson, J., Karlsson, R., and Nordlund, P.-J. (2002). Particle filters for positioning, navigation, and tracking. *IEEE Transactions on Signal Processing*, 50:425–437.

[Hammer et al., 2009] Hammer, B., Koterba, S., Shi, J., Simmons, R., and Singh, S. (2009). Mobile robotic dynamic tracking for assembly tasks. In *IEEE/RSJ International Conference on Intelligent Robots and Systems, IROS2009*, St. Louis, MO.

[Hamner et al., 2011] Hamner, B., Bergerman, M., and Singh, S. (2011). Autonomous orchard vehicles for speciality crops production. In *2011 ASABE Annual International Meeting*, Lousville, Kentucky, USA.

[Han et al., 2008] Han, J., Sun, Y., Meng, C., and Han, J. (2008). Estimating the tire road friction for tire pressure monitoring using the result of a nonlinear observer. In *7th World Congress on Intelligent Control and Automation*, Chongqing, China.

[Hashim and Lu, 2009] Hashim, M. S. M. and Lu, T. F. (2009). Multiple waypoints trajectory planning with specific position, orientation, velocity and time using geometric approach for a car-like robot. In *Australasian Conf. on Robotics and Automation*, Sydney, Australia.

[Hoffmann et al., 2007] Hoffmann, G. M., Tomlin, C. J., Montemerlo, M., and Thrun, S. (2007). Autonomous automobile trajectory tracking for off-road driving: controller design, experimental validation and racing. In *American Control Conference*, USA.

[Huynh et al., 2010] Huynh, V. T., Katupitiya, J., Kwok, N. M., and Eaton, R. P. (2010). Derivation of an error model for tractor-trailer path tracking. In *International Conference on Intelligent Systems and Knowledge Engineering (ISKE)*, Hangzhou.

[Iagnemma and Dubowsky, 2002] Iagnemma, K. and Dubowsky, S. (2002). Terrain estimation for high speed rough terrain autonomous vehicle navigation. In *Unmanned Ground Vehicle Technology IV, SPIE*, Orlando, FL, USA.

[Iijima et al., 2010] Iijima, T., Raksincharoensak, P., Michitsuji, Y., and Nagai, M. (2010). Vehicle side slip angle estimation methodology using a drive recorder. *Journal of Vibration and Control*, 16:571–583.

[Johnson et al., 2009] Johnson, D. A., Naffin, D. J., Puhalla, J. S., Sanchez, J., and Wellington, C. K. (2009). Development and implementation of a team of robotic tractors for autonomous peat moss harvesting. *Journal of Field Robotics*, 26.

[Kim and Oh, 1998] Kim, D. H. and Oh, J. H. (1998). Globally asymptotically stable tracking control of mobile robots. In *Proceedings of the 1998 IEEE Int. Conf. on Control Applications*, Trieste, Italy.

[Kuwata et al., 2009] Kuwata, Y., Teo, J., Fiore, G., Karaman, S., Frazzoli, E., and How, J. P. (2009). Real-time motion planning with applications to autonomous urban drive. *IEEE Transactions on Control Systems Technology*, 17:1105–1118.

[Kuwata et al., 2008] Kuwata, Y., Teoy, J., Fiorex, S. K. G., Frazzoli, E., and How, J. P. (2008). Motion planning in complex environments using closed-loop prediction. In *AIAA Guidance, Navigation, and Control Conf. and Exhibition*, Honolulu, Hawaii.

[Lee et al., 2006] Lee, K., Kim, D., Chung, W., Chang, H. W., and Yoon, P. (2006). Car parking control using a trajectory tracking controller. In *SICE-ICASE Int. Joint Conf.*, Busan, Korea.

[Lee et al., 1999] Lee, S., Kim, M., Youm, Y., and Chung, W. (1999). Control of a car-like mobile robot for parking problem. In *Proceedings of the 1999 IEEE Int. Conf. on Robotics and Automation*, Detroit, USA.

[Lenain et al., 2010a] Lenain, R., Lucet, E., Grand, C., Thuilot, B., and Amar, F. B. (2010a). Accurate and stable mobile robot path tracking: An integrated solution for off-road and high speed context. In *IEEE/RSJ International Conference on Intelligent Robots and Systems (IROS)*, Taipei.

[Lenain et al., 2003] Lenain, R., Thuilot, B., Cariou, C., and Martinet, P. (2003). Rejection of sliding effects in car like robot control: application to farm vehicle guidance using a single rtk gps sensor. In *Proceedings of the 2003 IEEE/RSJ Int. Conf. on Intelligent Robots and Systems*, Las Vegas, USA.

[Lenain et al., 2005] Lenain, R., Thuilot, B., Cariou, C., and Martinet, P. (2005). Robust path following of car-like wmr in the presence of skidding effects. In *Proceedings of the 2005 IEEE Int. Conf. on Mechatronics*, Taipei, Taiwan.

[Lenain et al., 2006] Lenain, R., Thuilot, B., Cariou, C., and Martinet, P. (2006). Sideslip angles observer for vehicle guidance in sliding conditions: Application to agricultural path tracking tasks. In *Proceedings of the IEEE International Conference on Robotics and Automation*, Orlando, Florida, USA.

[Lenain et al., 2010b] Lenain, R., Thuilot, B., Cariou, C., and Martinet, P. (2010b). Mixed kinematic and dynamic sideslip angle observer for accurate control of fast off-road mobile robots. *Journal of Field Robotics*, 27:181–196.

[Li et al., 2006] Li, L., Wang, F.-Y., and Zhou, Q. (2006). Integrated longitudinal and lateral tire/road friction modeling and monitoring for vehicle motion control. *IEEE Transactions on Intelligent Transportation Systems*, 7:1–19.

[Libby and Kantor, 2011] Libby, J. and Kantor, G. (2011). Deployment of a point and line feature localization system for an outdoor agriculture vehicle. In *IEEE International Conference on Robotics and Automation*, Shanghai, China.

[Liegeois and Moignard, 1993] Liegeois, A. and Moignard, C. (1993). Optimal motion planning of a mobile robot on a triangulated terrain model. *Lecture Notes in Computer Science*, 708:51–65.

[Lindgren et al., 2002] Lindgren, D. R., Hague, T., Smith, P. J. P., and Marchant, J. A. (2002). Relating torque and slip in an odometric model for an autonomous agricultural vehicle. *Autonomous Robots*, 13:73–86.

[Low and Wang, 2008] Low, C. B. and Wang, D. (2008). Gps-based path following control of a car-like wheeled mobile robot with skidding and slipping. *IEEE Transactions on Control Systems Technology*, 16:340–347.

[Luca and Oriolo, 1997] Luca, A. D. and Oriolo, G. (1997). *Feedback control of a nonholonomic car-like robot: Planning Robot Motion*. Lamond Ed., Springer-Verlag.

[Matveev et al., 2010] Matveev, A. S., Hoy, M., and Savkin, A. V. (2010). Mixed nonlinear sliding mode control of an unmanned farm tractor in the presence of sliding. In *11th Int. Conf. Control, Automation, Robotics and Vision*, Singapore.

[Melonee and John, 2008] Melonee, W. and John, H. (2008). Application and analysis of a robust trajectory tracking controller for under-characterized autonomous vehicles. In *IEEE Int. Conf. on Control Applications*, San Antonio, USA.

[Mester, 2010] Mester, G. (2010). Intelligent mobile robot motion control in unstructured environments. *Acta Polytechnica Hungarica*, 7:153–165.

[Motte and Campion, 2000] Motte, I. and Campion, G. (2000). A slow manifold approach for the control of mobile robots not satisfying the kinematic constraints. *IEEE Transactions On Robotics and Automations*, 16:875–880.

[Nagasaka et al., 2009] Nagasaka, Y., Saito, H., Tamaki, K., Seki, M., Kobayashi, K., and Taniwaki, K. (2009). An autonomous rice transplanter guided by global positioning system and inertial measurement unit. *Journal of Field Robotics*, 26.

[Ojeda et al., 2006a] Ojeda, L., Borenstein, J., Witus, G., and Karlsen, R. (2006a). Terrain characterization and classification with a mobile robot. *Journal of Field Robotics*, 23:103–122.

[Ojeda et al., 2006b] Ojeda, L., D, C., G, R., and Borenstein, J. (2006b). Current based slippage detection and odometry correction for mobile robots and planetary rovers. *IEEE Trans. Robot*, 22:366–378.

[Ordonez et al., 2009] Ordonez, C., Jr., O. Y. C., Jr., E. G. C., and Liu, X. (2009). Rut detection and following for autonomous ground vehicles. In *Proceedings of Robotics: Science and Systems (RSS)*, Seattle, USA.

[Pacejka, 2006] Pacejka, H. B. (2006). *Tire and vehicle dynamics, Second Edition*. Elsevier, Butterworth-Heinemann.

[Peters and Iagnemma, 2008] Peters, S. C. and Iagnemma, K. (2008). Mobile robot path tracking of aggressive maneuvers on sloped terrain. In *IEEE/RSJ International Conference on Intelligent Robots and Systems*, Nice, France.

[Ray, 2008] Ray, L. E. (2008). Autonomous terrain parameter estimation for wheeled vehicles. In *Unmanned Systems Technology X, SPIE*, Orlando, FL, USA.

[Rezaei et al., 2003] Rezaei, S., Guivant, J., and Nebot, E. M. (2003). Car-like robot path following in large unstructured environments. In *Proceedings of the 2003 IEEE/RSJ Int. Conf. on Intelligent Robots and Systems*, Las Vegas, USA.

[Ryu et al., 2002] Ryu, J., Rossetter, E. J., and Gerdes, J. C. (2002). Vehicle sideslip and roll parameter estimation using gps. In *6th Int. Symposium on Advanced Vehicle Control (AVEC)*, Hiroshima, Japan.

[Salerno and Angeles, 2007] Salerno, A. and Angeles, J. (2007). A new family of two wheeled mobile robots: modeling and controllability. *IEEE Transactions on Robotics*, 23:169–173.

[Sidek and Sarkar, 2008a] Sidek, N. and Sarkar, N. (2008a). Dynamic modeling and control of nonholomonic mobile robot with lateral slip. In *7th Int. Conf. On Signal Processing, Robotics and Auto.*, Stevens Point, Wisconsin, USA.

[Sidek and Sarkar, 2008b] Sidek, N. and Sarkar, N. (2008b). Inclusion of wheel slips in mobile robot modeling to enhance robot simulator performance. In *The 3rd Int. Conf. on Mechatronics*, Kuala Lumpur, Malaysia.

[Silva et al., 2008] Silva, A. F. B., Santos, A. V., Meggiolaro, M. A., and dos Reis, N. R. S. (2008). Traction control of all-wheel-drive independent suspension mobile robots in 2d rough terrain. *ABCM Symposium Series in Mechatronics*, 3:256–265.

[Singh et al., 2009] Singh, S., Baugher, T., Bergerman, M., Ellis, K., Grocholsky, B., Hamner, B., Harper, J., Hoheisel, G.-A., Hull, L., Jones, V., Kantor, G., Kliethermes, B., Koselka, H., Lewis, K., Libby, J., Messner, W., Ngugi, H., Owen, J., Park, J., Seavert, C., Shi, W., and Teza, J. (2009). Automation for specialty crops: A comprehensive strategy, current results, and future goals. In *The 4th IFAC International Workshop on Bio-Robotics, Information Technology, and Intelligent Control for Bioproduction Systems*, Champaign, IL.

[Singh et al., 2010] Singh, S., Bergerman, M., Cannons, J., Grocholsky, B., Hamner, B., Holguin, G., Hull, L., Jones, V., Kantor, G., Koselka, H., Li, G., Owen, J., Park, J., Shi, W., and Teza, J. (2010). Comprehensive automation for specialty crops: Year 1 results and lessons learned. *Intel Serv Robotics*, 3:245–262.

[Solea and Nunes, 2007] Solea, R. and Nunes, U. (2007). Trajectory planning and sliding-mode control based trajectory-tracking for cybercars. *Int. Journal of Integrated Computer-Aided Engineering*, 14:33–47.

[Song et al., 2004] Song, Z., Hutangkabodee, S., Zweiri, Y. H., Seneviratne, L. D., and AIthoefer, K. (2004). Identification of soil parameters for unmanned ground vehicles track-terrain interaction dynamics. In *SICE Annual Conference*, Sapporo, Japan.

[Sotelo, 2003] Sotelo, M. A. (2003). Lateral control strategy for autonomous steering of ackerman-like vehicles. *Robotics and Autonomous Systems*, 45:223–233.

[Stentz et al., 2002] Stentz, A., Dima, C., Wellington, C., Herman, H., and Stager, D. (2002). A system for semi-autonomous tractor operations. *Autonomous Robots*, 13:87–104.

[Stonier et al., 2007] Stonier, D., Cho, S.-H., Choi, S., Kuppuswamy, N. S., and Kim, J.-H. (2007). Nonlinear slip dynamics for an omniwheel mobile robot platform. In *IEEE Int. Conf. on Robotics and Auto.*, Roma, Italy.

[Tian et al., 2009] Tian, Y., Sidek, N., and Sarkar, N. (2009). Modeling and control of a nonholonomic wheeled mobile robot with wheel slip dynamics. In *IEEE Symposium on Computational Intelligence in Control and Automation*, Nashville, Tennessee.

[Tsai et al., 2004] Tsai, P.-S., Wang, L.-S., Chang, F.-R., and Wu, T.-F. (2004). Point stabilization control of a car-like mobile robot in hierarchical skew symmetry chained form. In *Proceedings of the 2004 IEEE Int. Conf. on Networking, Sensing and Control*, Taipei, Taiwan.

[Ward and Iagnemma, 2008] Ward, C. C. and Iagnemma, K. (2008). A dynamic-model-based wheel slip detector for mobile robots on outdoor terrain. *IEEE Transactions on Robotics*, 24:821–831.

[Webers and Zimmer, 2002] Webers, C. and Zimmer, U. R. (2002). Motion control of mobile robots-from static targets to fast drives in moving crowds. *Autonomous Robots*, 12:173–185.

[Wei et al., 2009] Wei, B., Gao, J., Li, K., and Chen, H. (2009). Navigation and slope detection system design for autonomous mobile robot. In *The Ninth International Conference on Electronic Measurement and Instruments*, Beijing, China.

[Weiss and Biber, 2011] Weiss, U. and Biber, P. (2011). Plant detection and mapping for agricultural robots using a 3d lidar sensor. *IEEE Transaction on Robotics and Automation*, 59:265–273.

[Williams et al., 2002] Williams, R. L., Carter, B. E., Gallina, P., and Rosati, G. (2002). Dynamic model with slip for wheeled omnidirectional robots. *IEEE Transactions on Robotics and Automation*, 18:285–293.

[Wong, 2001] Wong, J. Y. (2001). *Theory of ground vehicles, Third Edition*. John Wiley and Sons, USA.

[Xiang et al., 2007] Xiang, Z. Z., Jun, C., Toyofumi, Y., Ryo, T., He, S. Z., and Rong, M. E. (2007). Path tracking control of autonomous agricultural mobile robots. *Journal of Zhejiang University Science-A*, 8:1596–1603.

[Yang et al., 2004] Yang, E., Gu, D., Mita, T., and Hu, H. (2004). Nonlinear tracking control of a car-like mobile robot via dynamic feedback linearization. In *Control 2004*, University of Bath, UK.

[Ye and Borenstein, 2004] Ye, C. and Borenstein, J. (2004). A method for mobile robot navigation on rough terrain. In *IEEE International Conference on Robotics and Automation*, New Orleans, LA, USA.

[Yi et al., 2007] Yi, J., Song, D., Zhang, J., and Goodwin, Z. (2007). Adaptive trajectory tracking control of skid steering mobile robot. In *IEEE Int. Conf. Robot. Autom.*, Rome, Italy.

[Yun, 1995] Yun, X. (1995). State space representation of holonomic and nonholonomic constraints resulting from rolling contacts. In *IEEE lnternational Conference on Robotics and Automotion*, Nagoya, Aichi, Japan.

[Yun and Yamamoto, 1993] Yun, X. and Yamamoto, Y. (1993). Internal dynamics of a wheeled mobile robot. In *IEEE/RSJ International Conference on Intelligent Robots and Systems*, Yokohama, Japan.

[Yun and Yamamoto, 1997] Yun, X. and Yamamoto, Y. (1997). Stability analysis of the internal dynamics of a wheeled mobile robot. *Journal of Robotic Systems*, 14:697–709.

[Zhu et al., 2010] Zhu, J., Wang, Y., Yu, H., Wang, W., and Wen, Y. (2010). Sensing incline terrain for mobile robot autonomous navigation under unknown environment. In *IEEE International Conference on Information and Automation*, Harbin, China.

CURRICULUM VITAE

Gökhan Bayar

Middle East Technical University
Mechanical Engineering Department
Mechatronics Laboratory, D-107
Ankara, Turkey
Tel: +90.210.5208
email: gbayar@gmail.com

Education:

- Doctor of Philosophy in Mechanical Engineering Department (Mechatronics), Middle East Technical University.
- Master in Mechanical Engineering Department (Mechatronics), Middle East Technical University.
- Bachelor of Science with First Rank Honour in Mechanical Engineering Department, Eskisehir Osmangazi University.

Research Interests:

- Unmanned autonomous ground vehicles, mobile robots.

Academic and Professional Experience:

- Research-Teaching Assistant, Mechanical Engineering Department, Middle East Technical University, Ankara, Turkey.
- Research Engineer, ASELSAN, Ankara, Turkey (Unmanned Ground Vehicle Development Project).
- Research Engineer, Mechanical Engineering Department, Middle East Technical University, Ankara, Turkey, DPT Project (Mobile Robot Design for Mixed Terrain Applications.
- Researcher, Carnegie Mellon University, Robotics Institute, Pittsburgh, PA, USA, Long Distance Autonomous Trajectory Tracking for an Orchard Vehicle.